NASA Contractor Report 4286

Development of a Defect Stream Function, Law of the Wall/Wake Method for Compressible Turbulent Boundary Layers

Richard A. Wahls

NASA

NASA Contractor Report 4286

Development of a Defect Stream Function, Law of the Wall/Wake Method for Compressible Turbulent Boundary Layers

Richard A. Wahls
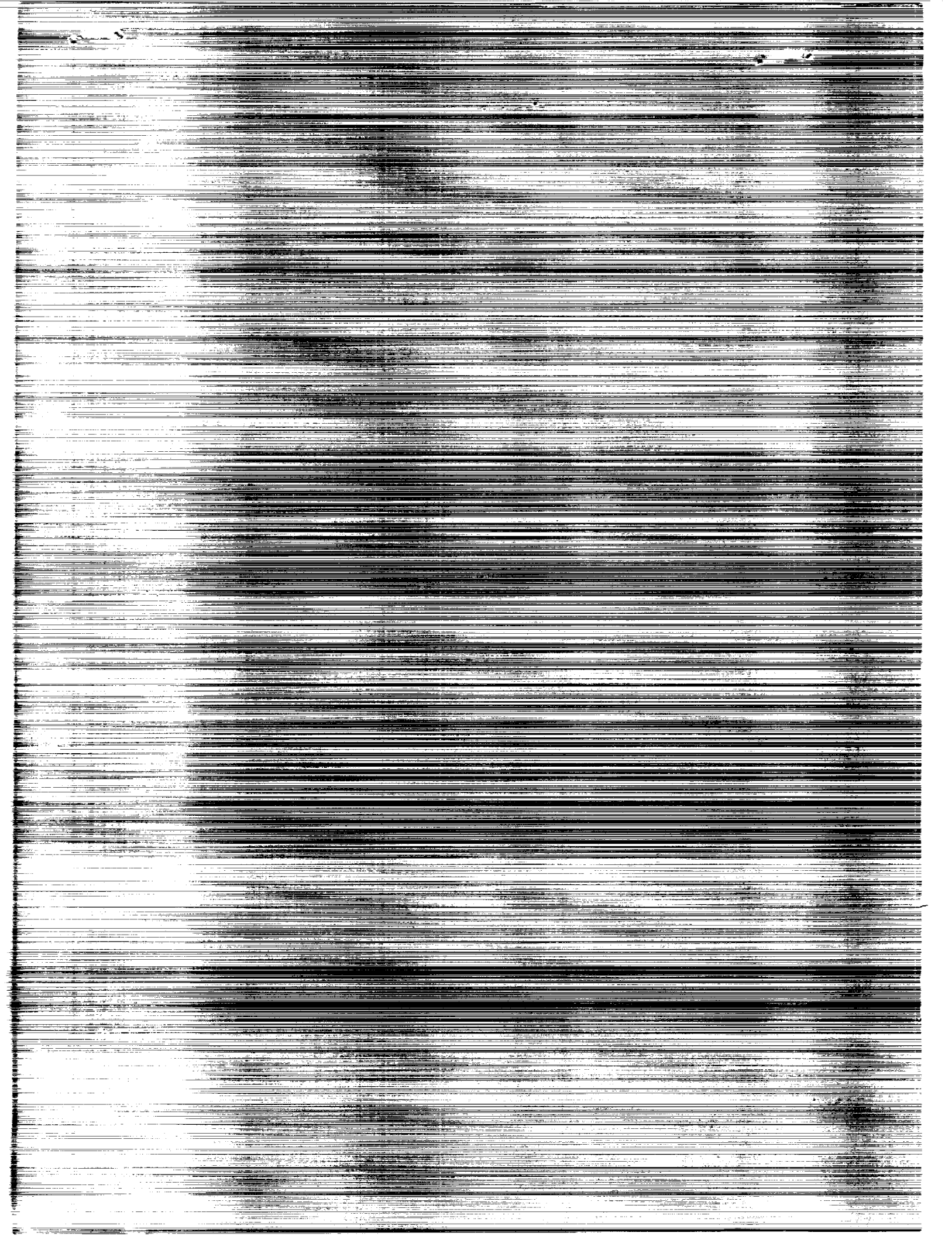*North Carolina State University*
Raleigh, North Carolina

NASA

National Aeronautics and
Space Administration

Office of Management

Scientific and Technical
Information Division

1990

Abstract

WAHLS, RICHARD A. Development of a Defect Stream Function, Law of the Wall/Wake Method for Compressible Turbulent Boundary Layers (Under the direction of Dr. Fred R. DeJarnette)

The method presented is designed to improve the accuracy and computational efficiency of existing numerical methods for the solution of flows with compressible turbulent boundary layers. A compressible defect stream function formulation of the governing equations assuming an arbitrary turbulence model is derived. This formulation is advantageous because it has a constrained zero-order approximation with respect to the wall shear stress and the tangential momentum equation has a first integral. Previous problems with this type of formulation near the wall are eliminated by using empirically based analytic expressions to define the flow near the wall. The van Driest law of the wall for velocity and the modified Crocco temperature-velocity relationship are used. The associated compressible law of the wake is determined and it extends the valid range of the analytic expressions beyond the logarithmic region of the boundary layer. The need for an inner-region eddy viscosity model is completely avoided. The near-wall analytic expressions are patched to numerically computed outer region solutions at a point determined during the computation. A new boundary condition on the normal derivative of the tangential velocity at the surface is presented; this condition replaces the no-slip condition and enables numerical integration to the surface with a relatively coarse grid using only an outer region turbulence model. The method has been evaluated for incompressible and compressible equilibrium flows and has been implemented into an existing Navier-Stokes code using the assumption of local equilibrium flow with respect to the patching. The method has proven to be accurate and efficient.

Acknowledgements

Table of Contents

List of Tables

List of Figures

1 INTRODUCTION

It is generally accepted that turbulence is the most complicated kind of fluid motion. Many researchers have directed extensive effort towards the physical understanding and computation of turbulent flows. Turbulence has been described by Hinze[1] as "...an irregular condition of flow in which the various quantities show a random variation with time and space coordinates so that statistically distinct average values can be discerned." The major problem when attempting to compute a turbulent flowfield from first principles is that the time and space scales of the turbulent motion are extremely small. The computational grid required to fully resolve such a flow in this manner are beyond the limits of todays computer technology. Anderson et al[2] provide an estimate of the spacing required for a typical flowfield in which "10^5 points may be required to resolve just 1 cm^3 of the flowfield." It is because "statistically distinct average values can be discerned" that modeling techniques can be developed that allow us to solve turbulent flowfields for engineering purposes.

Currently there are two basic approaches for computing turbulent flowfields[3]. The first approach is known as a large eddy simulation. This approach attempts to compute the maximum amount of information about the turbulent motion as it attempts to capture the turbulence on a real-time, real-space basis. Large eddies, which are responsible for the majority of the momentum transport, are resolved on the scale of the grid. Subgrid modeling is used to describe the effects of the small eddies, which cannot be resolved with practical grids. It has been projected[3] that fully converged large eddy simulations for simple airfoils is beyond the capability of current computers.

The second, and more prevalent, approach is to calculate the mean motion of the fluid by use of the time-averaged Navier-Stokes equations. These equations are often referred to as the Reynolds equations. They are derived by decomposing the dependent

variables into mean and fluctuating components and then averaging the equations over time. The resulting equations are expressed primarily in terms of mean variables with the transient effects of turbulence being described by the fluctuating quantities that appear in the turbulent or Reynolds stress terms; the Reynolds stress terms require modeling. This approach does not attempt to capture the turbulence on a real-time, real-space basis but instead relies on a turbulence model to convey the effects of the turbulent motion on the mean flow. Also, the solution schemes do not need to be time accurate and are able to converge much more rapidly than with large eddy simulations. On the other hand, information on the dynamics of turbulence is lost. It is fortunate that the simpler statistical approach is adequate for general engineering purposes[4].

Turbulence modeling is the most important and most difficult aspect of the statistical methods. The turbulence model is necessary to mathematically close the system of governing equations and must fully describe all of the effects of the turbulent motion on the mean flow. Several excellent review papers on the state of turbulence modeling have been given by Rubesin[3], Lakshminarayana[5], Marvin[6], and Rubesin and Viegas[7]. Turbulence models can be categorized as either zonal or global in reference to their range validity[3]. The zonal model is one which is designed for a specific application and is usually developed from this specific class of experiments. In general, these models do an excellent job of predicting flows of the particular class but begin to lose accuracy and break down when extending beyond these flows. The global models, however, involve more complex functions, such as the field equations for the turbulence quantities, and have a wider range of applicability. The more complex models require more empirically based coefficients than do the zonal models; these coefficients are determined from more than one class of experiments. The basic necessity of empirical coefficients restricts the global models from successfully predicting flows of all types. At present, a true global, or universal, model

2

which is accurate for all flows has yet to be determined. Thus, it can be stated that current turbulence models are restricted to various zones of application.

Turbulence models can also be classified as either eddy-viscosity or stress-transport models[6]. Eddy-viscosity models rely on the Boussinesq[8] concept, which models the turbulent shear stress as the product of an effective viscosity and a mean rate of strain. The effective viscosity is proportional to the velocity and length scales of the turbulence in the various regions of the flow. Eddy-viscosity models can be further classified according to the method of determining the effective viscosity; in other words, the various eddy-viscosity models are functions of the method used to describe the velocity and length scales of turbulence. They are classified as either zero-, one-, or two-equation models, where the designation refers to number of field equations used in addition to the usual mean flow equations. The simplest is, of course, the zero-equation model, which determines the eddy viscosity based entirely on the properties of the mean flow. The two primary examples of this type are those of Cebeci and Smith[9] and Baldwin and Lomax[10]. These models are widely used in practical engineering applications for simple shear flows and in many Navier-Stokes codes[5]. The one-equation models typically rely on the solution of the turbulent kinetic energy equation to represent the velocity scale, and the two-equation models incorporate the solution of an additional equation which represents the length scale of the problem. The one- and two-equation models are more general than the zero-equation models but, in many instances, do not improve the accuracy of the solutions.

The stress-transport models use the Reynolds-stress equations to model turbulence in the mean flow equations. Here closure is achieved through the solution of the mean turbulent field and requires the solution of up to six additional differential equations for the Reynolds stresses, thus significantly increasing the computational effort required beyond the capability of current computers[5]. As a result, several attempts to simplify the stress-transport equations have been made and are discussed in detail in reference 5. These

approaches make assumptions, some arbitrary and others based on the physics of the flow, that allow the stress-transport equations to be reduced to an algebraic form. Note that even in differential form, these equations still require modeling of several terms which involve a number of empirical coefficients. The main advantage relative to eddy-viscosity models is that the stresses are able to respond immediately to changes in the rate of strain. These models are appropriate for a wider range of flow conditions including separated and recirculation regions for which eddy-viscosity models are not valid.

The current investigation is concerned with the solution of compressible turbulent boundary layers over solid surfaces. The flowfields studied are restricted to attached boundary layers under adiabatic wall conditions. The formulation is derived such that it is consistent with the eddy-viscosity concept. Over the years, considerable research has been devoted to the development of numerical methods for just such situations. The computational effort required of these methods is highly dependent on the number of grid points necessary to accurately resolve the flowfield. Boundary-layer flows in general require a finely spaced grid in order to accurately calculate their properties and their influence on the external flow. Turbulent boundary layers, in particular, demand a very fine grid near the wall in order to resolve the high gradients of the physical properties in this region; however, a much coarser grid similar to that necessary for a laminar boundary layer can be used in the outer region away from the wall. Blottner[11] presented an excellent example demonstrating the different grid requirements for laminar and turbulent boundary layers. Blottner's figure is reproduced here in figure 1. With a common outer edge of the boundary layer defined and the requirement of one percent accuracy of the shear stress at the wall, Blottner estimated the number of uniform intervals necessary to resolve laminar and turbulent boundary layers on a flat plate. He found that the turbulent profile required twenty times the number of intervals as the laminar profile. The additional intervals required are a direct result of the high gradient region near the wall, and to a lesser extent,

the increased thickness of the turbulent boundary layer. An obvious solution to this problem is the use of a nonuniform grid which clusters grid points where the most resolution is needed; in this case, grid points are clustered in the high gradient region near the wall. Nonuniform grids are in everyday use and have been for many years. Despite this technique, the grid requirements still become excessive when dealing with complex two-dimensional and even the simplest three-dimensional flows as computational time can take many hours or days even on the fastest available computers.

An additional technique which has become popular recently is the use of wall functions. In effect, wall functions replace the highly clustered grid points and corresponding numerical computations near the surface with empirically based, analytic expressions for velocity, temperature, and other quantities as necessary for compatibility with a particular turbulence model. It is, in fact, the potential reduction of computational effort that is the main incentive behind the development of wall function techniques. Experimental investigations of turbulent flows, and the corresponding analytic investigations, have established expressions for the near-wall region which have proven to be quite accurate and robust. The use of such expressions should not be a concern as it is apparent that all turbulent flow analyses are based on empiricism to some extent. The logarithmic law of the wall for velocity is one of the most widely used and accepted expressions of this type. It is, in fact, one of the most widely accepted empiricisms in all of fluid mechanics and has proven useful even beyond the bounds of its strict assumptions.

The basic concept of the wall function methods is to determine analytically the flowfield variables from the surface to a point near the surface where the analytic description is valid. This is the first grid point off of the surface. From this point outward, the flowfield is resolved with an appropriate numerical method and associated turbulence model. The analytic description of the flowfield variables at the first grid point provides boundary conditions used to compute the remainder of the flowfield. Most methods simply

patch the analytic and numeric solutions at this point while some, such as the recent method of Walker, Ece, and Werle[12], formally match the outer limit of the inner solution to the inner limit of the outer solution. A common characteristic of current wall function approaches is the precomputation designation of the first grid point off of the wall; that is, the section of the flowfield to be determined analytically is decided prior to the computation. This characteristic is independent of the numerical method and turbulence model. The grid point location is crucial because it must be within the range of validity of the analytic model at all streamwise locations. This grid point is typically chosen to lie within the viscous sublayer or logarithmic region of the boundary layer. As such, this approach does not take full advantage of the analytic expressions because their use is limited to only a portion of their valid range. It follows that near-wall turbulence models are still required although not to the same extent as without the use of wall functions.

Rubesin's review of turbulence modeling[3] points out several major advantages that wall function methods have over methods that integrate to the surface. First of all, wall function methods have proven to be quite economical due to the reduction in the number of grid points required to resolve the flowfield as well as to the increase in the allowable time step due to the increased size of the minimum grid spacing. Secondly, present near-wall turbulence models have inherent physical uncertainties and, in some instances, result in a numerically stiff set of equations near the surface. The use of the wall functions has been shown to increase the accuracy of the solutions near the surface in many cases while relieving this near-wall stiffness. As far as the accuracy is concerned, it should be advantageous to model the inner region with an empirical representation which can be validated by direct experimental observation rather than with another model, such as an eddy-viscosity model, which cannot be validated by direct experimental observation. The point is that error can enter through a model if said model is based on indirect empiricism

6

such as velocity measurements being correlated and put in the form of an eddy viscosity; the eddy viscosity is not a property which can be measured directly.

One of the most effective wall function methods to date is that of Viegas, Rubesin, and Horstman[13], which is an extension of the method originally developed by Viegas and Rubesin[14] to increase computational efficiency for their study of shock wave/boundary layer interactions. Their method has proven to be successful not only by increasing the efficiency of their solution procedure by an order of magnitude with respect to the computer time per solution, but also by improving the accuracy of their solutions. The method has proven successful over a variety of flowfields including two-dimensional separated flows. However, several parameters, such as the skin-friction coefficient and shock locations, remain somewhat sensitive to the choice of the first grid point off of the surface (the patch point of the analytic and numeric solutions). More recently Wilcox[15] reports the sensitivity of the location of the first grid point on the skin friction.

The method put forth in this investigation combines traditional wall function ideas with features designed to further improve computational efficiency and address some of the shortcomings of previous methods. The improvement in efficiency will be a direct result of further grid reduction, and the primary shortcoming addressed is the choice of the location of the first grid point. The method proposed considers the turbulent boundary layer as a composite consisting of an inner region near the surface with an outer region beyond. The two regions are similar to those encountered with zero-equation turbulence models, which use separate eddy-viscosity models in the different regions. The inner region is to be resolved in a completely analytic manner while the outer region is resolved numerically. The inner region exploits the law of the wall for velocity in conjunction with an associated law of the wake. The law of the wake enables the effects of streamwise pressure gradients to influence the region near the wall. The energy equation is replaced by a modified form of the Crocco temperature-velocity relationship. The outer region is formulated and

7

resolved in terms of the defect stream function. This formulation properly characterizes the outer portion of the boundary layer as it relates the local mean velocity to the velocity at the outer edge of the boundary layer.

As stated earlier, the law of the wall for velocity is probably the most widely accepted empiricism in fluid mechanics. The most common form of this law is known as the logarithmic law of the wall and is valid in the fully turbulent, logarithmic region of the inner part of the boundary layer. Others have devised laws that are valid from the wall through the viscous sublayer and the logarithmic region. One such example for incompressible flow is the law given by Liakopolous[16], which was used in a prior investigation[17,18] by the present author. Far and away the most popular compressible law of the wall is that described as the effective, or generalized, velocity approach of van Driest[19], which effectively relates the velocity in a compressible fluid to a corresponding velocity in an incompressible fluid. The van Driest law is used in the present method and is discussed further in section 2.2.

Law of the wake empiricisms have not been developed or used to the extent as law of the wall empiricisms, particularly for compressible flows. The most popular law of the wake is that presented by Coles[20] for incompressible flow. Moses[21] also gives a commonly used incompressible law of the wake. Several other laws for incompressible flow are given by White in reference 22. McQuaid[23] proposed an incompressible law that used a modified shear-stress velocity as the normalizing variable, such that pressure gradients from the most favorable to separation could be handled with relative ease, while the more common laws of the wake simply use the shear-stress velocity as the normalizing variable. The most popular form of a compressible law of the wake appears to be the incorporation of Coles' law into the van Driest effective velocity approach. Maise and McDonald[24] merely speculated on this extension without a rigorous derivation and found this to be a valid approach. This extension was used in the work of Alber and Coats[25] and

8

further scrutinized by Mathews, Childs, and Paynter[26] also with favorable results. Squire[27] used a compressible flow extension of McQuaid's law and found the law to give questionable results with Mach numbers of 3.6 and above.

It was felt that an additional contribution of the present investigation could be a compressible law of the wake determined directly from compressible flow solutions rather than relying on correlations with a law that is based entirely on incompressible flow data. This has been accomplished and is discussed in detail in the upcoming sections. The precise law of the wake determined here is valid through the inner region and into the inner portion of the outer region. The significant effect of including a law of the wake is the extension of the region of the boundary layer that is described by the analytic expressions beyond the logarithmic region. This provides an additional grid reduction leading to increased computational efficiency. Physically speaking, the law of the wake allows for the influence of the streamwise pressure gradient on the inner region of the boundary layer. The importance of this effect has been discussed by many including McDonald[28], Patel[29], the present author in references 17 and 18, and more recently by Wilcox in reference 15.

A primary feature of the present method is the approach used to patch the inner and outer solutions. Specifically, the location of the patching is not predetermined by the researcher, but rather is determined as part of the computation. This approach has several advantages. First of all, the arbitrary choice of the location of the the patching is eliminated. Secondly, the choice is made as part of the computation in a manner which extends the use of the analytic expressions at each streamwise location. Various means of implementing such an approach are discussed in section 3.3.

The formulation in the outer region is also a key factor with the present technique. A prior investigation by the present author[17,18] formulated the outer region in terms of the conventional stream function; the outer region velocity was nondimensionalized by the velocity at the edge of the boundary layer. The critical implementation feature was the

9

algorithm developed to interact the inner and outer region treatments. Solutions were obtained for incompressible flows over flat plates, and two-dimensional ellipses and circular cylinders. Once pressure gradient effects were included in the inner region treatment, successful computations were made, although a fair amount of numerical difficulty was encountered. The present formulation reduces the numerical difficulty by replacing, when possible, computational steps in the interaction routine with equivalent analytic steps. This process was facilitated by reformulating the outer region in terms of the defect stream function; the outer region is characterized by a velocity deficit, relative to the edge velocity, normalized by the shear-stress velocity.

Much of the outer region analysis to follow is based on previous analyses by Clauser[30,31] and by Mellor and Gibson[32]. Clauser's analysis resulted from a desire to study turbulent boundary layers excluding upstream history effects. The comparison is made to the self-similar laminar solutions of Blasius, and Falkner and Skan, as shown in most fluids textbooks, where the governing equations reduce exactly to ordinary differential equation form, resulting in a solution independent of the streamwise location. The problem for turbulent flows is much more difficult, as not only must the mean velocity profiles be similar, but also the profiles of the turbulence quantities. Clauser observed that experimental tangential velocity profiles for incompressible turbulent boundary layers on a flat plate reduce to a single curve, independent of the Reynolds number, when plotted in terms of the velocity defect normalized by the shear-stress velocity. Several of Clauser's figures from his 1956 paper[31] are reprinted here in figure 2 for the purpose of demonstration. Figure 2a shows several turbulent velocity profiles from flat plate experiments plotted in the conventional velocity ratio format. Figure 2b demonstrates the collapse of the data to a single curve when plotted in the velocity defect format. Clauser further proved that velocity defect profiles of turbulent boundary layers with streamwise pressure gradients are also self-similar if the pressure and skin friction forces are, in his

terminology, in equilibrium. Clauser determined, with much effort, that a pressure gradient parameter normalized by the ratio of the (incompressible) displacement thickness to the shear stress at the wall designates the various families of similar solutions for turbulent boundary layer flow. A similar parameter for compressible flow is determined in the present investigation.

Another of Clauser's contributions was the definition of a highly accurate eddy-viscosity model valid in the outer region. The model is a result of Clauser's observation of the laminar-like behavior of the outer region of the turbulent boundary layer. To demonstrate this similarity, Clauser solved the Blasius equation with various nonzero wall velocities, as shown in figure 2c, and compared to the turbulent profiles shown in figure 2b. The similarity away from the wall, as shown in figure 2d, is remarkable. Clauser determined the proper velocity and length scales to be the edge velocity and the (incompressible) displacement thickness, respectively, and a corresponding constant which completed an outer region eddy-viscosity model that remains constant normal to the surface. These scales were subsequently verified for compressible flow by Maise and McDonald[24] and variations of the model are still widely used today.

Clauser did not derive the governing equations in terms of the defect stream function, but rather used the conventional stream function. Although others studied equilibrium turbulent boundary layers after Clauser, it was not until ten years after Clauser that Mellor and Gibson[32] put forth a clear, accurate derivation of the governing equations in terms of the defect stream function variables. It should be noted that a significant portion of the work described in reference 32 was originally presented four years earlier in Gibson's doctoral dissertation[33]. The work of reference 32 is restricted to the analysis of incompressible, equilibrium turbulent boundary layers. Mellor and Gibson obtained an extremely accurate, approximate solution to the governing equations in the limit of vanishing shear-stress velocity to edge velocity ratio. They also determined a completely

11

analytic solution of the governing equations by using this approximate equation and taking advantage of the first-integral property of the tangential momentum equation. With this solution, they established the extremes of Clauser's pressure gradient parameter from the most favorable pressure gradient to separation. The two major problems with their formulation concerned the enforcement of law of the wall behavior near the wall and the implementation of the wall-layer eddy-viscosity model. Also, the wall boundary condition, which is inversely proportional to the shear-stress velocity to edge velocity ratio (the ratio is a small number), presents numerical difficulties. The computational complexity Mellor and Gibson encountered near the wall probably explains the general lack of popularity of the defect stream function formulation. Even Mellor[34] abandoned this formulation for his analysis of nonequilibrium, incompressible turbulent boundary layers. The present technique completely overcomes the difficulty near the wall by use of analytic expressions in the inner region.

A significant accomplishment of the present investigation is the extension of the defect stream function formulation to nonequilibrium, compressible turbulent boundary layers. The derivation follows in chapter 2. Chapter 3 presents the inner region treatment and discusses its implementation. Finally, chapter 4 discusses the results of the present technique. The equilibrium class of boundary layers has been used extensively over the years in the development and testing of analytic and numerical methods. The process is continued in the current investigation: section 4.1 shows solutions for equilibrium, incompressible flow; and section 4.2 discusses equilibrium, compressible flow solutions. Section 4.3 discusses the initial implementation of the method into an existing Navier-Stokes code and presents results for several cases of compressible flow over a flat plate.

2 DEFECT STREAM FUNCTION FORMULATION

The basic formulation parallels that of Mellor and Gibson[32] for incompressible, equilibrium, turbulent boundary-layer flow. However, the present treatment is for compressible, nonequilibrium, turbulent boundary layers; and the eddy viscosity model for the present treatment is much more general than that of reference 32. In fact, it is unnecessary to specify the eddy viscosity in the inner layer at all.

2.1 Basic Equations

The Reynolds-averaged continuity and tangential momentum equations for compressible turbulent boundary-layer flow in two dimensions are

$$\frac{\partial(\rho u)}{\partial x} + \frac{\partial(\rho v)}{\partial y} = 0$$

$$\rho u \frac{\partial u}{\partial x} + \rho v \frac{\partial u}{\partial y} - \rho_e u_e \frac{du_e}{dx} = \frac{\partial \tau}{\partial y} \tag{2.1}$$

where x and y are the tangential and normal coordinates, u and v are the respective velocity components, ρ is the density, and the subscript 'e' designates values at the edge of the boundary layer. The shear stress τ is

$$\tau = \mu \frac{\partial u}{\partial y} - \rho \overline{u'v'} \tag{2.2}$$

where μ is the molecular viscosity of the fluid and $(-\rho \overline{u'v'})$ is the Reynolds stress term, a direct result of fluctuations inherent to turbulent flow. The Reynolds stress term must be modeled because an exact, analytic form is not known. In the present investigation the Boussinesq[8] eddy viscosity concept is used rather than a more complex stress transport

equation model. The Boussinesq concept imitates the Newtonian assumption that the shear stress is linearly proportional to the mean rate of strain; the Reynolds stress is modeled as

$$-\rho \overline{u'v'} = \mu_t \frac{\partial u}{\partial y} \tag{2.3}$$

where μ_t is the eddy viscosity. The eddy viscosity is proportional to a velocity scale and a length scale; the choice of these scales distinguishes the various eddy viscosity models from one another. The present derivation models the sum of μ and μ_t as

$$\mu + \mu_t = K(x,y)\rho u_e \delta_i^* \tag{2.4}$$

where K is a general nondimensional function of x and y and δ_i^* is the incompressible displacement thickness. The incompressible displacement thickness δ_i^* is sometimes referred to as the velocity thickness[35] and is defined as

$$\delta_i^* = \int_0^\infty (1 - \frac{u}{u_e}) \, dy$$

This model (equation (2.4)) is of the form proposed by Clauser[31] for the outer region of incompressible turbulent boundary layers. The generality of the present form is achieved by the use of the arbitrary function K(x,y), which allows this model to duplicate other existing turbulence models without affecting the present derivation. Although the function K(x,y) can have separate definitions in the inner and outer regions of the boundary layer, only an outer region definition is required with the present technique. The present solutions were computed assuming K(x,y) = k in the interest of simplicity, where k is the Clauser constant.

The energy equation is accounted for by use of the modified Crocco temperature-velocity relationship. The basic relationship was derived by Crocco[36] with following

14

assumptions: steady flow of a perfect gas, Prandtl number (Pr) of one, which implies a perfect balance of viscous dissipation and heat conduction, streamwise pressure gradient of zero, and a constant value of the specific heat coefficient c_p. The basic relationship is

$$T = T_w + (T_{aw} - T_w)\frac{u}{u_e} - \frac{u^2}{2c_p}$$

where T_w is the wall temperature and T_{aw} is the adiabatic wall temperature. Baronti and Libby[37] have made a detailed investigation of the accuracy of the Crocco relation for adiabatic flows and state that they found deviations of less than plus or minus four percent in the static temperature ratios obtained throughout the boundary layer. Gran, Lewis, and Kubota[38] have compared this relation to nonadiabatic experimental cases and found no significant deviation. White[22] shows a modification to this equation in which a recovery factor is introduced as follows:

$$T = T_w + (T_{aw} - T_w)\frac{u}{u_e} - \frac{ru^2}{2c_p}$$

where r is the recovery factor and is defined as $r=Pr^{1/3}$ for turbulent flow ($r=Pr^{1/2}$ for laminar flow). This equation has proven to be a very good approximation[22] of the energy equation even beyond the bounds of the strict assumptions.

Adiabatic wall conditions are assumed in the present study; the modified Crocco temperature-velocity relationship for adiabatic walls is

$$\frac{T_w}{T} = \frac{\rho}{\rho_w} = 1 + r\frac{(\gamma-1)}{2}(\frac{u}{a})^2 = 1 + r\frac{(\gamma-1)}{2}M^2 \tag{2.5}$$

where $\bar{\gamma}$ is the ratio of specific heats (taken to be 1.4), a is the speed of sound, and M is the Mach number. The Prandtl number is assumed to be 0.72 in this study. The simplicity and effectiveness of this relationship avoids the use of the differential energy equation and the corresponding need for temperature laws of the wall and wake.

In this treatment, the defect stream function of Clauser[30,31] is modified to account for compressibility. The defect stream function $f(\xi,\eta(x,y))$ of this formulation is defined such that

$$\frac{\partial f}{\partial \eta} = f'(\xi,\eta) = \frac{u-u_e}{u^*} \tag{2.6}$$

where the transformed coordinates are

$$\xi = x \quad \text{and} \quad \eta = \frac{1}{\Delta} \int^y \frac{\rho}{\rho_e} \, dy$$

The coordinate transformation incorporates a density weighting integral similar to that originally proposed by Mager[39]. This particular transformation of the normal coordinate was chosen because it reduces to the form used by Clauser, and then Mellor and Gibson, for incompressible flow. The shear-stress velocity u^* is defined as

$$u^* = \sqrt{\frac{\tau_w}{\rho_w}}$$

where ρ_w and τ_w are the density and shear stress at the wall. The compressibility transformation yields the density-weighted velocity thickness δ_v^*, which appears throughout the derivation and is defined as

$$\delta_v^* = \int_0^\infty \frac{\rho}{\rho_e} \left(1 - \frac{u}{u_e}\right) dy$$

The boundary layer defect thickness parameter Δ is defined as

16

$$\Delta = -\int_0^\infty \frac{\rho}{\rho_e} \frac{\partial f}{\partial \eta} dy = \frac{u_e}{u^*} \int_0^\infty \frac{\rho}{\rho_e} (1 - \frac{u}{u_e}) dy = \frac{u_e \delta_v^*}{u^*}$$

or

$$\Delta u^* = u_e \delta_v^*$$

Partial derivatives with respect to x and y are of the form

$$\frac{\partial}{\partial x} = \frac{\partial}{\partial \xi} + \frac{\partial \eta}{\partial x} \frac{\partial}{\partial \eta} \quad \text{and} \quad \frac{\partial}{\partial y} = \frac{\rho}{\Delta \rho_e} \frac{\partial}{\partial \eta}$$

2.2 Law of the Wall and Wake

It is assumed that a law of the wall and wake for velocity in the inner part of the boundary layer is known. This law is of the form

$$\frac{u}{u^*} = g(y^+, M_e) + h(\beta, \bar{\eta}, M_e) \tag{2.7}$$

where g is the law of the wall and h is the law of the wake. The inner variable y^+ is defined as

$$y^+ = \frac{u^* y}{\nu_w} = \frac{Re_{\delta^*}}{\omega} \bar{\eta}$$

where ω and $\bar{\eta}$ are defined as

$$\omega = \frac{\delta_i^*}{\delta_v^*} \quad \text{and} \quad \bar{\eta} = \frac{y}{\Delta}$$

and the Reynolds number based on the edge velocity, the incompressible displacement thickness, and kinematic viscosity at the wall is defined as

$$Re_{\delta^*} = \frac{u_e \delta_i^*}{\nu_w} = \frac{u^* \Delta}{\nu_w} \omega$$

17

The compressible pressure gradient parameter, which reduces to Clauser's pressure gradient parameter for incompressible flow, is defined as

$$\beta = \frac{\delta_v^*}{\tau_w}\frac{dp}{dx}$$

where p is the pressure. A modified form of the parameter β will be defined later and shown to be the compressible equilibrium parameter. For nonequilibrium flow, this new parameter is a function of x and hence ξ; for equilibrium flow, this parameter is constant.

In the present treatment, van Driest's[19] effective velocity (or generalized velocity) approach, as simplified for adiabatic flows and modified by the recovery factor, is used for the law of the wall:

$$g(y^+,M_e) = \sqrt{\frac{2}{r(\bar{\gamma}-1)}} \left(\frac{a_{aw}}{u^*}\right) \sin\left\{ \sqrt{\frac{r(\bar{\gamma}-1)}{2}} \left(\frac{u^*}{a_{aw}}\right) \left(\frac{1}{\kappa}\ln y^+ + B\right) \right\} \qquad (2.8)$$

where a_{aw} is the adiabatic wall speed of sound and κ and B are the law of the wall constants. Van Driest's derivation parallels Prandtl's[40] derivation for incompressible flow. The assumptions used are that the shear stress in the fluid is constant and approximately equal to the shear stress at the wall and the mixing length is linearly proportional to the distance from the wall. Van Driest incorporated a variable density into the derivation in the form of the Crocco relationship. Again, equation (2.8) has been simplified for flows with adiabatic wall conditions. Because the ratio (u^*/a_{aw}) is generally small, the law of the wall is often used as

$$g(y^+,M_e) = \frac{1}{\kappa}\ln y^+ + B + O[(\frac{u^*}{a_{aw}})^2]$$

Neither of these expressions is valid in the laminar sublayer.

Law of the wake empiricisms have not been developed and used to the extent that law of the wall empiricisms have, particularly for compressible flow. It is widely accepted that the leading term of the incompressible law of the wake is proportional to y^2. There is, however, disagreement over the order of the second term[22]. Moses[21], for example, uses a second term proportional to y^3 while Coles'[20] second term is proportional to y^4. If the law of the wake needs to be valid from the wall through the inner part of the outer region of the boundary layer only, a single term proportional to y^2 is sufficient to define the wake function. In the present compressible treatment, a functional form proportional to y^2 for the law of the wake is assumed and is modeled after the leading term of the Moses incompressible law of the wake. The present law of the wake for compressible flow is

$$h(\beta,\bar{\eta},M_e) = \frac{6}{\kappa} w\, \bar{\eta}^2 \tag{2.9}$$

where $w = w(\beta,M_e)$ is a coefficient determined as part of the computation. The procedure for determining this coefficient is discussed later, and an analytic expression is given as a result of the present computations.

2.3 Shear-Stress Velocity Ratio

The nondimensional shear-stress velocity is defined as

$$\gamma = \frac{u^*}{u_e}$$

In the present treatment, the ratio γ is evaluated with the laws of the wall and wake. From equations (2.6) and (2.7) it is seen that the velocity u at the match point η_m between the inner and outer regions of the boundary layer can be expressed as

$$u_m = u^*[\, g(y_m^+) + h(\bar{\eta}_m)\,] = u_e + u^* f'\,(\xi,\eta_m) \tag{2.10}$$

The equation for γ is obtained from equation (2.10) as

$$\gamma = \frac{1}{[\ g_m + h_m - f'_m\ ]} \tag{2.11}$$

In the analysis that follows an expression for the gradient of γ with respect to ξ is needed. Differentiation of the above expression yields

$$\dot{\gamma} = -\gamma^2\ [\ \dot{g}_m + \dot{h}_m - \dot{f}'_m\ ] \tag{2.12}$$

where

$$(\dot{\ }) = \frac{d}{d\xi}$$

The derivative of the law of the wall (equation (2.8)) with respect to ξ is

$$\dot{g} = \frac{1}{\kappa}[\ \frac{\dot{\gamma}}{\gamma} + \frac{\dot{u}_e}{u_e} + \frac{\dot{\Delta}}{\Delta} - \frac{\dot{v}_w}{v_w}] + O[(\frac{u^*}{a_{aw}})^2] \tag{2.13}$$

Substitution of equation (2.13) into (2.12) yields

$$\frac{u_e\ \dot{\gamma}}{\dot{u}_e\ \gamma} = \frac{-(\frac{\gamma}{\kappa})}{(1\ +\ \frac{\gamma}{\kappa})}\ [\ 1 + \frac{u_e}{\dot{u}_e}(\frac{\dot{\Delta}}{\Delta} - \frac{\dot{v}_w}{v_w})\ ] + \frac{\rho_e}{\rho_w}\frac{\Delta}{\beta}\frac{(\dot{h}_m - \dot{f}'_m)}{(1\ +\ \frac{\gamma}{\kappa})}$$

This term was neglected by Clauser[31] but was found to be important and included by Mellor and Gibson[32] in their incompressible analysis. The present compressible analysis will also require the following relationships:

$$\frac{\dot{\rho}_e}{\rho_e} = -M_e^2\ \frac{\dot{u}_e}{u_e}$$

$$\frac{\dot{v}_w}{v_w} = \frac{\dot{\mu}_w}{\mu_w} - \frac{\dot{\rho}_w}{\rho_w}$$

$$\frac{\dot{\mu}_w}{\mu_w} = \left[\frac{1 + 3\frac{\bar{s}}{T_w}}{2(1 + \frac{\bar{s}}{T_w})} \right] \left[2(1 - \frac{\rho_w}{\rho_e})\frac{(r-1)}{r} \right] \frac{\dot{u}_e}{u_e}$$

$$\frac{\dot{\rho}_w}{\rho_w} = -\left[M_e^2 + 2(1 - \frac{\rho_w}{\rho_e})(1 + \frac{\frac{\rho_e}{\rho_w} - 1}{r}) \right] \frac{\dot{u}_e}{u_e}$$

These relationships are derived from the perfect gas equation of state, the modified Crocco relation for adiabatic wall conditions (equation(2.5)), and Sutherland's viscosity law[22] where $\bar{s} = 199°R$. Note that the term $\frac{u_e}{\dot{u}_e}\frac{\dot{v}_w}{v_w}$ is a known function of M_e.

2.4   Governing Equations

Now one equation for the defect stream function f can be written. The gradients of u with respect to x and y are

$$\frac{\partial u}{\partial x} = \frac{du_e}{dx}(1 + \gamma f') + u_e \frac{\partial}{\partial x}(\gamma f') + u_e \gamma f'' \frac{\partial \eta}{\partial x}$$

$$\frac{\partial u}{\partial y} = \frac{\rho u_e \gamma f''}{\rho_e \Delta}$$

respectively. From the definition of the stream function

$$\rho u = \frac{\partial \Psi}{\partial y} \quad \text{and} \quad -\rho v = \frac{\partial \Psi}{\partial x}$$

it can be shown that

$$\Psi = \rho_e u_e \Delta (\eta + \gamma f)$$

and the flux ρv is obtained as

$$-\rho v = \frac{d}{dx}(\rho_e u_e \Delta)\,(\eta + \gamma f) + \rho_e u_e \Delta \frac{\partial}{\partial x}(\gamma f) + \rho_e u_e \Delta\,(1 + \gamma f')\frac{\partial \eta}{\partial x} \tag{2.14}$$

In the defect stream function formulation, the tangential momentum equation, equation (2.1), is

$$
\frac{\omega}{\beta}\frac{\rho_e}{\rho_w}\Big[K\,\Big(\frac{\rho}{\rho_e}\Big)^2 f''\Big]' + \frac{\rho_e}{\rho_w}(2f' + \gamma f'^2) - (1 + \frac{u_e}{\dot u_e}\frac{\dot\Delta}{\Delta})\Big[(\eta + \gamma f)f''
$$

$$
+ \frac{(\frac{\gamma}{\kappa})}{(1 + \frac{\gamma}{\kappa})}(f' + \gamma f'^2 - \gamma f f'')\Big] + M_e^2(\eta + \gamma f)f'' + \frac{(\frac{\gamma}{\kappa})}{(1 + \frac{\gamma}{\kappa})}\frac{u_e}{\dot u_e}\frac{\dot v_w}{v_w}(f' + \gamma f'^2 - \gamma f f'')
$$

$$
+ \frac{(\frac{\gamma}{\beta})}{(1 + \frac{\gamma}{\kappa})}\frac{\rho_e}{\rho_w}\Big(\frac{dh_m}{ds} - \frac{df'_m}{ds}\Big)(f' + \gamma f'^2 - \gamma f f'') \tag{2.15}
$$

$$
= \frac{\rho_e}{\rho_w}\frac{1}{\beta}\Big[\frac{\partial f'}{\partial s} + \gamma f'\frac{\partial f'}{\partial s} - \gamma f''\frac{\partial f}{\partial s}\Big]
$$

where s is the nondimensional tangential coordinate defined as

$$s = \int^{\xi} \frac{\gamma}{\Delta}\,d\xi$$

2.5 Boundary Conditions

There are two surface boundary conditions and one far-field boundary condition. From equation (2.14) for the flux ρv, the normal flow boundary condition at the surface, $v = 0$ at $\eta = 0$, is observed to correspond to

$$f(s,0) = 0$$

The far-field boundary condition is obtained from the definition of the boundary-layer defect thickness Δ:

$$\Delta = - \int_0^\infty \frac{\rho}{\rho_e} \frac{\partial f}{\partial \eta} dy = -\Delta \int_0^\infty \frac{\partial f}{\partial \eta} d\eta = \Delta \ (f(s,0) - f_\infty(s))$$

It follows that

$$f_\infty \ (s) = -1 \tag{2.16}$$

This boundary condition requires that u approach u_e as y approaches infinity. The final boundary condition involves the shear stress at the wall. The shear-stress boundary condition is

$$\tau_w = \lim_{y \to 0} (\mu + \mu_t) \frac{\partial u}{\partial y}$$

This boundary condition can be written as

$$\rho_w u^{*2} = \lim_{\eta \to 0} \frac{K(\xi,\eta)\rho^2 u_e^2 \delta_i^* \gamma f''}{\rho_e \Delta}$$

or

$$\lim_{\eta \to 0} K(\xi,\eta) \left(\frac{\rho}{\rho_e}\right)^2 f'' = \frac{1}{\omega} \frac{\rho_w}{\rho_e} \tag{2.17}$$

This boundary condition replaces the usual no-slip boundary condition at the surface $(u(s,0)=0)$ and states simply that the shear stress must approach the wall shear stress as y approaches zero.

It should be noted that these boundary conditions reduce to those used by Mellor and Gibson[32] for incompressible flow.

23

2.6 First Integral of Governing Equation

It is always desired to reduce the governing equations to their simplest form analytically before turning to numerical analysis. The advantage of such an analytic integration is twofold: the order of the equation to be solved numerically can be reduced, and boundary conditions can be absorbed and not imposed numerically. The defect stream function governing equation has a first integral, and one boundary condition is absorbed analytically. As will be seen, however, a limited advantage is gained for the full equation. It is only upon making the zero-order approximation in the limit of vanishing shear-stress velocity ratio that the full advantage is gained.

Equation (2.15) can be written as

$$
\begin{aligned}
&\left[\frac{\omega}{\beta} \frac{\rho_e}{\rho_w} K \left(\frac{\rho}{\rho_e}\right)^2 f'' \right. \\
&+ 2 \frac{\rho_e}{\rho_w} f - \left(1 + \frac{u_e}{\dot{u}_e} \frac{\dot{\Delta}}{\Delta}\right) \left\{ \eta f' - \frac{(1-\gamma f')f}{(1 + \frac{\gamma}{\kappa})} \right\} + \frac{(\frac{\gamma}{\beta})}{(1 + \frac{\gamma}{\kappa})} \frac{\rho_e}{\rho_w} \left(\frac{dh_m}{ds} - \frac{df'_m}{ds}\right) (1-\gamma f')f \\
&+ M_e^2 \eta f' - \frac{(1-\gamma f')f}{(1 + \frac{\gamma}{\kappa})} \left(M_e^2 + \frac{\gamma}{\kappa} \{M_e^2 - \frac{u_e}{\dot{u}_e} \frac{\dot{v}_w}{v_w}\}\right) - \frac{\rho_e}{\rho_w} \frac{1}{\beta} \frac{\partial f}{\partial s} + \frac{\rho_e}{\rho_w} \frac{\gamma}{\beta} f' \frac{\partial f}{\partial s} \right]' \\
&= \frac{-\gamma f'^2}{(1 + \frac{\gamma}{\kappa})} \left[(1 + \frac{u_e}{\dot{u}_e} \frac{\dot{\Delta}}{\Delta}) - M_e^2 + \frac{\rho_e}{\rho_w} \frac{\gamma}{\kappa} ((1 + \frac{u_e}{\dot{u}_e} \frac{\dot{\Delta}}{\Delta}) \right. \\
&\left. + M_e^2 - 2 \frac{u_e}{\dot{u}_e} \frac{\dot{v}_w}{v_w} - \frac{\rho_e}{\rho_w}) + 2 \frac{\gamma}{\beta} \frac{\rho_e}{\rho_w} \left(\frac{dh_m}{ds} - \frac{df'_m}{ds}\right) \right] + \frac{\rho_e}{\rho_w} \frac{\gamma}{\beta} \frac{\partial f'^2}{\partial s}
\end{aligned}
$$

Using the boundary condition given in equation (2.17), the above equation can be integrated across the boundary layer to evaluate the quantity $1 + \frac{u_e}{\dot{u}_e} \frac{\dot{\Delta}}{\Delta}$. This value is

$$1 + \frac{u_e}{\dot{u}_e}\frac{\dot{\Delta}}{\Delta} = -\left[\left(1+\frac{\gamma}{\kappa}\right)\left(\frac{1}{\beta}+\frac{\rho_e}{\rho_w}\{2-\gamma G\}\right) - M_e^2\{1-\gamma G\} - \frac{\left(\frac{\gamma}{\kappa}\right)}{\left(1+\frac{\gamma}{\kappa}\right)}\frac{u_e}{\dot{u}_e}\frac{\dot{v}_w}{v_w}(2\gamma G - 1)\right.$$

$$\left.+\frac{\rho_e}{\rho_w}\frac{\gamma}{\beta}\frac{dG}{ds}\right) + \frac{\gamma}{\beta}\frac{\rho_e}{\rho_w}\left(\frac{dh_m}{ds}-\frac{df'_m}{ds}\right)(1-2\gamma G)\right]\left[1-\gamma G\left(1-\frac{\gamma}{\kappa}\right)\right]^{-1} \qquad (2.18)$$

$$= 1 + \frac{1}{m(s)}$$

where the defect shape factor G is defined as

$$G = \int_0^\infty f'^{\,2}\,d\eta$$

It is necessary to incorporate a Mach number scaling effect into the coordinates in order to determine the conditions for compressible equilibrium flow. The following transformation allows for this effect:

$$\hat{s} = \int_0^s \frac{\rho_w}{\rho_e}\,ds \qquad \text{and} \qquad \hat{\eta} = \sqrt{\frac{\rho_w}{\rho_e}}\,\eta \qquad (2.19)$$

Applying this transformation and integrating across the boundary layer, the first integral of the governing equation for arbitrary $\hat{\eta}$ is

$$(1-\hat{\gamma f'})\frac{\partial f}{\partial \hat{s}} = \omega\left(\frac{\rho}{\rho_e}\right)^2 Kf'' - \beta\left(1+\frac{1}{m}-M_e^2\right)\left(\hat{\eta}f' - \frac{(1-\hat{\gamma f'})f}{\left(1+\frac{\gamma}{\kappa}\right)}\right)$$

$$- \frac{\left(\frac{\gamma}{\kappa}\right)}{\left(1+\frac{\gamma}{\kappa}\right)}\beta(1-\hat{\gamma f'})f\left(M_e^2-\frac{u_e}{\dot{u}_e}\frac{\dot{v}_w}{v_w}\right) + 2\beta\frac{\rho_e}{\rho_w}f - 1 + \frac{\hat{\gamma}}{\left(1+\frac{\gamma}{\kappa}\right)}\left[\beta\left(1+\frac{1}{m}-M_e^2+\frac{\rho_e}{\rho_w}\right)\left(1-\frac{\gamma}{\kappa}\right)\right.$$

$$\left. - 2\frac{\gamma}{\kappa}\beta\left(M_e^2-\frac{u_e}{\dot{u}_e}\frac{\dot{v}_w}{v_w}-\frac{\rho_e}{\rho_w}\right)+2\gamma\left(\frac{dh_m}{d\hat{s}}-\sqrt{\frac{\rho_w}{\rho_e}}\frac{df'_m}{d\hat{s}}\right)\right]\int_0^{\hat{\eta}} f'^{\,2}\,d\hat{\eta} \qquad (2.20)$$

25

$$-\frac{\rho_e}{\rho_w}\frac{\beta}{r}(1-\frac{\rho_w}{\rho_e})(1-(1-r)\frac{\rho_w}{\rho_e})[\hat{\eta}f' + \hat{\gamma}\int_0^{\hat{\eta}} f'^2\,d\hat{\eta})] - \hat{\gamma}\frac{\partial}{\partial\hat{s}}\int_0^{\hat{\eta}} f'^2\,d\hat{\eta}$$

$$+\frac{\gamma}{(1+\frac{\gamma}{\kappa})}(\frac{dh_m}{d\hat{s}} - \sqrt{\frac{\rho_w}{\rho_e}}\frac{df'_m}{d\hat{s}})(1-\hat{\gamma}f')\,f$$

where the prime denotes partial differentiation with respect to $\hat{\eta}$. The term $(1+\frac{1}{m})$ is defined in equation (2.18), and the parameter $\hat{\gamma}$ is defined as

$$\hat{\gamma} = \sqrt{\frac{\rho_w}{\rho_e}}\,\gamma$$

Note that for the adiabatic wall conditions of this investigation, the density ratio (ρ_w/ρ_e) has values between zero and one, which assures that $\hat{\gamma}$ is less than or equal to γ. Expressions for the ratios ω and (ρ_e/ρ) can also be written in defect stream function form:

$$\omega = \frac{\delta_i^*}{\delta_v^*} = 1 + \varepsilon\,[\int_0^\infty f'^2\,(1+\frac{\gamma}{2}\sqrt{\frac{\rho_w}{\rho_e}}\,f')\,d\hat{\eta}]$$

$$\frac{\rho_e}{\rho} = 1 + r\frac{(\gamma-1)}{2}M_e^2\,[1-(\frac{u}{u_e})^2] = 1 - \varepsilon f'\,[1+\frac{\gamma}{2}\sqrt{\frac{\rho_w}{\rho_e}}\,f']$$

where

$$\varepsilon = 2\gamma\sqrt{\frac{\rho_e}{\rho_w}}(1-\frac{\rho_w}{\rho_e})$$

For edge Mach numbers from incompressible to supersonic this parameter is small so that the ratios (δ_i^*/δ_v^*) and (ρ_e/ρ) are approximately one. However, because ε has the limiting form

$$\lim_{M_e \to \infty} \varepsilon = 2 \sqrt{\frac{r(\bar{\gamma}-1)}{2}} \ \gamma M_e$$

it is not small for large values of the edge Mach number. The term ε is similar to Coles'[41] parameter $c_f M_\infty^2$ which remains finite for large Mach numbers. The skin friction coefficient c_f is equal to $(2\tau_w/\rho_\infty u_\infty^2)$.

It is apparent that the analytic integration shown in equation (2.20) provides an advantage over equation (2.15), the equation before integration. The governing equation, which is now in the form of an integro-differential equation, has been reduced to second order (leading derivative of f") and one boundary condition (equation (2.17)) has been absorbed analytically. The integral terms in equation (2.20) are of higher order, and are evaluated easily when solving this equation. The full advantage of the first integral equation is seen in the next section where the zero-order approximation is made.

2.7 Zero-Order Approximation

As mentioned previously, the shear-stress velocity ratio γ is generally small. As a result, the dependent variable of the defect stream function formulation f can be expanded in terms of the shear-stress velocity ratio. Mellor and Gibson[32] used this expansion in their incompressible analyses to obtain a zero-order, asymptotic form of the governing equations with respect to the shear-stress velocity ratio. The expansion of f is

$$f = f_0 + \gamma f_1 + \gamma^2 f_2 + \dots.$$

Asymptotic forms are obtained for equations (2.18) and (2.20). For hypersonic flow, these asymptotic forms are not the strict zero-order forms because the term ε appears in both ω and (ρ_e/ρ) and is not negligible. The constrained zero-order forms of equations (2.18) and (2.20) are

$$1 + \frac{u_e}{\dot{u}_e}\frac{\dot{\Delta}}{\Delta} = -\left(\frac{1}{\beta} + 2\frac{\rho_e}{\rho_w} - M_e^2\right)$$

$$\frac{\partial f_0}{\partial \hat{s}} = \omega\left(\frac{\rho}{\rho_e}\right)^2 K f_0'' + (1+2\hat{\beta})\,\hat{\eta}f_0' - f_0 - 1 \tag{2.21}$$

where the pressure gradient parameter $\hat{\beta}$ is defined as

$$\hat{\beta} = \frac{\rho_e}{\rho_w}\beta\left[1 - \frac{(1-\frac{\rho_w}{\rho_e})}{2r}(1-\frac{\rho_w}{\rho_e}(1-r))\right]$$

Note that equation (2.21) is linear from incompressible to supersonic flow because ω and (ρ_e/ρ) are approximately one. An additional transformation is necessary to obtain a governing equation which is linear in the hypersonic range. This transformation is described in reference 42 and shown in Appendix A.

The full advantage of analytically integrating the governing equation is now apparent. The terms in equation (2.20) are either simplified or eliminated when making the zero-order approximation; the integral terms of equation (2.20) are considered to be small and are neglected. The result is simply a second order differential equation and one boundary condition has been absorbed analytically.

2.8 Equilibrium Flow Approximation

The equilibrium condition, as defined by Mellor and Gibson[32], occurs mathematically when the profile of f, and hence u, depend only on the nondimensional normal coordinate and not on the streamwise coordinate. These authors noted that the streamwise partial derivatives are zero when the coefficients of the governing equation are independent of the streamwise coordinate, and they showed that this condition can be met exactly for the zero-order incompressible equation and approximately when higher order terms are included. This same situation pertains for compressible flow. If K does not

depend on $\hat{s}$, $\hat{\beta}$ is constant, and both ω and (ρ_e/ρ) are approximately one, the coefficients of equation (2.21) are independent of $\hat{s}$ and, since the boundary conditions are also independent of $\hat{s}$, the derivative on the left side of equation (2.21) is zero. The more complicated coefficients of equation (2.20) depend weakly on $\hat{s}$.

The equilibrium form of the full equation (equation(2.20)) is

$$
\omega\left(\frac{\rho}{\rho_e}\right)^2 Kf'' - \beta\left(1 + \frac{1}{m} - M_e^2\right)\left(\hat{\eta}f' - \frac{(1-\hat{\gamma}f')f}{(1+\frac{\gamma}{\kappa})}\right) - \frac{(\frac{\gamma}{\kappa})}{(1+\frac{\gamma}{\kappa})}\beta(1-\hat{\gamma}f')\,f\left(M_e^2 - \frac{u_e}{\dot{u}_e}\frac{\dot{v}_w}{v_w}\right)
$$

$$
+ 2\beta\frac{\rho_e}{\rho_w}f - 1 + \frac{\hat{\gamma}}{(1+\frac{\gamma}{\kappa})}\left[\beta\left(1+\frac{1}{m} - M_e^2 + \frac{\rho_e}{\rho_w}\right)\left(1-\frac{\gamma}{\kappa}\right) - 2\frac{\gamma}{\kappa}\beta\left(M_e^2 - \frac{u_e}{\dot{u}_e}\frac{\dot{v}_w}{v_w} - \frac{\rho_e}{\rho_w}\right)\right]\int_0^{\hat{\eta}}f'^2\,d\hat{\eta}
$$

$$
- \frac{\rho_e}{\rho_w}\frac{\beta}{r}\left(1-\frac{\rho_w}{\rho_e}\right)\left(1-(1-r)\frac{\rho_w}{\rho_e}\right)\left[\hat{\eta}f' + \hat{\gamma}\int_0^{\hat{\eta}}f'^2\,d\hat{\eta}\right] = 0 \tag{2.22}
$$

The equilibrium form of the constrained zero-order equation (equation (2.21)) is

$$
\omega\left(\frac{\rho}{\rho_e}\right)^2 Kf_0'' + (1+2\hat{\beta})\,\hat{\eta}f_0' - f_0 - 1 = 0 \tag{2.23}
$$

It will be shown that numerical solutions to the nonlinear, equilibrium equation (equation (2.22)) and solutions to the approximately linear form of equation (2.23) are virtually identical. Each of these equilibrium equations is an ordinary differential equation.

Mellor and Gibson[32] have shown that the zero-order incompressible equation is in the form of a confluent hypergeometric equation, which has an analytic solution[43]. They showed equilibrium solutions to exist from $\beta = -0.5$, the most favorable pressure gradient case, to $\beta = \infty$, the incipient separation case. The corresponding compressible analysis is

presented in reference 42, and the analytic solution for compressible flow is given in Appendix A.

3 Inner Region Treatment

It is this treatment which most distinguishes the present method of solution from previous methods. In effect, the treatment replaces the inner region numerical computations with an empirical representation. The inner region generally encompasses the inner-most twenty percent of the boundary layer and can extend beyond the logarithmic region of the boundary layer. It can also be thought of as the region where an inner eddy-viscosity model is used in the zero-equation eddy-viscosity approach. The need for an eddy-viscosity model in this region is completely eliminated. The empirical representation is in the form of the law of the wall and the law of the wake for velocity as defined in equation (2.7) and the modified Crocco relation for the temperature as defined in equation (2.5). The laws of the wall and wake need only be valid in the inner region for the present method; the Crocco relation is used across the entire boundary layer. The outer region of the boundary layer is where the outer eddy-viscosity model pertains.

In general, there is one point, the "match point," where both the laws of the wall and wake and the outer eddy-viscosity model are correct. The present treatment assures that the derivatives of the defect stream function through f'' are continuous at this point. The term "match point" should not be construed to mean that the inner and outer solutions are being matched in the formal sense. Actually, these solutions are being patched at one point. As discussed in references 17 and 18, this procedure is completely analogous to patching the inner and outer eddy viscosity models in the zero-equation modeling approach.

It should be noted that the inclusion of the law of the wake in the inner layer model means that the match point is not confined to the logarithmic part of the boundary layer.

Several key points must be addressed when deriving and implementing this inner region treatment. First of all, an equation relating the velocity, as represented by f', and its integral, represented by f, through the inner region must be available to insure a continuous solution across the match point. Secondly, an equation which allows the determination of

31

the match point as part of the computation must be determined. Finally, a procedure must be developed which allows the implementation of the patching of the inner empirical and outer numerical solutions in an efficient manner. These points will now be addressed.

3.1   Equation relating f and f'

An equation can be established which relates f and f' throughout the inner region of the boundary layer. This equation follows from the definitions of f and the laws of the wall and wake:

$$f = \int_0^\eta \frac{\partial f}{\partial \eta} \, d\eta = \eta \frac{\partial f}{\partial \eta} - \int_0^{\bar\eta} \eta \left(\frac{\partial g}{\partial \bar\eta} + \frac{\partial h}{\partial \bar\eta}\right) d\bar\eta$$

A relationship between the η and $\bar\eta$ is needed to form the final inner region relationship between f and f'. Such a relationship is

$$\frac{\eta}{\bar\eta} = \frac{\rho_w}{\rho_e} \left\{ 1 + \frac{1}{\cos^2\theta}\left[\sin^2\theta - 2\chi(\tan\theta - \frac{3\chi}{\cos^2\theta} + 2\chi)\right] + O\left[\left(\frac{u^*}{a_{aw}}\right)^4\right] \right\} \tag{3.1}$$

where the terms θ and χ result from the modified van Driest law of the wall (equation (2.8)) and are defined as

$$\chi = \frac{\gamma}{\kappa}\sqrt{1 - \frac{\rho_w}{\rho_e}} \quad \text{and} \quad \theta = \chi\kappa\left(\frac{1}{\kappa}\ln y^+ + B\right)$$

Note that the term $\chi\kappa$ is no larger than the shear-stress velocity ratio γ and the term θ is typically small, which enables use of the small angle approximation in equation (3.1). The relationship between f and f' is written as

$$f = \eta\left(\frac{\partial f}{\partial \eta} - \frac{\cos\theta}{\kappa}\left\{\frac{\cos^2\theta - 3\chi\sin\theta\,\cos\theta + 12\chi^2 - 7\chi^2\cos^2\theta}{\cos^2\theta - 2\chi\sin\theta\,\cos\theta + 6\chi^2 - 4\chi^2\cos^2\theta}\right\}\right) - \int_0^{\bar{\eta}}\eta\frac{\partial h}{\partial\bar{\eta}}d\bar{\eta}$$

$$+ O\left[\left(\frac{u^*}{a_{aw}}\right)^4\right]$$

The lowest order approximate relationship between f and f' is written as

$$f = \eta\left(\frac{\partial f}{\partial\eta} - \frac{1}{\kappa}\right) - \int_0^{\bar{\eta}}\eta\frac{\partial h}{\partial\bar{\eta}}d\bar{\eta} + O\left[\left(\frac{u^*}{a_{aw}}\right)^2\right] \qquad (3.2)$$

This equation pertains throughout the inner region, where the empirical law of the wall and wake is valid. Note that because h is proportional to $\bar{\eta}^2$, the integral term is proportional to $\bar{\eta}^3$; the integral term is small throughout the inner region because $\bar{\eta}_m$ is small. The use of this equation at the match point insures the continuity of f and f'. The match point is positioned so that the derivative f" is continuous. The transformation given in equation (2.19) is easily applied to the equations of this section.

3.2   Match Point Location

The match point location is determined using the equilibrium form of equation (2.20), which is the first integral of the tangential momentum equation as given in equation (2.22), and equations (2.7) and (2.8) for the law of the wall and wake, which are used to evaluate the f" term in equation (2.20). The equilibrium flow assumption can be used because the derivatives with respect to $\hat{s}$ in equation (2.20) are small in the inner region where the match point is located. Equation (3.2) is used to relate f and f'. Equation (2.22) is evaluated at the match point and, with some manipulation, the constrained zero-order form of the governing equation is

$$K\omega\frac{\rho_m}{\rho_w}\left\{\frac{1}{\kappa\bar{\eta}_m}+\left(\frac{\partial h}{\partial\bar{\eta}}\right)_m\right\}+(1+2\hat{\beta})\hat{\eta}_m\left(\frac{\partial f}{\partial\hat{\eta}}\right)_m-f_m-1=0 \tag{3.3}$$

Using the transformation given in equation (2.19) and equation (3.1), the lowest order relation between $\hat{\eta}$ and $\bar{\eta}$ is

$$\hat{\eta}=\bar{\eta}\left(\frac{\rho_w}{\rho_e}\right)^{3/2}$$

Because the law of the wake in equation (2.9) is of order $\bar{\eta}^2$ near the wall, the integral term in equation (3.2) is of order $\bar{\eta}^3$ and can be neglected as $\bar{\eta}_m$ is small. If equation (3.2) is substituted into equation (3.3), the equation for the match point location is

$$A\bar{\eta}_m^2-\bar{\eta}_m+\frac{K}{\kappa}\omega\frac{\rho_m}{\rho_w}=0 \tag{3.4}$$

where the constrained zero-order form of the term A is

$$A=\left(\frac{\rho_w}{\rho_e}\right)^{3/2}\left\{\frac{1}{\kappa}\sqrt{\frac{\rho_e}{\rho_w}}+2\hat{\beta}\left(\frac{\partial f}{\partial\hat{\eta}}\right)_m\right\}+\frac{12w}{\kappa}K\omega\frac{\rho_m}{\rho_w} \tag{3.5}$$

It is in equation (3.4) that the law of the wake plays its most significant role in the analysis and, from equation (3.5), it is the leading coefficient of the law of the wake which is truly significant. The solution for $\bar{\eta}_m$ is easily determined from equation (3.4) as

$$\bar{\eta}_m=\frac{1-\sqrt{1-4A\frac{K}{\kappa}\omega\frac{\rho_m}{\rho_w}}}{2A} \tag{3.6}$$

3.3 Implementation of Inner Region Treatment

There are several methods with which to implement this inner region treatment. The essential feature is that the inner region formulation properly interact with the numerically computed outer region solution. As discussed earlier, the formulation is such

that f, f', and f'' are continuous at the interface between the two regions. In primitive variable terminology, this means that the integral of the velocity profile, the velocity u, and the velocity gradient $\partial u/\partial y$ are continuous across the match point. In effect, the inner region formulation provides boundary conditions for the outer numerical solution. This is the same concept that has been used in other wall function methods. Again, the main differences of the present method are the increased region of the boundary layer that is modeled empirically and the fact that the size of this region is not predetermined by the researcher (ie. previous methods limit the use of empirical expressions to a predetermined distance from the wall) but is determined as part of the solution process.

Once the match point is determined, empirical expressions are evaluated at this point so that the properties of the flow are determined and used as boundary conditions for the numerical computation of the outer region. These new boundary conditions replace the traditional no-slip at the wall boundary conditions normally enforced at the wall for viscous flows. The region of the boundary layer requiring numerical computation on a highly clustered grid is significantly reduced. This is true for previous wall function methods and was, in fact, the main incentive behind the development of these methods. As mentioned before, the present treatment increases the savings.

At a given streamwise location, the present treatment yields a single, physically accurate match point location; this location, however, is variable in the streamwise direction. Problems with the implementation of the new boundary conditions arise because the grid is typically established prior to the numerical computations; it would be fortuitous if the variable location of the match point would always, or ever for that matter, fall on an existing grid point. Computationally, there are several options as to the point of application of the empirically determined, match point boundary conditions.

The obvious first option is to apply an adaptive grid technique that forces the grid point nearest the wall to coincide with the match point at each streamwise location; the first

grid point off of the wall adjusts itself with each iteration, or time step, during the computation such that it is always located at the current match point. The match point boundary conditions are enforced at the first grid point. This approach is very complex for the general case of nonequilibrium flows, but is relatively simple for equilibrium flows. This is the primary approach used in the present investigation when computing equilibrium flows (both incompressible and compressible); the details of this technique as applied here for equilibrium flows are given later.

An approach must be developed that relates the match point to a general, fixed grid. Several options present themselves. Since the inner region of the boundary layer is thin relative to the boundary layer thickness, it should be admissible as a first approximation to impose the match point boundary conditions at the geometric surface. This is comparable to translating the point of application of boundary conditions in thin airfoil theory to the airfoil chordline. A more accurate approximation is to apply the match point boundary conditions at the grid point closest to the match point. Flowfield information at the grid points between the match point and the surface is supplied by the law of the wall and wake.

Another possibility is the definition of a new transformed normal coordinate that is defined such that the match point is located at a constant value of the new coordinate for all streamwise locations. Such an approach requires the definition of a scaling function used in the transformation of the normal coordinate. The scaling function is dependent on the streamwise location and varies from flowfield to flowfield. Melnik[44] and Walker, Ece, and Werle[12] have developed methods incorporating this approach.

The notion of applying surface slip velocity boundary conditions is reminiscent of Clauser's[31] analysis of the outer region of turbulent boundary layers and comparison to laminar boundary layers with slip velocities. Note the slip velocity corresponding to the outer region shown in figure 2d. It would be desirable to use information determined from the inner region treatment and the matching process to define surface boundary conditions

36

which enable the proper numerical computation of the outer region of the boundary layer. In effect, the outer region is assumed to extend all the way down to the wall so that only an outer eddy-viscosity model is required. The shear stress at the wall associated with the outer eddy-viscosity model is forced to be equal to the physically accurate wall shear stress. As a result, the numerical computations from the wall to the match point yield nonphysical information. However, the numerical solution becomes physically accurate upon reaching the match point, thus providing the proper description of the outer region. The condition specified in this approach is on the velocity gradient at the wall, which implies a condition on the shear stress at the wall. In words, the numerically computed wall shear stress must be equal to the physically accurate wall shear stress which is determined from the empirical inner region and matching treatments. Mathematically, the boundary condition on the velocity gradient enforced at the wall is

$$\left(\frac{\partial u}{\partial y}\right)_{y=0} = \frac{\tau_w}{\mu + \mu_t} = \frac{\rho_w u^{*2}}{K \rho_s u_e \delta_i^*} \tag{3.7}$$

and is written in defect stream function variables as

$$\left[\frac{\partial}{\partial \eta}\left(\frac{\partial f}{\partial \eta}\right)\right]_{\eta=0} = \frac{\rho_w}{\rho_e}\left(\frac{\rho_e}{\rho_s}\right)^2 \frac{\delta_i^*}{K \delta_v^*}$$

This equation is a direct result of the definition of the shear stress (equation(2.2)) using the eddy-viscosity concept (equation(2.3)). The arbitrary function K is chosen in the form of an outer region model, such as K=k where k is the Clauser constant. This outer solution includes a nonzero surface slip velocity and the associated surface density ρ_s.

Conditions on the velocity gradient at the wall have been used prior to this investigation by other researchers. The condition used by Gorski et al[45] is common among wall function approaches. The condition is of the form

$$\left(\frac{\partial u}{\partial y}\right)_{y=0} = \frac{u^*}{\kappa y}$$

and is simply the derivative of the common logarithmic law of the wall. This condition does not enforce the outer region model at the wall, but rather provides the compatibility between the velocity, as determined from the law of the wall, and its normal derivative in the near wall region. Melnik[44], on the other hand, has developed a condition for incompressible flow that is also in the tradition of Clauser. His condition, which was developed independently from the present investigation, is essentially the same condition as the incompressible form of the present boundary condition.

It is felt that the implementation of the inner region treatment will be best handled in the general, nonequilibrium case by use of the slip-velocity approach just described. This approach is used in the primitive variable applications of this investigation. It has also been successfully implemented into the equilibrium boundary layer solution procedure using defect stream function variables.

4 Results and Discussion

This chapter traces the development of the present method in chronological order. The initial phase of the investigation involved the derivation of the nonequilibrium defect stream function formulation for incompressible flows. The formulation reduces to that of Mellor and Gibson[32] for equilibrium flow. The primary accomplishment of the incompressible studies was, however, the development and implementation of the technique used to match the empirical inner region solutions with numerically computed outer region solutions. Another new feature was the use of a law of the wake in addition to the law of the wall. An existing law of the wake was used in this part of the investigation.

The primary phase of the investigation was the development of the nonequilibrium, compressible defect stream function formulation and the corresponding compressible inner region treatment in conjunction with the matching of the inner and outer region solutions. The compressible formulation was designed to reduce to the incompressible form of the initial work. A method for determining the coefficients of a postulated compressible law of the wake was also developed. This resulted in an analytic equation for the compressible law of the wake valid from the wall through the inner part of the outer region.

The final phase consisted of the application of the present techniques in primitive variable form. The method was incorporated into an existing two-dimensional Navier-Stokes code and tested for several cases of compressible flow over a flat plate.

4.1 Incompressible Flow

Solutions for incompressible, equilibrium boundary layers have been computed with the asymptotic, or zero-order, and full-equation forms of the present method. As discussed earlier, the zero-order form is taken in the limit of vanishing shear-stress velocity ratio. All solutions of this section were computed using the incompressible law of the wake of Moses[21] which is one of the widely accepted incompressible laws along with that

of Coles[20]. The Moses law was chosen because of its simple, polynomial form. Moses' incompressible law of the wake is

$$h(\xi,\bar{\eta}) = \frac{2}{\kappa}\Pi(\beta)\left[3\left(\frac{\Delta\bar{\eta}}{\delta}\right)^2 - 2\left(\frac{\Delta\bar{\eta}}{\delta}\right)^3\right]$$

where δ is the boundary layer thickness. The ratio (Δ/δ) and the coefficient Π are functions of β, and β is a function of the streamwise coordinate ξ. White[22] gives empirical expressions for these terms with regard to incompressible, equilibrium turbulent flow as follows:

$$\frac{\Delta}{\delta} = \frac{(1 + \Pi)}{\kappa}$$

and

$$\Pi = \frac{4}{5}(0.5 + \beta)^{3/4} \tag{4.1}$$

The law of the wall given in equation (2.8) reduces exactly to the common logarithmic-law form. The empirical coefficients for the computations of this section were chosen to conform with the work of Mellor and Gibson[32]; the law of the wall constants κ and B have the values 0.41 and 4.9, respectively, and the arbitrary function $K(x,y)$ in the outer region eddy-viscosity model is assumed to be the Clauser[31] constant and has the value 0.016 after Mellor and Gibson.

The equilibrium boundary layer problem is solved easily using a shooting technique. A value for the match point velocity defect f'_m is iterated until the far-field boundary condition on f (equation(2.16)) is satisfied. With the guess of f'_m, the match point location and then the corresponding value of f_m are determined. A fourth order Runge-Kutta integration routine given by White[22] is used to integrate from the match point across the outer region of the boundary layer.

The present solutions are compared with the full-equation solutions of Mellor and Gibson[32]. All of these results are for a Reynolds number based on the edge velocity and displacement thickness ($Re_{\delta*}$) of 10^5. The comparison shown in figure 3 includes the zero-order closed form solution for the most favorable pressure gradient, $\beta=-0.5$. This solution is shown in Appendix B. The present zero-order numerical solution is seen to be in complete agreement with the closed form solution and in close agreement with Mellor and Gibson's full-equation solution. The zero-order solutions provide an indication of the accuracy of the numerical scheme; the numerical solutions give an early indication of the accuracy of the zero-order equations.

It should be noted in figure 3 that the present method has resolved a turbulent boundary layer with only eleven grid points across the boundary layer. It is fair to question the accuracy of a solution with so few grid points. Figure 4 compares various grids for a typical value of β ($\beta = 2$) and shows that the eleven point grid solution is in agreement with the 51 and 101 point solutions. Only the six point solution deviates noticeably from the fine grid solutions, and this deviation is negligible. On the basis of these observations, the present solutions were computed with eleven uniformly spaced grid points. The first grid point is always at the match (patch) point, and the edge value of the normal coordinate is fixed. This is the adaptive grid approach mentioned in section 3.3. The normal coordinate reduces to $\bar{\eta}$ for incompressible flow and is plotted as such. During the iteration of the velocity defect f'_m, the first grid point $\bar{\eta}_m$ shifts with f'_m according to equation (3.6). The uniform grid is recomputed for each value of f'_m. This grid procedure was used for convenience rather than necessity as the grid points other than the first could have been fixed. By eliminating the inner region computations, a grid-point savings on the order of fifty percent was realized as was the case in references 12, 13, 17, and 18.

Equilibrium velocity defect profiles are presented in figure 5 for several small-β cases ($\beta \leq 1$); and in figure 6, results are presented for large-β cases ($\beta > 1$). The

distinction between small and large β cases was made by Mellor and Gibson[32] because the standard velocity defect variables become unbounded as β approaches infinity and the shear-stress velocity u^* approaches zero. They also observed the edge value of the normal coordinate $\bar{\eta}_e$ also approaches zero as β approaches infinity. Mellor and Gibson presented a transformation to overcome these difficulties. The transformation effectively replaces the shear-stress velocity u^* with a "pressure velocity" u_p which is defined as

$$u_p = \sqrt{\frac{\delta_i^*}{\rho} \frac{dp}{dx}}$$

for incompressible flow. This quantity is related to u^* and β as

$$u_p = u^* \sqrt{\beta}$$

The incompressible coordinates are defined as

$$S = \beta s \quad \text{and} \quad N = \bar{\eta} \sqrt{\beta}$$

and the velocity defect normalized by the pressure velocity and the transformed shear-stress velocity ratio are

$$\frac{\partial F}{\partial N} = F'(N) = \frac{u - u_e}{u_p} = \frac{f'(\bar{\eta})}{\sqrt{\beta}} \quad \text{and} \quad \lambda = \gamma \sqrt{\beta}$$

respectively. Although it was not necessary to invoke this transformation in order to achieve the solutions presented in this section, the variables F' and N are used for the large-β cases to facilitate comparison with the results of Mellor and Gibson.

It can be seen in these figures that the full-equation form of the present method compares extremely well with the full-equation solutions of Mellor and Gibson. Even more important is the excellent agreement of the present zero-order solutions with the full-

equation solutions. The relative simplicity of the zero-order approach and its excellent results makes it a desirable alternative to the full-equation approach.

The differences seen in the inner region are caused by the differences between Mellor and Gibson's inner region eddy-viscosity model and the present combination of the law of the wall and law of the wake. Mellor and Gibson's solutions approach the law of the wall in the limit as $\bar{\eta}$ goes to zero. As will be seen later, Mellor and Gibson's approach allows a large deviation from the law of the wall and wake in the inner region. This effect becomes more noticeable with increasingly strong adverse pressure gradients (increasing β).

The $\beta = 10$ case shown in figure 6 was computed with the Clauser constant $k = 0.0154935$ rather than $k = 0.016$. As demonstrated in figure 7 for the zero-order approach, a match point does not exist for $\beta = 10$ with $k = 0.016$ because the far-field boundary condition $F_\infty = -1$ cannot be satisfied. This failure to obtain a solution indicates the problem is overspecified. Figure 7 shows that the value $k = 0.0154935$ yields a single value of F'_m that satisfies the far-field boundary condition for $\beta = 10$. The maximum value of β for which a solution exists for $k = 0.016$ is approximately 8.6. For values of β less than 8.6, there are two values of f'_m which allow the far-field boundary condition to be satisfied. The physically correct value is the smaller of the two.

The problem of overspecification is alleviated by allowing the law of the wake to be computed as part of the solution, as discussed in section 4.2, rather than relying on a fixed law of the wake as done when computing the solutions shown in this section. The flexibility of computing the law of the wake allows solutions to be computed without altering the Clauser constant as was done for the $\beta = 10$ case shown in figure 4.

Results for the shear-stress velocity ratio γ from the present solutions are compared with the results of Mellor and Gibson in figure 8. The two sets of results are in close agreement but are not identical.

The present method for evaluating γ differs substantially from that of Mellor and Gibson[32], Walker et al[12], and others in that the value of γ is obtained from a patching of the inner and outer solutions at a particular point in the present method whereas a matching of the outer limit of the inner solution with the inner limit of the outer solution is used in the other methods. These methods are not strictly asymptotic in that the inner and outer eddy-viscosity models are patched at a point analogous to the patch point used in the present method. The equation Mellor and Gibson used to evaluate γ is very similar to equation (2.11), the equation used in the present method. The difference is one of application; equation (2.11) is evaluated at a point a finite distance from the surface in the present method, while the equation used by Mellor and Gibson is evaluated as close to the surface as possible (the inner limit of the outer solution). As a result, the values of γ obtained by Mellor and Gibson are consistently smaller than those obtained by the present method. However, larger values of γ can be obtained from the results of Mellor and Gibson by evaluating their equation at the point where the eddy viscosities are patched.

The inner region velocity profiles of the present method differ from those of Mellor and Gibson. The differences increase with an increasingly strong adverse pressure gradient (increasing β) and are best displayed using inner variable coordinates. Figure 9a shows the $\beta = 4$ case. It is clear in this figure that, although the inner solutions are identical near the wall, Mellor and Gibson's solution deviates from the logarithmic behavior at least an order of magnitude (in y^+ units) closer to the wall than in the present method. This shows the difference between applying an eddy-viscosity model that approaches the logarithmic form when approaching the wall and enforcing the logarithmic behavior throughout the inner region. In view of this difference, a comparison with experimental data seems appropriate. Figure 9b compares the present solution with experimental data taken from reference 46 for Clauser's[30] second equilibrium flow. The data shown in figure 9b correspond to profile 2305 in reference 46. For this profile, $\beta = 7.531$ and

$Re_{\delta^*} = 30692.5$. Figure 9b shows excellent agreement between the experimental data the present solution. Given the relatively large value of β, one would expect less agreement, especially in the logarithmic region, between a Mellor and Gibson solution and experiment. The present solution and experiment were also in close agreement for γ where a 0.87 percent difference was found. Present solutions were computed and compared with experimental data from reference 46 for many values of β and good agreement was generally observed. Table 1 shows several comparisons of the experimentally and numerically determined shear-stress velocity ratios where the numerical solutions were computed with the zero-order formulation. The analytic solution from the method of reference 42 (see Appendix A) is also shown.

Another feature of the present method can be observed quite well in figure 9b. Notice that the match point of the present solution is well beyond the logarithmic region. This result demonstrates the advantage gained when including the law of the wake in the present formulation. For all present solutions, the law of the wake allows the match point to move beyond the logarithmic region thus extending the usefulness of the analytic inner region treatment and further reducing the region which must be resolved numerically. As one would expect, the influence of the law of the wake increased as β increased.

4.2 Compressible Flow

Solutions for compressible, equilibrium boundary layers have been computed with the constrained zero-order and full-equation forms of the present method. The full-equation solutions, however, were generated with the equations of the matching procedure truncated to second-order. As discussed earlier, the constrained zero-order form is not the strict asymptotic form taken in the limit of vanishing γ as the term ε, which is of order γM_e, is not always a small parameter and thus remains in the formulation. The significance of the term ε increases with increasing M_e and has been included in all of the present computations for compressible flow. The term, however, is practically negligible until

45

reaching the high supersonic and hypersonic flow regimes. To fulfill the goal of determining a compressible law of the wake, solutions were computed with an iterative curve fit technique supplying the coefficient w of the postulated law of the wake given in equation (2.9). An analytic expression for the coefficient w is determined from these results.

The compressible equilibrium boundary-layer problem is solved using a shooting technique in the same fashion as described for incompressible flow. The primary difference is the determination of the law of the wake as part of the computational procedure. The specific procedure for determining the coefficient w is discussed later; suffice it to say that a new value of the coefficient w is determined with each iteration of f'_m. The empirical parameters κ and B for the law of the wall and the outer region eddy-viscosity parameter k retain their values from the incompressible flow cases; they are 0.41, 4.9, and 0.016, respectively. Note that the additional empiricism of the Crocco relationship is also incorporated in the compressible flow computations.

Both the constrained zero-order and full-equation solutions have been computed over M_e, $\hat{\beta}$, and $Re_{\delta*}$ ranges. The solutions shown were computed with 32 uniformly spaced grid points across the outer region (the first point being the match point) in order to facilitate the law of the wake curve fit procedure. Fewer points could have been used with the same success if the points had been nonuniformly spaced and clustered near the match point. Significantly fewer points were needed when the analytic law of the wake was used (ie once the compressible law of the wake was determined and the curve fit procedure no longer needed). The inner region solutions shown in the following figures were determined analytically from the laws of the wall and wake and the Crocco relationship.

Figure 10 compares velocity defect profiles for the constrained zero-order and full-equation formulations over a Mach number range for $Re_{\delta*} = 10^4$ and $\hat{\beta} = 0$ (the flat-plate case). It can be seen that the agreement between the formulations is extremely good. Table

2a shows the shear-stress velocity ratio γ computations to be in agreement on the order of one percent across the M_e range. The percent error of the constrained zero-order formulation for the prediction of γ, as compared to the full-equation formulation prediction, increases as the edge Mach number decreases, but we have previously seen that the predictions show excellent agreement for incompressible flow.

Figure 11 shows the comparison over a Reynolds number ($Re_{\delta*}$) range for $M_e = 3$ and $\hat{\beta} = 0$. Again, the velocity defect profiles are nearly identical and, as shown in Table 2b, the shear-stress velocity ratios as computed by the constrained zero-order formulation show an error on the order of one percent. As the Reynolds number decreases, the percent error of the constrained zero-order prediction of γ increases.

Figure 12 shows the comparison for several $\hat{\beta}$ values for $M_e = 3$ and $Re_{\delta*} = 10^4$. The $\hat{\beta} = 1$ case represents a relatively strong adverse pressure gradient case for supersonic flow. The velocity defect agreement for the $\hat{\beta} = 1$ case, although not as good as for the flat plate case, is still quite good. Table 2c shows the comparison of the shear-stress velocity ratios computed by the two formulations. The percent error of the constrained zero-order formulation increases with increasingly strong adverse pressure gradient. Although the error seen here is larger than for variations of M_e and $Re_{\delta*}$, the error over this practical range of $\hat{\beta}$'s remains below five percent.

The reduced complexity of the constrained zero-order formulation and the excellent agreement of the results above justify it as an excellent approximation and alternative to the full-equation formulation. All subsequent solutions shown in this section are based on the constrained zero-order formulation.

The determination of the law of the wake coefficient w is an important part of the present solution procedure. The assumed, or postulated, functional form of the law of the wake is shown in equation (2.9), where w is the unknown coefficient that is determined by a least squares curve fit during each iteration of f'_m. Recall that for the present treatment the

law of the wake need only be valid in the inner most part of the outer region; the curve fit to determine w focuses on this region of the boundary layer. In effect, a value for the law of the wake h is determined at each point in the outer region as

$$h(\bar{\eta}) = \sqrt{\frac{\rho_w}{\rho_e} \frac{\partial f}{\partial \hat{\eta}} - g(\bar{\eta}) + \frac{1}{\gamma}}$$ (4.2)

where g is the law of the wall, γ is the current value of the shear-stress velocity ratio, and f' is determined from the numerical solution. A least squares curve fit of the values of h is made with the value of the coefficient w as a result. A standard least squares correlation factor was used to judge the accuracy of the fit. The number of points used for the curve fit varied from case to case in order to maintain approximately the same correlation factor; that is, approximately the same level of accuracy with regard to the fit was maintained from case to case. Note that this procedure can be used for any general postulated law of the wake with any number of unknown coefficients. More complex laws of the wake which could be valid over more of the outer region of the boundary layer can be determined.

Figure 13 compares the resulting analytic law of the wake as defined by equation (2.9) and the determined value of the coefficient w with the numerically computed values of the law of the wake as determined by equation (4.2) for several Mach numbers. The profiles shown are for $Re_{\delta^*} = 10^4$ and $\hat{\beta} = 0$. It can be seen that the number of points accurately fit by the postulated law of the wake decreases as the Mach number increases; the fit is always accurate near the match point. From this figure, as well as other solutions not presented, it appears that the y^2 dominance of the law of the wake in the inner region begins to diminish as M_e approaches 4.

It can be seen in figure 13 that the law of the wake coefficient w is a function of M_e in addition to being dependent on $\hat{\beta}$. Figure 14a shows the variations of w as a function of M_e and $\hat{\beta}$ for $Re_{\delta^*} = 10^4$. It is seen that w increases significantly as $\hat{\beta}$ increases, especially

at small values of M_e. As the Mach number approaches 4, w becomes a relatively small number for all $\hat{\beta}$, and the strong dependence of h on $\bar{\eta}^2$ in the inner part of the boundary diminishes. Figure 14b shows the variations of the coefficient w as a function of M_e and Re_{δ^*} for $\hat{\beta} = 0$; the coefficient w is a weak function of Re_{δ^*}.

An analytic model for the law of the wake coefficient based on the above solutions can be written as

$$w(M_e,\hat{\beta}) = w(0,\hat{\beta}) \left(\frac{\rho_w}{\rho_e}\right)^{\alpha(\hat{\beta})}$$

where $w(0,\hat{\beta})$ is the law of the wake coefficient for incompressible flow and the exponent α is a function of $\hat{\beta}$ only. An equation for the coefficient w in incompressible flow follows from section 4.1 as

$$w(0,\hat{\beta}) = \Pi \left(\frac{\Delta}{\delta}\right)^2 = \Pi \left(\frac{1 + \Pi}{\kappa}\right)^2 \tag{4.3}$$

where the coefficient Π is a function of β. White's[22] equation for Π, as given in equation (4.1), can be used. Values of equation (4.3) based on equation (4.1) are shown in figure 14a in comparison to the values determined by the curve fit procedure. The present zero-order solutions have been used to determine a new expression for Π. The equation is

$$\Pi = \sigma_1(0.5 + \beta)^{\sigma_2} \tag{4.4}$$

where σ_1 and σ_2 are functions of β, rather than constants as in equation (4.1), and are defined as

$$\sigma_1 = \frac{4}{5} + \sqrt{\frac{0.5 + \beta}{250}} \quad \text{and} \quad \sigma_2 = \frac{1}{2} + \frac{2}{5}\exp\left[-\frac{1}{2}(0.5 + \beta)^{3/8}\right]$$

Figure 15a compares equations (4.1) and (4.4) with values of Π deduced from the numerically determined values of the coefficient w. Figure 15b compares the corresponding values of the coefficient w. Equation (4.4) is seen to be an excellent approximation to the numerical data throughout the range of β. White never intended equation (4.1) to be used for high β cases, so the improvement in this range is not unexpected. The agreement between equations (4.1) and (4.4) is much better in the low β range, but the new expression does fit the numerical data better. The equation for α was determined from the solutions shown in figure 14a and is written as

$$\alpha(\hat{\beta}) = 2 - \exp\left[-\frac{5}{4}\sqrt{2\hat{\beta} + 1}\,\right] \tag{4.5}$$

The resulting curve is shown in figure 16.

As mentioned previously, significant grid reduction can be realized when using the analytic law of the wake. Figure 17 shows this grid reduction when the analytic equation is used rather than the curve fit procedure. The solutions shown for the case where $M_e = 3$, $\hat{\beta} = 0$, and $Re_{\delta^*} = 10^4$ are virtually identical with only the seven point grid solution deviating ever so slightly. The computed values of γ were also essentially identical as the difference between the 32-point and the 7-point solutions was less than a quarter of one percent.

Figure 18 presents a series of constrained zero-order solutions over a $\hat{\beta}$ range from -0.3 to 2 for $Re_{\delta^*} = 10^4$ and $M_e = 3$. Profiles of the velocity defect, velocity ratio, and the density ratio are given. Since it is unnecessary to evaluate the inner region solution in order to compute the outer region solution, only the outer region results are shown. Figure 19 presents a series of flat plate solutions for a Mach number range from 0 to 4 and for $Re_{\delta^*} = 10^4$. Figures 18 and 19 are presented to document the effect of parameter variations on the profiles. It is interesting to observe that M_e variations have a minimal effect on the velocity defect profiles. The velocity defect profiles for variations of Re_{δ^*} with fixed M_e

and $\hat{\beta}$, although not presented here, were virtually identical. The fact that the velocity defect profiles are relatively insensitive to variations of M_e and Re_{δ^*} supports the definition of $\hat{\beta}$ as the compressible equilibrium flow parameter. The parameter $\hat{\beta}$ effectively designates the various families of similar solutions for compressible equilibrium flow, at least under adiabatic wall conditions, in the manner shown by Clauser with his parameter β for incompressible flow. Note that the present parameter $\hat{\beta}$ reduces to Clauser's β for incompressible flow.

Figure 20a shows the effect of M_e and $\hat{\beta}$ on the shear-stress velocity ratio for $Re_{\delta^*} = 10^4$. It is observed that γ increases with increasing M_e while decreasing with increasing $\hat{\beta}$ (increasingly strong adverse pressure gradient). For any combination of M_e and $\hat{\beta}$, γ increases as the Reynolds number decreases. Figure 20b demonstrates this trend for flat plate flow. The trend was documented in reference 32 for incompressible flow.

Figure 21 shows the effect of M_e, $\hat{\beta}$, and Re_{δ^*} on the compressibility parameter ω. Recall that this parameter is the ratio of the velocity thickness to the density-weighted velocity thickness and appears throughout the present formulation. Figure 21a shows the Mach number and pressure gradient effects on ω for $Re_{\delta^*} = 10^4$. By definition, ω remains one for all incompressible flows. It is observed that ω increases with increasing M_e as well as with increasing $\hat{\beta}$. The effect of the pressure gradient is magnified with increasing M_e. Figure 21b shows the effect of Re_{δ^*} on ω for $M_e = 3$ and $\hat{\beta} = 0$. It is observed that ω decreases with increasing Reynolds number. The curves of figure 21a would shift upwards for Re_{δ^*} less than 10^4 and downwards for Re_{δ^*} greater than 10^4 with the exception of the incompressible flow curve which remains fixed.

Comparisons of the constrained zero-order solutions with experimental data compiled by Fernholz and Finley[47] have also been made. Figure 22 shows the profile comparisons for two flat plate cases; each numerical solution was computed with 32 grid points across the outer region and the curve fit procedure was used to determine the law of

the wake coefficient. The agreement of the velocity defect and velocity ratio profiles is good, while the density ratio profiles are in reasonable agreement. The use of the Crocco relationship for the density ratio magnifies the velocity differences, especially near the edge of the boundary layer. The modification of the outer eddy-viscosity model by including the intermittency factor would improve the comparisons because the gradient of f' would increase as the boundary layer edge is approached. An intermittency factor could be incorporated into the formulation easily by allowing the arbitrary function K in equation (2.4) to be variable rather than using the Clauser constant k.

Table 3 compares the computed and experimental shear-stress velocity ratios. The computed solutions are from the constrained zero-order formulation and the experimental values are based on the values of skin friction as measured by a force balance. The analytic solutions shown were determined with the method of reference 42. The agreement for the flat plate cases is excellent; the experimental and computed values differ by no more than two percent. The 5801 series of experimental data represents a nonequilibrium flow in which data was taken in both favorable and adverse pressure gradients. The agreement shown for this series is not as good as seen with the flat plate cases. However, the largest difference occurs with the larger of the two adverse pressure gradient cases and the difference approximately 6.5 percent. The editors of reference 47 cast some doubt on the accuracy of the experimental values due to a lack of upstream history information and unknown conditions at the edge of the boundary layer. The value of the shear-stress velocity ratio should decrease between profiles 5801/0501 and 5801/0801 as M_e decreases, $\hat{\beta}$ increases, and Re_{δ^*} increases; these trends, as observed in the present investigation, indicate a decrease in γ that apparently was not observed experimentally.

4.3 Primitive Variable Application

The ultimate objective of the present investigation is implementation of the present concepts into existing three-dimensional, Navier-Stokes methods. It should be at this level

that the greatest rewards with regard to computational efficiency and accuracy will be realized. Coarse grids are often used near the wall in the interest of computational efficiency; the result is a loss of accuracy. Accurate numerical computations near the wall require a fine grid, which results in a loss of computational efficiency. The numerical computations near the wall can be replaced by an empirical treatment that does not rely on a fine grid for accuracy. The initial effort towards the final goal is discussed in this section.

The concepts developed in the present investigation have been implemented into the computer code known as NASCRIN (Numerical Analysis of Scramjet Inlets)[48,49]. The code solves the two-dimensional Navier-Stokes equations in conservation law form. Turbulence is modeled with the zero-equation eddy-viscosity model of Baldwin and Lomax[10]. The zero-equation model of Cebeci and Smith[9] has also been incorporated into NASCRIN and is used in the present investigation. A numerical coordinate transformation is used which generates a set of boundary-fitted curvilinear coordinates in order to facilitate the resolution of flowfields with general geometries. The transformation allows for the clustering of grid points in regions of high gradients. The transformed governing equations are solved using an unsplit, explicit, predictor-corrector, finite-difference method developed by MacCormack[50]. This finite-difference method is second-order accurate in both time and space. The flowfield variables at the inflow boundary are fixed at some designated initial condition; the variables at the outflow boundary are determined by a first-order extrapolation. No-slip and adiabatic wall conditions are applied on solid surfaces. The adiabatic wall condition used in NASCRIN ($\partial T/\partial y = 0$ at y =0) has been replaced by a more accurate[51] condition ($\partial H/\partial y = 0$ at y =0) in the present investigation.

The present inner region and matching treatments were incorporated into NASCRIN with relatively minor modifications to the code. The no-slip condition at the wall was replaced with the condition on the gradient of the velocity $\partial u/\partial y$ given in equation (3.7), and an additional subroutine was incorporated to determine the inner/outer match

point location, and the shear-stress velocity. A general description of the use of this boundary condition was given in section 3.3. The finite-difference method is used throughout the flowfield; only the outer region eddy viscosity of the zero-equation turbulence model (the Cebeci-Smith model, for example) is required. In essence, the resulting numerical solution is not physically accurate near the wall, as it is based on the outer region eddy-viscosity model and the velocity gradient boundary condition at the wall. However, the solution away from the wall is accurate, where the outer region eddy-viscosity model is physically correct. The physically accurate solution near the wall is determined from the empirical expressions used in the inner region treatment after the numerical solution of the outer region has converged.

The velocity gradient boundary condition (equation (3.7)) depends on the value the shear-stress velocity u^*. This parameter varies in the streamwise direction and is updated during the computation after every twenty time-steps. This updating scheme was chosen because NASCRIN updates the eddy-viscosity after every twenty time-steps. The shear-stress velocity is determined from the matching of the inner and outer region treatments. In this initial effort, the present concepts have been incorporated in the form of the method of reference 42 (see Appendix A). The numerical method provides the values of M_e, $\hat{\beta}$, and Re_{δ^*} needed in the matching subroutine, which is the new subroutine that has been incorporated into NASCRIN. This subroutine is, in fact, the method of reference 42, which solves analytically for the value of u^* at each streamwise location. Note that the analytic solution of reference 42 is for the constrained zero-order equation with equilibrium flow.

The NASCRIN code was used with and without the present modifications. Solutions with the present modifications are referred to as the slip-velocity solutions. Solutions computed without modification are referred to as the baseline solutions. The Cebeci-Smith turbulence model was used with the Clauser constant $k = 0.0168$; the law of

54

the wall constants κ and B have the values 0.41 and 5.0, respectively, and are used in the present inner region and matching treatments. Baseline and slip-velocity solutions are compared with experimental data.

The test cases considered in this initial effort were for compressible flow on flat plates. The two cases presented here are for $M_e = 2.578$ and 4.544; test conditions and experimental results for these two flows are found in reference 47 as part of the 5301 series of data. These two cases were discussed previously in section 4.2. Inflow conditions were determined by the analytic method of reference 42 for a specified $Re_{\delta*}$; the $M_e = 2.578$ case was started with $Re_{\delta*} = 2500$, and the $M_e = 4.544$ case was started with $Re_{\delta*} = 400$ at the inflow boundary. In each case, the experimental measurement station, corresponding to $Re_{\delta*} = 5295$ and 902 for $M_e = 2.578$ and 4.544, respectively, is near the middle of the computational field. The numerical solution was considered to be converged when one of the following criteria was met: (1) the maximum change in the density at each grid point was less than or equal to 10^{-7}, or (2) the average change in the density over the entire field was less than or equal to 10^{-8}. Each case was computed with fifty-one uniformly-spaced grid points in the streamwise direction and a constant Δx of 0.0168 meters.

The grid reduction, and corresponding increase in computational efficiency, is directly related to the grid-spacing normal to the surface. It was found that fifty-one grid points normal to the surface was adequate to resolve the flowfields for each case with the baseline method. The first grid point off of the wall was located at $y = 0.000027$ meters, which corresponds to y^+ values of approximately 3.9 and 0.9 for the $M_e = 2.578$ and 4.544 cases, respectively. Slip-velocity solutions were determined with far fewer grid points normal to the surface. To demonstrate, each case was computed with twenty-six points. The first grid point off of the wall is located at $y = .000142$ meters, or approximately five times further off of the wall than was used in the baseline solutions.

The values of y^+ were approximately 21 and 4.9 for the $M_e = 2.578$ and 4.544 cases, respectively. The match point was located at $y = 0.0021$ and 0.00145 meters, with corresponding y_m^+ values of 312 and 50, for the $M_e = 2.578$ and 4.544 cases, respectively. Recall that from the match point outward, the slip-velocity solution is physically accurate; empirical expressions provide the physically accurate solution between the wall and the match point.

Velocity ratio and density ratio profiles for the two cases are shown in figures 23 and 24. The baseline and slip-velocity solutions show excellent agreement in the outer region; the empirical inner region solution, based on the matching process, is in excellent agreement with the inner region solution of the baseline method. The only significant deviation from experiment occurs near the edge of the boundary layer. The predicted values of the shear-stress velocity ratio for $M_e = 2.578$ were 0.0430 and 0.0423 for the baseline and slip-velocity solutions, respectively; the shear-stress velocity ratios for $M_e = 4.544$ were 0.0522 and 0.0532 for the baseline and slip-velocity solutions, respectively. The corresponding experimental values were 0.0426 and 0.0544 for $M_e = 2.578$ and 4.544, respectively. In each case, the slip-velocity solution provides the better prediction.

The time-step is directly proportional to the minimum grid spacing normal to the surface. As discussed earlier, the slip-velocity procedure enables an increase in the minimum spacing (by moving the first grid point off of the wall further from the wall). The effect on the rate of convergence is dramatic. The baseline solution for the $M_e = 2.578$ case required 26250 steps, at an average Δt of approximately 0.00000008 seconds; the corresponding slip-velocity solution required only 5900 steps at an average Δt of approximately 0.0000004 seconds. The average time-step increases by approximately five for the slip-velocity solution. The baseline solution for the $M_e = 4.544$ case required 21250 steps, at an average Δt of approximately 0.00000008 seconds; the corresponding

slip-velocity solution required only 9000 steps at an average Δt of approximately 0.0000004 seconds. Again, the average time-step increases by approximately five for the slip-velocity solution.

Slip-velocity solutions were computed for a variety of grids; the twenty-six point solutions just discussed should not be taken as the optimum result. In fact, the slip-velocity solutions were relatively insensitive to the number of grid points normal to the surface. This statement holds for the resulting parameter profiles as well as the predicted shear-stress velocity ratio. The effect of reducing the amount of grid clustering (near the wall) and the number of grid points is to increase the rate of convergence.

5   Concluding Remarks

Equations governing two-dimensional, nonequilibrium, compressible turbulent boundary-layer flow have been derived using a defect stream function formulation. This formulation is of particular interest because it has a constrained zero-order approximation for which the tangential momentum equation has a first integral. The approximation is obtained in the limit of vanishing shear-stress velocity to edge velocity ratio and the constraint exists because the parameter γM_e cannot be neglected for high-speed flows. The modified Crocco temperature-velocity relationship has been used as an approximation to the energy equation. Compressible equilibrium flow has been defined with this formulation. Solutions for incompressible and compressible equilibrium flows have shown the constrained zero-order form to compare well with the full-equation form and experimental data.

The lack of popularity of previous defect stream function formulations is probably due to the difficulty encountered in enforcing the no-slip surface boundary condition. The present method overcomes this difficulty with a law of the wall/law of the wake formulation for the inner part of the boundary layer. This inner region treatment is mathematically patched to the outer region formulation. This formulation eliminates the need for an inner region eddy-viscosity model. The method also significantly reduces the grid requirements by eliminating numerical computations in the inner region.

A compressible law of the wake has been developed. The law of the wake was assumed to be proportional to y^2 and an iterative curve fitting procedure was used to determine its coefficient as part of the computation. Solutions generated with this technique allowed the definition of an analytic expression for the coefficient, and thus a completely analytic compressible law of the wake. Results show that use of the law of the wake permits patch point locations beyond the logarithmic region of the boundary layer.

The method, in its constrained zero-order equilibrium flow form, has been implemented into an existing two-dimensional Navier-Stokes code. Solutions for compressible, turbulent boundary-layer flow on flat plates have been computed. As implemented, solutions were computed using only an outer region eddy-viscosity model from the surface to the edge of the boundary layer. The no-slip boundary condition for the velocity at the surface was replaced by a boundary condition on the normal derivative of the tangential velocity at the surface. Solutions showed a significant increase in computational efficiency as a result of a coarse grid near the wall and increased time steps. The solutions showed excellent agreement with experimental data, analytic solutions, and the baseline, Navier-Stokes computations.

Future investigations should include the incorporation of the nonequilibrium, defect stream function equations and matching treatments into NASCRIN, in addition to other Navier-Stokes solvers with various turbulence models. The current defect stream function treatment should be modified to account for nonadiabatic wall effects. Finally, the treatment should be extended to and implemented in three dimensions. An initial look at the extension to three dimensions, for adiabatic wall conditions, is given in reference 52.

6 Appendices

6.1 Appendix A: Analytic Solution for Compressible Turbulent Flow

The constrained zero-order analytic solution for compressible, turbulent boundary layers and resulting skin friction law are discussed in detail in reference 42. This appendix provides a general outline of the solution.

As discussed in section 2.7, the constrained zero-order equation for equilibrium flow given in equation (2.21) is essentially linear from incompressible to supersonic flow, but an additional transformation is necessary to obtain a linear governing equation for hypersonic flow. The transformation is

$$\tilde{s} = \hat{s} \quad \text{and} \quad \tilde{\eta} = \int^{\hat{\eta}} \frac{\rho_e}{\rho} \, d\hat{\eta} = \hat{\eta} - \varepsilon f$$

The transformed governing equation is

$$\frac{\partial f}{\partial \tilde{s}} = \omega K \frac{\partial^2 f}{\partial \tilde{\eta}^2} + (1+2\hat{\beta}) \, (\tilde{\eta} - \tilde{\eta}_0) \, \frac{\partial f}{\partial \tilde{\eta}} - f - 1 - \varepsilon \, \tilde{\beta} \, f \frac{\partial f}{\partial \tilde{\eta}} \tag{6.1}$$

where f is understood to be f_0 and

$$\tilde{\beta} = 2\beta \frac{(1 - r)}{r} \left(\frac{\rho_e}{\rho_w} - 1\right) \quad \text{and} \quad \tilde{\eta}_0 = \frac{\varepsilon}{(1 + 2\hat{\beta})}$$

This equation is linear if the inequality

$$\varepsilon \, |\tilde{\beta}| \ll 1 \tag{6.2}$$

is satisfied. This inequality is satisfied for all pressure gradients from incompressible to supersonic flow and for small pressure gradients in hypersonic flow. An equilibrium form

60

of equation (6.1) can be determined in the same manner as discussed in section 2.8 with the additional condition that the inequality of equation (6.2) is satisfied. The equilibrium form of equation (6.1) is

$$\omega k \frac{d^2 f}{d\tilde{\eta}^2} + (1+2\hat{\beta})\,(\tilde{\eta} - \tilde{\eta}_0)\,\frac{df}{d\tilde{\eta}} - f - 1 = 0 \tag{6.3}$$

where the arbitrary function K is assumed to be the Clauser constant k.

As mentioned in section 2.8, Mellor and Gibson[32] showed that the incompressible equation is in the form of a confluent hypergeometric equation. Following Mellor and Gibson, the present independent variable is defined as

$$N = \frac{1 + 2\hat{\beta}}{\omega k} \frac{(\tilde{\eta} - \tilde{\eta}_0)^2}{2}$$

The dependent variable for the present problem is defined as

$$\hat{f} = (1 + f)\exp(N)$$

which has the free-stream boundary condition

$$\hat{f}_\infty = 0$$

In terms of these variables, equation (6.3) is

$$N\frac{d^2 \hat{f}}{dN^2} + \left(\frac{1}{2} - N\right)\frac{d\hat{f}}{dN} - \frac{1}{2}\left(1 + \frac{1}{1 + 2\hat{\beta}}\right)\hat{f} = 0$$

Confluent hypergeometric equations are of the form[43]

$$N\frac{d^2 \hat{f}}{dN^2} + (b - N)\frac{d\hat{f}}{dN} - a\hat{f} = 0$$

The parameters a and b for the present problem are

$$b = \frac{1}{2} \quad \text{and} \quad a = \frac{1}{2}\left(1 + \frac{1}{1 + 2\hat{\beta}}\right)$$

and the solution is

$$\hat{f} = C\, M(a,b,N) + D\, N^{1-b}\, M(1+a-b, 2-b, N)$$

where C and D are coefficients related to the boundary conditions and $M(a,b,N)$ is Kummer's function which is given as[43]

$$M(a,b,N) = 1 + \frac{a}{b}N + \frac{a(a+1)}{b(b+1)}\frac{N^2}{2!} + \dots$$

The resulting equation for the velocity profile in the outer region of the compressible, equilibrium turbulent boundary layer is

$$\frac{df}{d\tilde{\eta}} = -C\left\{\frac{a}{\sqrt{(a-1/2)\omega k}}\frac{\Gamma(1/2+a)}{\Gamma(1+a)}M(a-1/2, 1/2, N) - \frac{(\tilde{\eta}-\tilde{\eta}_0)}{\omega k}M(a, 3/2, N)\right\}\exp(-N)$$

where Γ is the gamma function and the coefficient C is given in reference 42.

The inner region empirical formulation is identical to that previously described. The matching of the velocity and velocity gradients of the inner and outer region solutions gives an equation for the match point $\tilde{\eta}_m$, and finally an equation for the shear-stress velocity which is

$$\frac{u^*}{u_e} = \left\{ \frac{1}{\kappa}\ln\left(\frac{Re_{\delta^*}}{\omega}\sqrt{\frac{\rho_e}{\rho_w}}\,\tilde{\eta}_m\right) + B + \frac{6}{\kappa}w\frac{\rho_e}{\rho_w}\tilde{\eta}_m^2 \right.$$

$$+ C\frac{\rho_e}{\rho_m}\sqrt{\frac{\rho_w}{\rho_e}}\left[\frac{a}{\sqrt{(a-1/2)\omega k}}\frac{\Gamma(1/2+a)}{\Gamma(1+a)}M(a-1/2, 1/2, N_m)\right.$$

$$\left.\left. - \frac{(\tilde{\eta}_m - \tilde{\eta}_0)}{\omega k}M(a, 3/2, N_m)\right]\exp(-N_m)\right\}^{-1}$$

This equation is written in terms of the simplified form of equation (2.8) for the law of the wall. Solutions presented here, however, were computed using the full van Driest form of the law of the wall as given in equation (2.8).

6.2 Appendix B: Analytic Solution for Incompressible Turbulent Flow at $\beta = -0.5$

A closed-form solution exists for the zero-order equilibrium flow case with regard to the most favorable pressure gradient ($\beta = -0.5$). The zero-order governing equation for equilibrium flow with $\beta = -0.5$ and K defined as the Clauser constant k is

$$kf_0'' - f_0 = 1$$

Evaluation of equation (4.1) for Π shows that the law of the wake vanishes for $\beta = -0.5$. Therefore, equation (3.2) has the form

$$f_{0,m} = \bar{\eta}_m \left(f_{0,m}' - \frac{1}{\kappa} \right)$$

The equation for $\bar{\eta}_m$ is

$$\bar{\eta}_m = \frac{\sqrt{1 + 4f_{0,m}k/(\bar{\eta}_m \kappa)} - 1}{2f_{0,m}/\bar{\eta}_m}$$

The solution is

$$f_0(\bar{\eta}_m) = \frac{k}{\kappa \bar{\eta}_m} \exp\left[(\bar{\eta}_m - \bar{\eta}) / \sqrt{k} \right] - 1$$

where

$$\bar{\eta}_m = 0.5 \left[\kappa - \sqrt{k} - \sqrt{(\kappa - \sqrt{k})^2 - 4k} \right]$$

63

The velocity defect is

$$\frac{u - u_e}{u^*} = \zeta_0 = -\frac{\sqrt{k}}{\kappa \bar{\eta}_m} \exp\left[(\bar{\eta}_m - \bar{\eta}) / \sqrt{k}\right]$$

and the shear-stress velocity is

$$\frac{u^*}{u_e} = \frac{1}{\left[\dfrac{1}{\kappa} \ln\left(Re_{\delta^*} \bar{\eta}_m\right) + B + \dfrac{\sqrt{k}}{\kappa \bar{\eta}_m}\right]}$$

7 References

1. Hinze, J. O.: Turbulence. second edition, McGraw-Hill Book Company, New York, 1975.

2. Anderson, D. A.; Tannehill, J. C.; and Pletcher, R. H.: Computational Fluid Mechanics and Heat Transfer. McGraw-Hill Book Company, New York, 1984.

3. Rubesin, M. W.: Turbulence Modeling for Aerodynamic Flows. AIAA Paper 89-0606, January 1989.

4. Bradshaw, P.(editor): Topics in Applied Physics: Turbulence, vol. 12, second edition, Springer-Verlag, Berlin Heidelberg New York, 1978.

5. Lakshminarayana, B.: Turbulence Modeling for Complex Shear Flows. AIAA Journal, vol. 24, no. 12, December 1986, pp. 1900-1917.

6. Marvin, J. G.: Turbulence Modeling for Computational Aerodynamics. AIAA Journal, vol. 21, no. 7, July 1983, pp. 941-955.

7. Rubesin, M. W.; and Viegas, J. R.: Turbulence and Modeling in Transonic Flow. Transonic Symposium: Theory, Application, and Experiment. NASA CP-3020, vol. 1, part 2, April 1988, pp.581-611.

8. Boussinesq, J.: Theorie de l'ecoulement tourbillant. Memoires Presentes par Divers Savants Sciences Mathematique at Physiques, Academie des Sciences, vol. 23, Paris,France, 1877, p.46.

9. Cebeci, T.; and Smith, A. M. O.: Analysis of Turbulent Boundary Layers. Academic Press, New York, 1974.

10. Baldwin, B. S.; and Lomax, H.: Thin Layer Approximation and Algebraic Model for Separated Turbulent Flows. AIAA Paper 78-0257, January 1978.

11. Blottner, F. G.: Nonuniform Grid Method for Turbulent Boundary Layers. Lecture Notes in Physics, vol. 35, 1975, pp.91-97.

12. Walker, J. D. A.; Ece, M. C. ; and Werle, M. J.: An Embedded Function Approach for Turbulent Flow Prediction. AIAA Paper 87-1464, June 1987.

13. Viegas, J. R.; Rubesin, M. W.; and Horstman, C. C.: On the Use of Wall Functions as Boundary Conditions for Two-Dimensional Separated Compressible Flows. AIAA Paper 85-0180, January 1985.

14. Viegas, J. R.; Rubesin, M. W.: Wall-Function Boundary Conditions in the Solution of the Navier-Stokes Equations for Complex Compressible Flows. AIAA Paper 83-1694, July 1983.

15. Wilcox, D. C.: Wall Matching, A Rational Alternative to Wall Functions. AIAA Paper 89-0611, January 1989.

16. Liakopolous, A.: Explicit Representation of the Complete Velocity Profile in a Turbulent Boundary Layer. <u>AIAA Journal</u>, vol. 22, no. 6, June 1984, pp.844-846.

17. Wahls, R. A.: Solution of the Turbulent Boundary-Layer Equations by a Finite-Difference Outer Layer and Integral Inner Layer Method. M.S. Thesis, North Carolina State University, June 1986.

18. Wahls, R. A.; Barnwell, R. W.; and DeJarnette, F. R.: Finite-Difference Outer-Layer, Analytic Inner-Layer Method for Turbulent Boundary Layers. <u>AIAA Journal</u>, vol. 27, no. 1, January 1989, pp.15-22.

19. van Driest, E. R.: Turbulent Boundary Layer in Compressible Fluids, <u>Journal of the Aeronautical Sciences</u>, vol. 18, no. 3, March 1951, pp. 145-160, 216.

20. Coles, D.: The Law of the Wake in the Turbulent Boundary Layer. <u>Journal of Fluid Mechanics</u>, vol. 1, 1956, pp.191-226.

21. Moses, H. L.: The Behavior of Turbulent Boundary Layers in Adverse Pressure Gradients. Report 73, Gas Turbine Laboratory, Massachusetts Institute of Technology, January 1964.

22. White, F. M.: <u>Viscous Fluid Flow</u>. McGraw-Hill Book Company, New York, 1974.

23. McQuaid, J.: A Velocity Defect Relationship for the Outer Part of Equilibrium and Near Equilibrium Turbulent Boundary Layers. Aeronautical Research Council CP-885, October 1965.

24. Maise, G.; and McDonald, H.: Mixing Length and Kinematic Eddy Viscosity in a Compressible Boundary Layer. <u>AIAA Journal</u>, vol. 6, no. 1, January 1968, pp.73-80.

25. Alber, I. E.; and Coats, D. E.: Analytical Investigation of Equilibrium and Nonequilibrium Compressible Turbulent Boundary Layers. Project SQUID: Technical Report DYN-1-PU, May 1969.

26. Mathews, D. C.; Childs, M. E.; and Paynter, G. C.: Use of Coles' Universal Wake Function for Compressible Turbulent Boundary Layers. <u>Journal of Aircraft</u>, vol. 7, no. 2, March-April 1970, pp.137-140.

27. Squire, L. C.: Further Experimental Investigations of Compressible Turbulent Boundary Layers with Air Injection. Aeronautical Research Council R & M 3627, 1968.

28. McDonald, H.: The Effect of Pressure Gradient on the Law of the Wall. <u>Journal of Fluid Mechanics</u>, vol. 35, part 2, 1969, pp.311-336.

29. Patel, V. C.: A Unified View of the Law of the Wall Using Mixing Length Theory. <u>Aeronautical Quarterly</u>, vol. 24, February 1973, pp.55-70.

30. Clauser, F. H.: Turbulent Boundary Layers in Adverse Pressure Gradients. <u>Journal of the Aeronautical Sciences</u>, vol. 21, February 1954, pp. 91-108.

31. Clauser, F. H.: The Turbulent Boundary Layer. Advances in Applied Mechanics, vol. 4, Academic Press Inc., New York, 1956, pp. 1-51.

32. Mellor, G. L.; and Gibson, D. M.: Equilibrium Turbulent Boundary Layers. Journal of Fluid Mechanics, vol. 24, part 2, February 1966, pp. 225-253.

33. Gibson, D. M.: Incompressible Turbulent Boundary Layers in Adverse Pressure Gradients. PhD Dissertation, Princeton University, 1962.

34. Mellor, G. L.: Incompressible, Turbulent Boundary Layers with Arbitrary Pressure Gradients and Divergent or Convergent Cross Flows. AIAA Journal, vol. 5, no. 9, September 1967, pp.1570-1579.

35. Schlichting, H.: Boundary-Layer Theory. McGraw-Hill Book Company, New York, 1979.

36. Crocco, L.: Su di un valor massimo del coefficiente di trasmissione del calore da una lamina piana a un fluido scorrente. L'Aerotecnica, vol. 12, 1932, pp. 181-197.

37. Baronti, P. O.; and Libby, P. A.: Velocity Profiles in Turbulent Compressible Boundary Layers. AIAA Journal, vol. 4, no. 2, February 1966, pp.193-202.

38. Gran, R. L.; Lewis, J. E.; and Kubota, T.: The effect of wall cooling on a compressible turbulent boundary layer. Journal of Fluid Mechanics, vol. 66, part 3, 1974, pp.507-528.

39. Mager, A.: Transformation of the Compressible Turbulent Boundary Layer. Journal of the Aeronautical Sciences, vol. 25, 1958, pp. 305-311.

40. Prandtl, L.: Zur Turbulenten Stromung in Rohren und langs Platten. Ergen Aerodyn. Versuchsanst. Gottingen, vol. 4, 1932, pp. 18-29.

41. Coles, D. E.: The Turbulent Boundary Layer in a Compressible Fluid. U.S. Air Force Proj. RAND. Report R-403-PR, Rand Corp. September 1962. (Available from DTIC as AD 285 651.)

42. Barnwell, R. W.; and Wahls, R. A.: A Skin Friction Law for Compressible Turbulent Flow. AIAA Paper No. 89-1864, June 1989.

43. Abramowitz, M.; and Stegun, I. A. (editors): Handbook of Mathematical Functions with Formulas, Graphs, and Mathematical Tables. John Wiley and Sons, New York, 1964, pp. 504-535.

44. Melnik, R. E.: An Asymptotic Theory of Turbulent Separation. Computers & Fluids, vol. 17, no. 1, 1989, pp.165-184.

45. Gorski, J. J.; Govindan, T. R.; and Lakshminarayana, B.: Computation of Three-Dimensional Turbulent Shear Flows in Corners. AIAA Journal, vol. 23, no. 5, May 1985, pp.685-692.

46. Coles, D. E.; and Hirst, E. A.(editors): Proceedings, Computation of Turbulent Boundary Layers, 1968, vol. II, Compiled Data, Stanford University, 1969.

47. Fernholz, H. H.; and Finley, P. J.(editors): A Critical Compilation of Compressible Turbulent Boundary Layer Data. AGARDograph no. 223, June 1977.

48. Kumar, A.: Numerical Analysis of the Scramjet-Inlet Flow Field by Using Two-Dimensional Navier-Stokes Equations. NASA TP-1940, December 1981.

49. Kumar, A.: User's Guide for NASCRIN - A Vectorized Code for Calculating Two-Dimensional Supersonic Internal Flow Fields. NASA TM-85708, February 1984.

50. MacCormack, R. W.: The Effect of Viscosity in Hypervelocity Impact Cratering. AIAA Paper 69-0354, April-May 1969.

51. Rudy, D. H.; Kumar, A.; Thomas, J. L.; Gnoffo, P. A.; and Chakravarthy, S. R.: A Comparitive Study and Validation of Upwind and Central-Difference Navier-Stokes Codes for High-Speed Flows. Validation of Computational Fluid Dynamics. AGARD-CP-437, vol. 1, December 1988, pp.37-1, 37-15.

52. Barnwell, R. W.; and Wahls, R. A.: Slip Velocity Method for Three-Dimensional Compressible Turbulent Boundary Layers. NASA TM-100586, March 1988.

Case[*]	M_e	$\hat{\beta}$	$Re_{\delta*}$	γ experiment	γ numerical	γ analytical[**]
1312	0	-0.230	5447.0	.0411	.0407	.0401
1410	0	0	6754.2	.0388	.0386	.0382
1422	0	0	19,321.1	.0350	.0351	.0348
2205	0	1.891	20,230.2	.0319	.0301	.0296
2305	0	7.531	30,692.5	.0231	.0229	.0225
2402	0	3.026	42,832.9	.0267	.0265	.0265

[*] experimental data from reference 46.
[**] analytical solution from method of reference 42.

Table 1. Shear-stress velocity ratio comparisons with experimental data
and analytical solutions for incompressible flow.

M_e	$\hat{\beta}$	Re_{δ^*}	$\gamma_{\text{full eqn}}$	$\gamma_{\text{zero-order}}$	% error
0	0	10^4	.0367	.0372	1.362
1	0	10^4	.0375	.0380	1.333
2	0	10^4	.0392	.0397	1.276
3	0	10^4	.0409	.0414	1.222
4	0	10^4	.0424	.0428	0.943
5	0	10^4	.0435	.0439	0.920

a) The effect of M_e variations.

M_e	$\hat{\beta}$	Re_{δ^*}	$\gamma_{\text{full eqn}}$	$\gamma_{\text{zero-order}}$	% error
3	0	10^3	.0511	.0523	2.348
3	0	10^4	.0409	.0414	1.222
3	0	10^5	.0341	.0344	0.880
3	0	10^6	.0293	.0295	0.683
3	0	10^7	.0256	.0258	0.781

b) The effect of Re_{δ^*} variations.

M_e	$\hat{\beta}$	Re_{δ^*}	$\gamma_{\text{full eqn}}$	$\gamma_{\text{zero-order}}$	% error
3	-0.15	10^4	.0418	.0421	0.718
3	0	10^4	.0409	.0414	1.222
3	0.5	10^4	.0386	.0394	2.073
3	1	10^4	.0367	.0378	2.997
3	2	10^4	.0339	.0352	3.835

c) The effect of $\hat{\beta}$ variations.

Table 2. Shear-stress velocity ratio comparisons of constrained zero-order and full equation equilibrium solutions.

Case[*]	M_e	$\hat{\beta}$	$Re_{\delta*}$	γ experiment	γ numerical	γ analytical[**]
5501/0101	1.724	0	4719	.0414	.0420	.0414
5301/0601	2.578	0	5295	.0426	.0431	.0424
5301/1302	4.544	0	902	.0544	.0555	.0533
5801/0101	1.947	-0.155	7949	.0397	.0412	.0407
5801/0501	1.918	.2175	8596	.0395	.0391	.0384
5801/0801	1.873	.7265	9024	.0395	.0370	.0360

[*] experimental data from reference 47.

[**] analytical solution from the method of reference 42.

Table 3. Shear-stress velocity ratio comparisons with experimental data and analytical solutions for compressible flow.
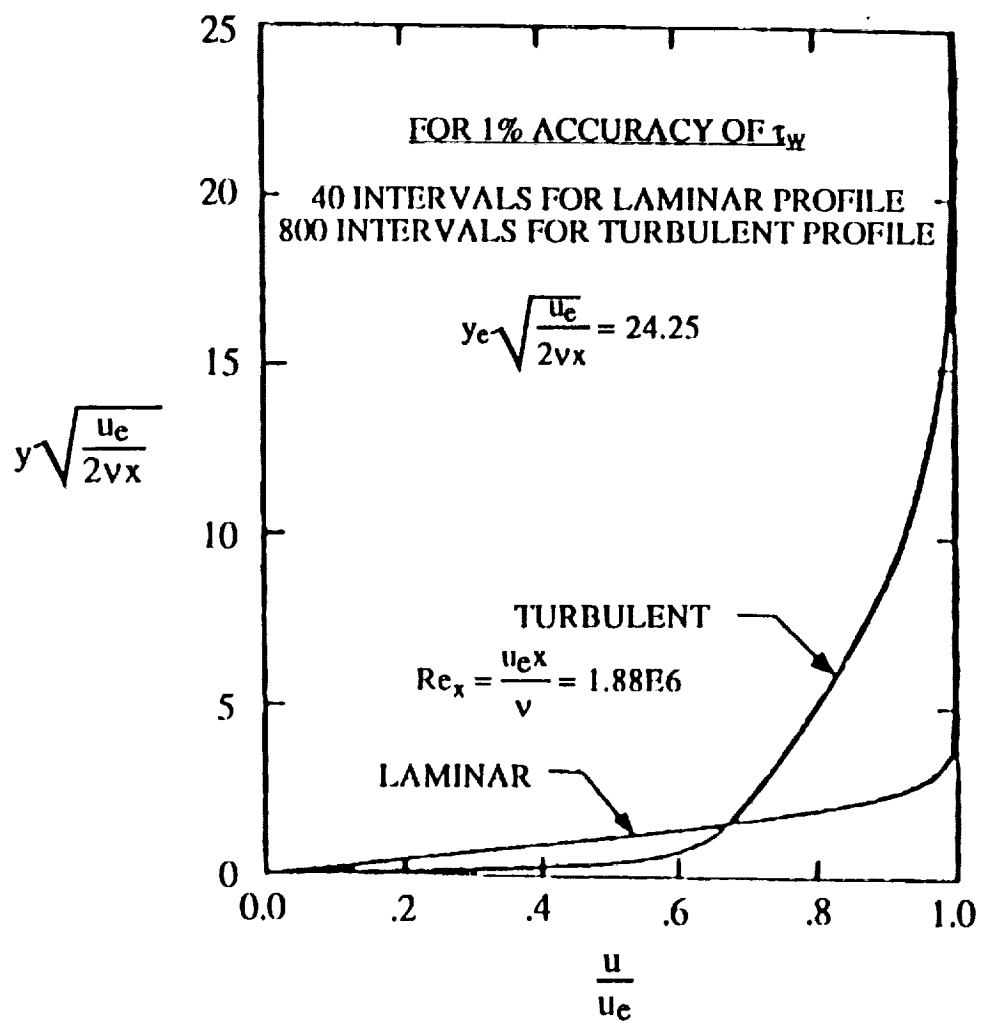
Figure 1. Laminar and turbulent velocity profiles on a flat plate.
(reprint from reference 11)
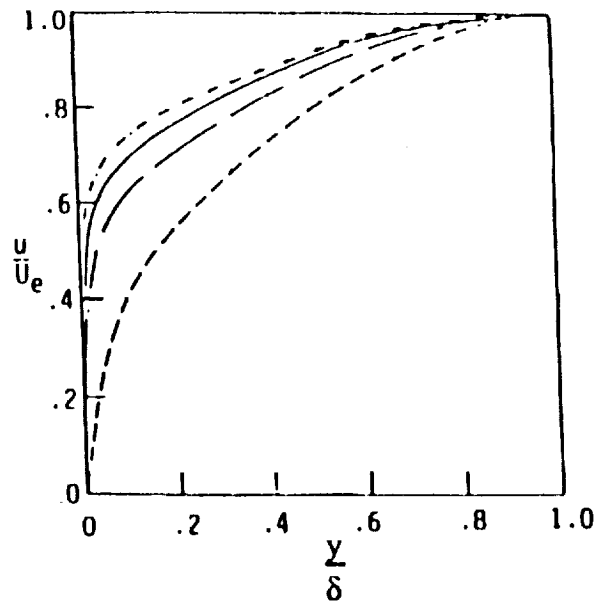
a) Several experimental turbulent velocity profiles on flat plates.
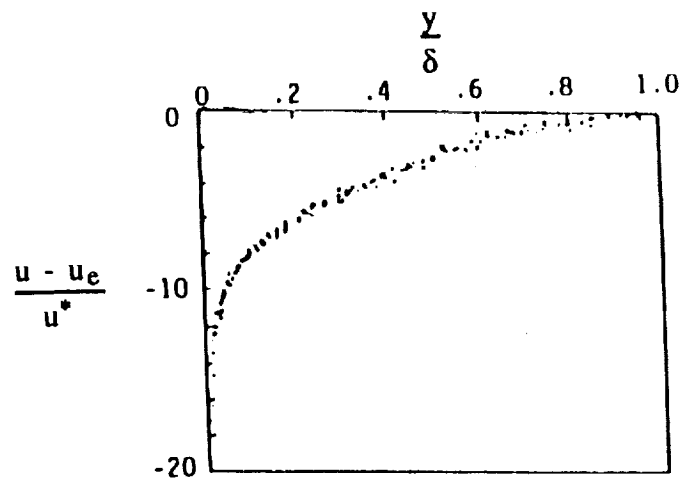
b) Universal plot of experimental turbulent velocity profiles on flat plates.

Figure 2.   Laminar-like behavior of the outer region of turbulent boundary layers.
(composite of reprints from reference 31)
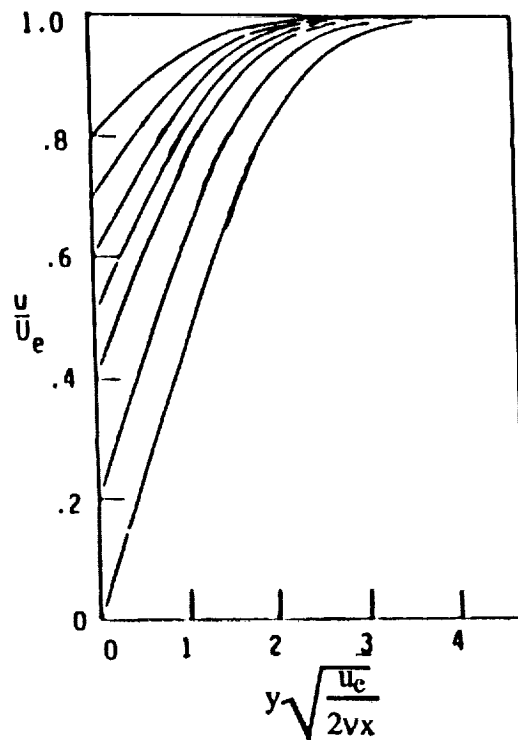
c) Solutions of the Blasius equation with nonzero surface velocities.
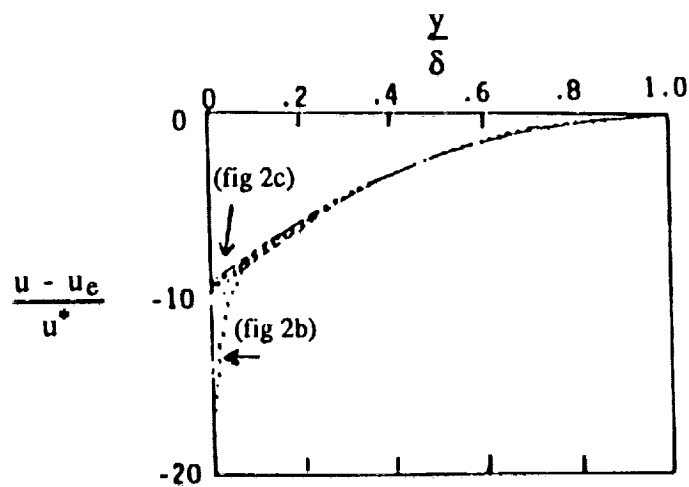
d) Comparison of the data shown in fig. 2b and 2c.

Figure 2.   Concluded.

74
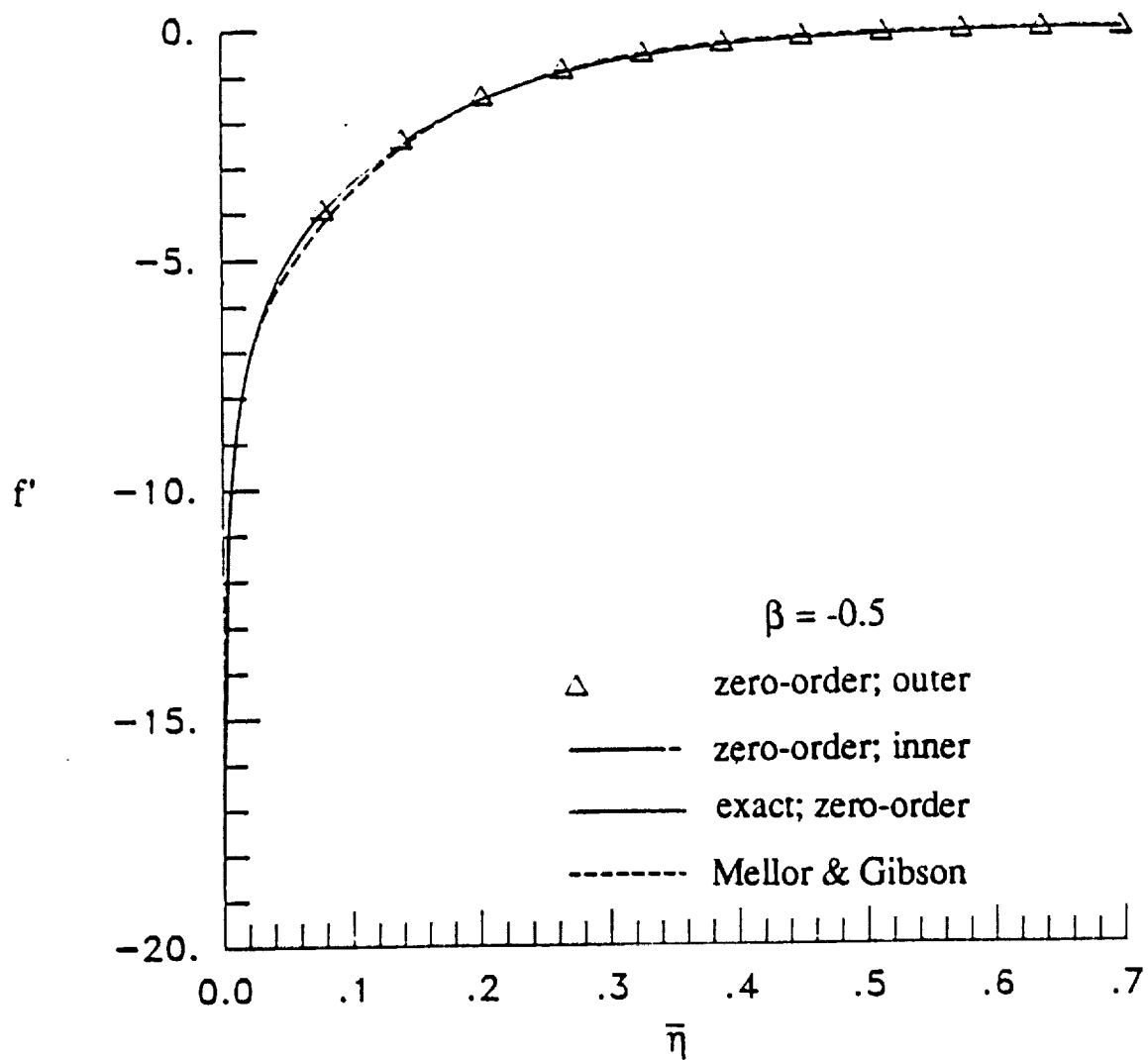
Figure 3.   Velocity defect profiles with β = -0.5 for incompressible flow.
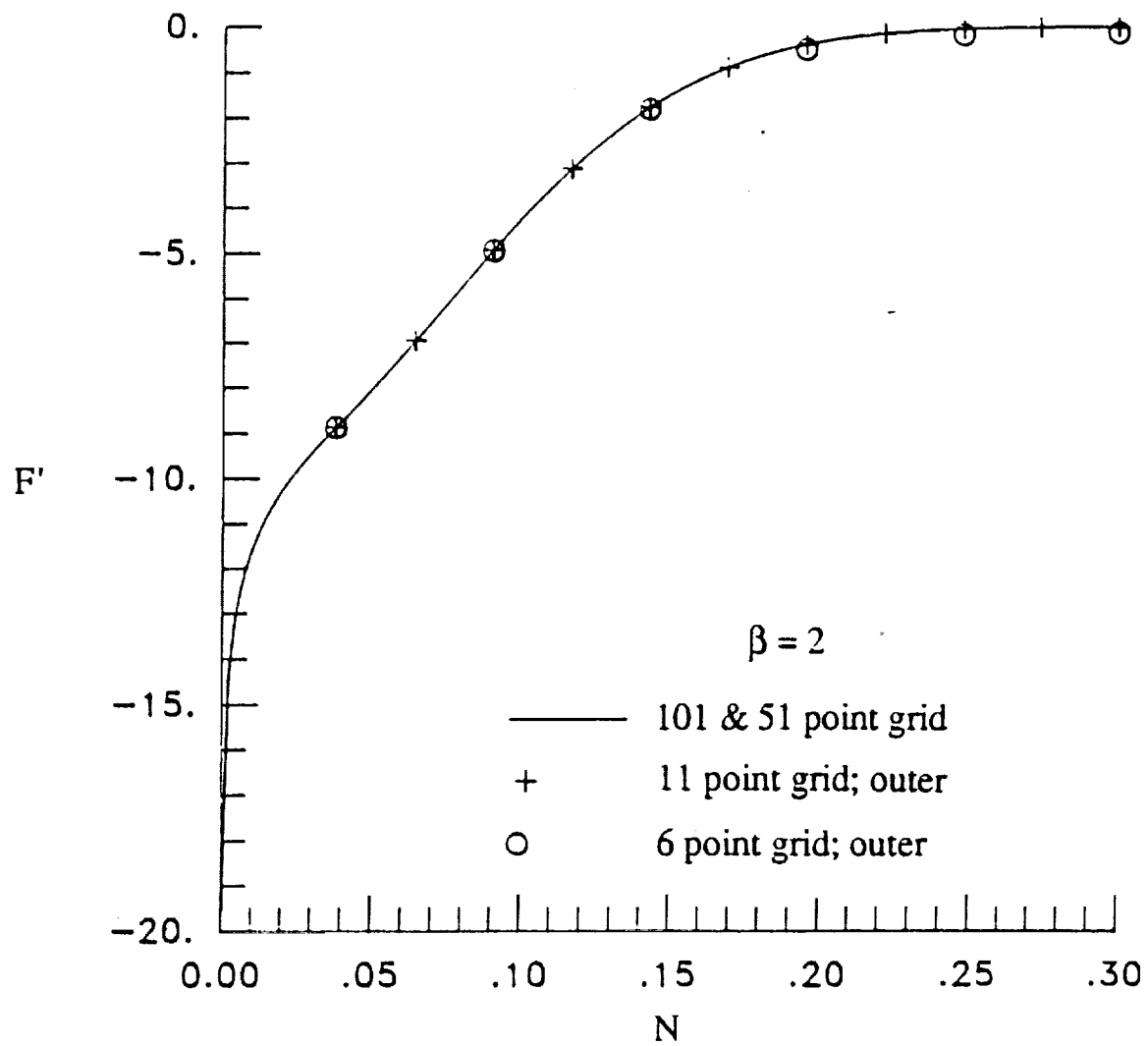
Figure 4. Grid resolution comparison for incompressible flow.
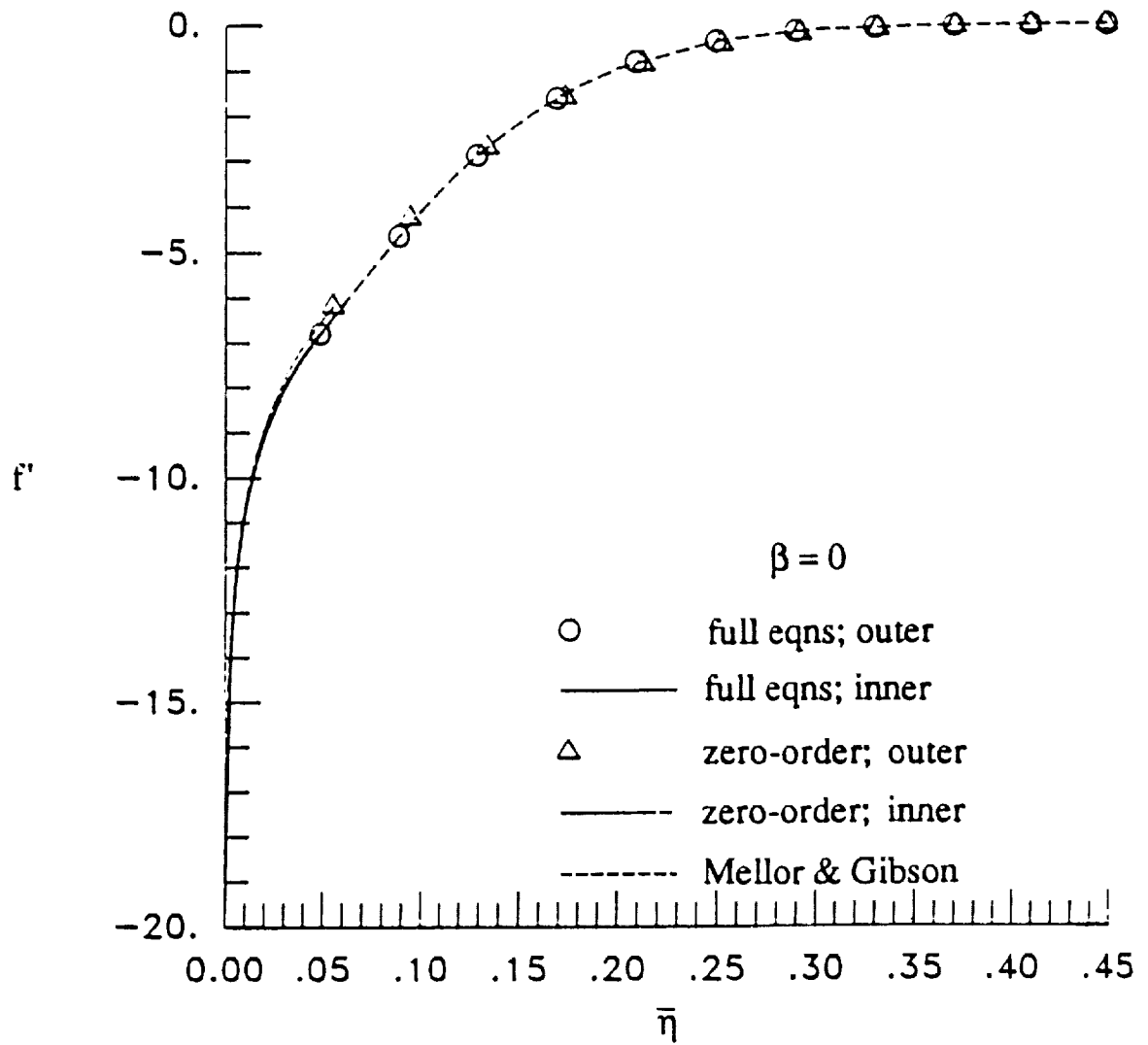
a) β = 0

Figure 5.   Velocity defect profiles with β ≤ 1 for incompressible flow.

b) $\beta = 0.5$

Figure 5.   Continued.
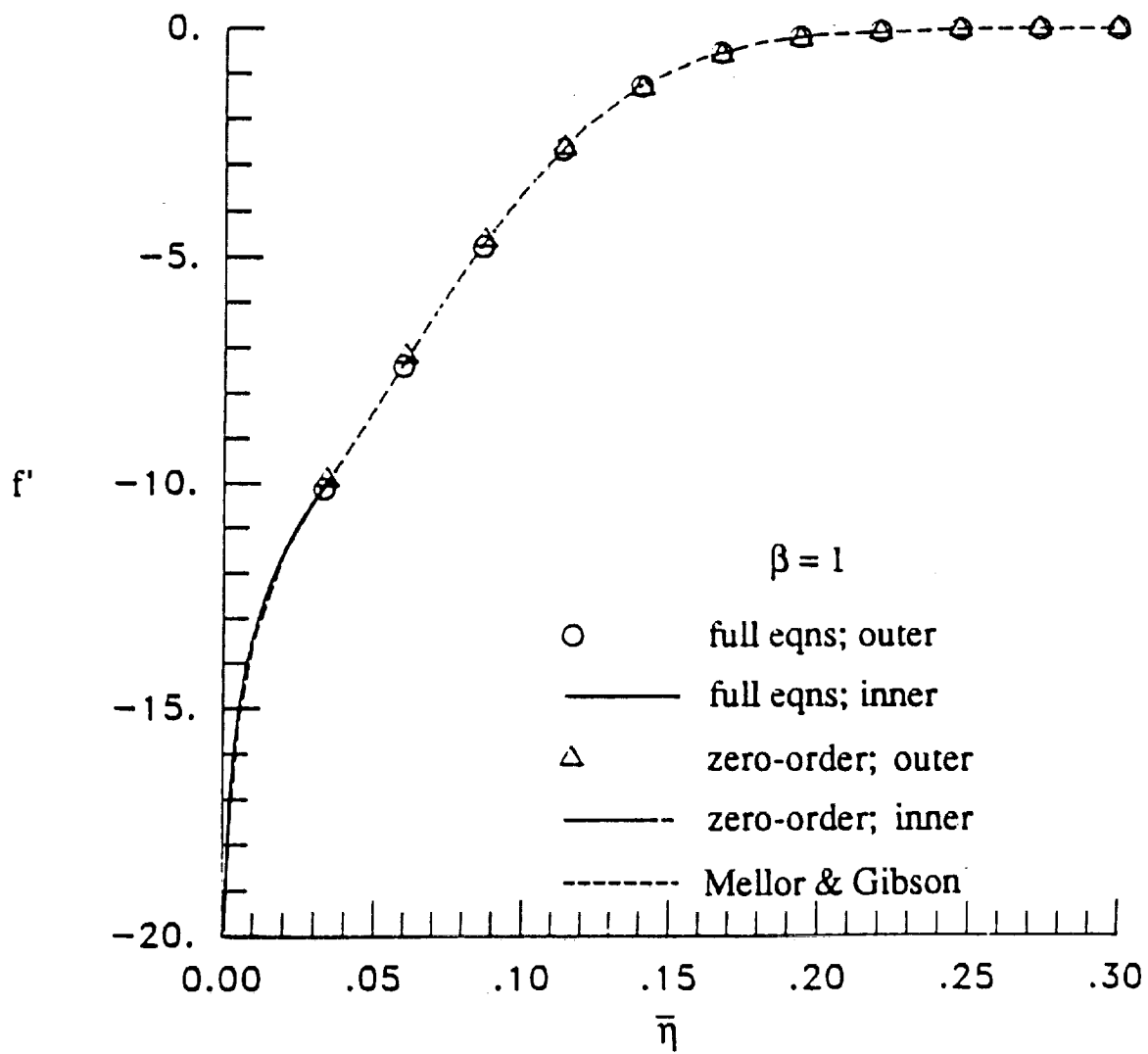
c) $\beta = 1$

Figure 5.   Concluded.
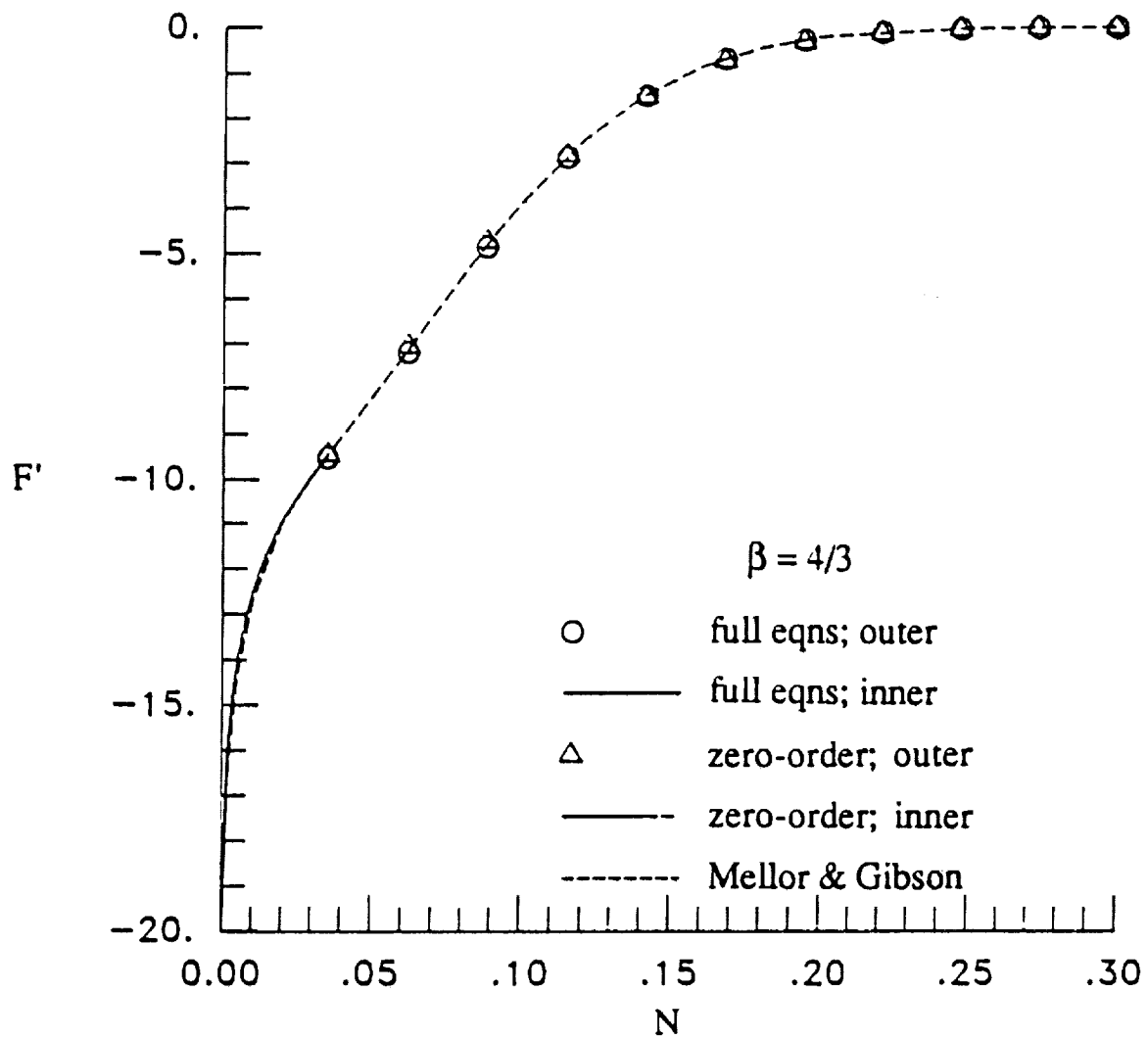
a) $\beta = 4/3$

Figure 6.   Velocity defect profiles with $\beta > 1$ for incompressible flow.

b) $\beta = 2$

Figure 6.   Continued.

$\beta = 4$

O	full eqns; outer
——	full eqns; inner
△	zero-order; outer
— - —	zero-order; inner
- - - - - -	Mellor & Gibson

F'

axis values: 0., -5., -10., -15., -20.

N

0.00 .05 .10 .15 .20 .25 .30 .35
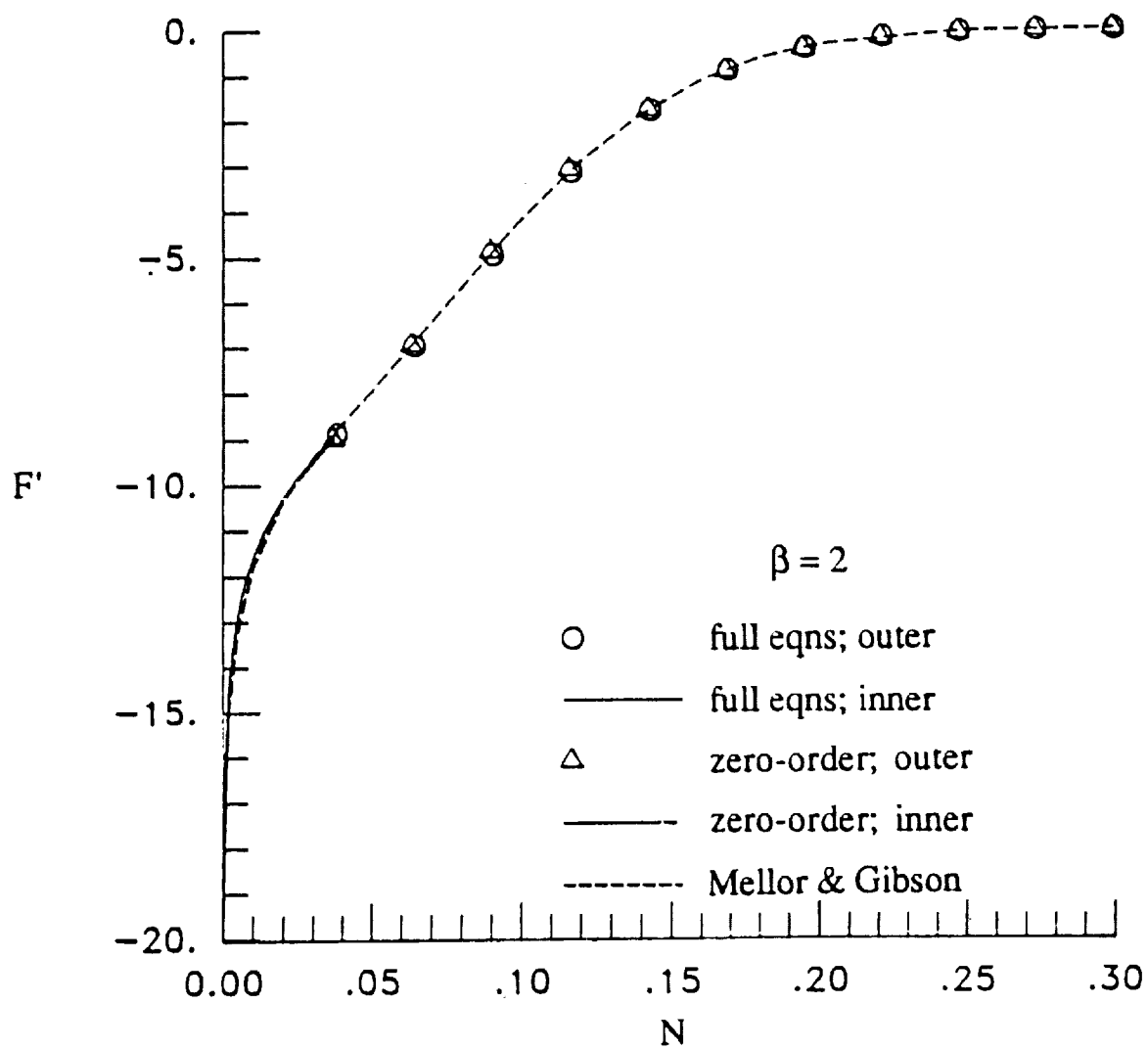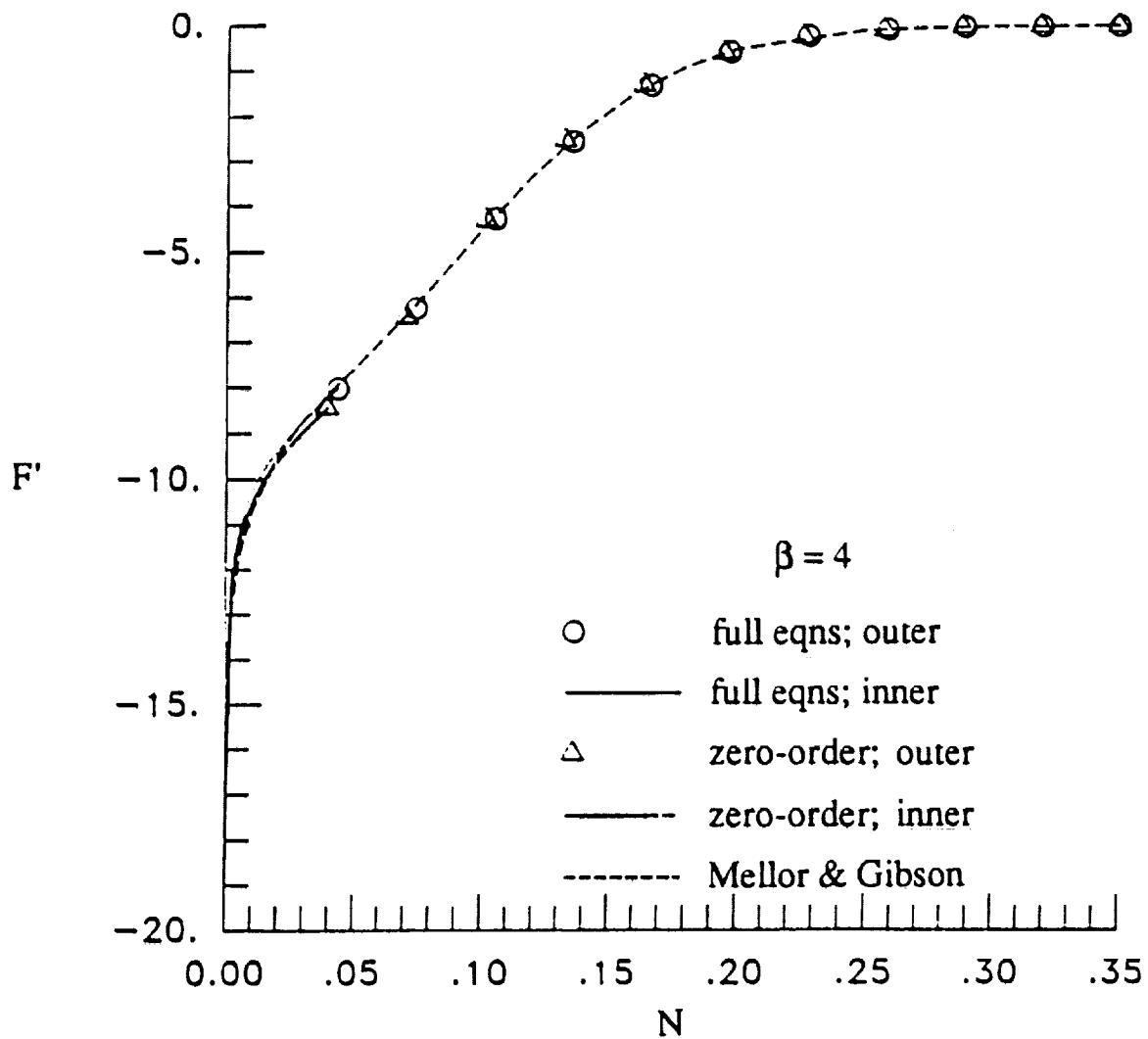
c) $\beta = 4$

Figure 6.   Continued.
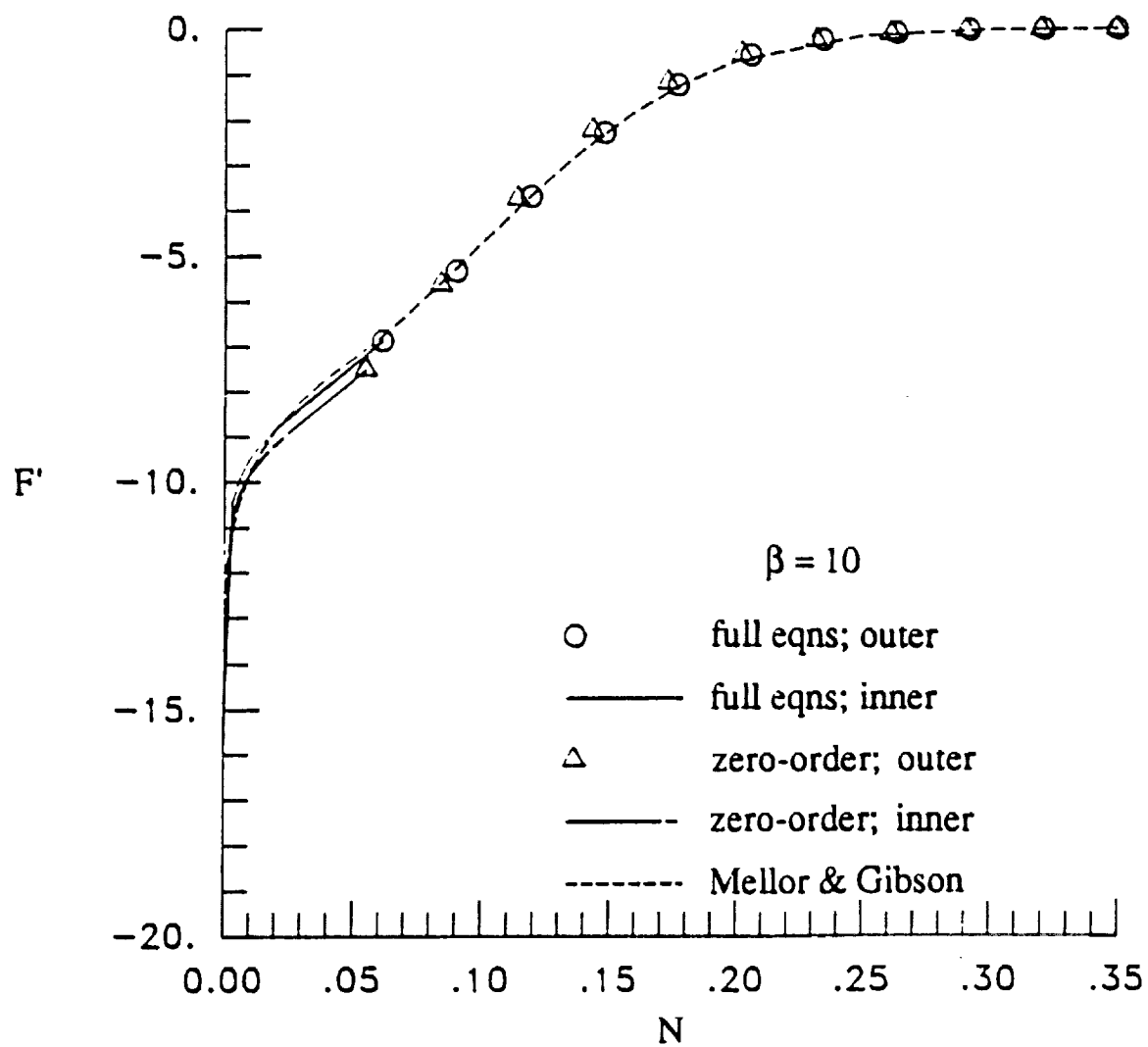
d) $\beta = 10$

Figure 6.   Concluded.
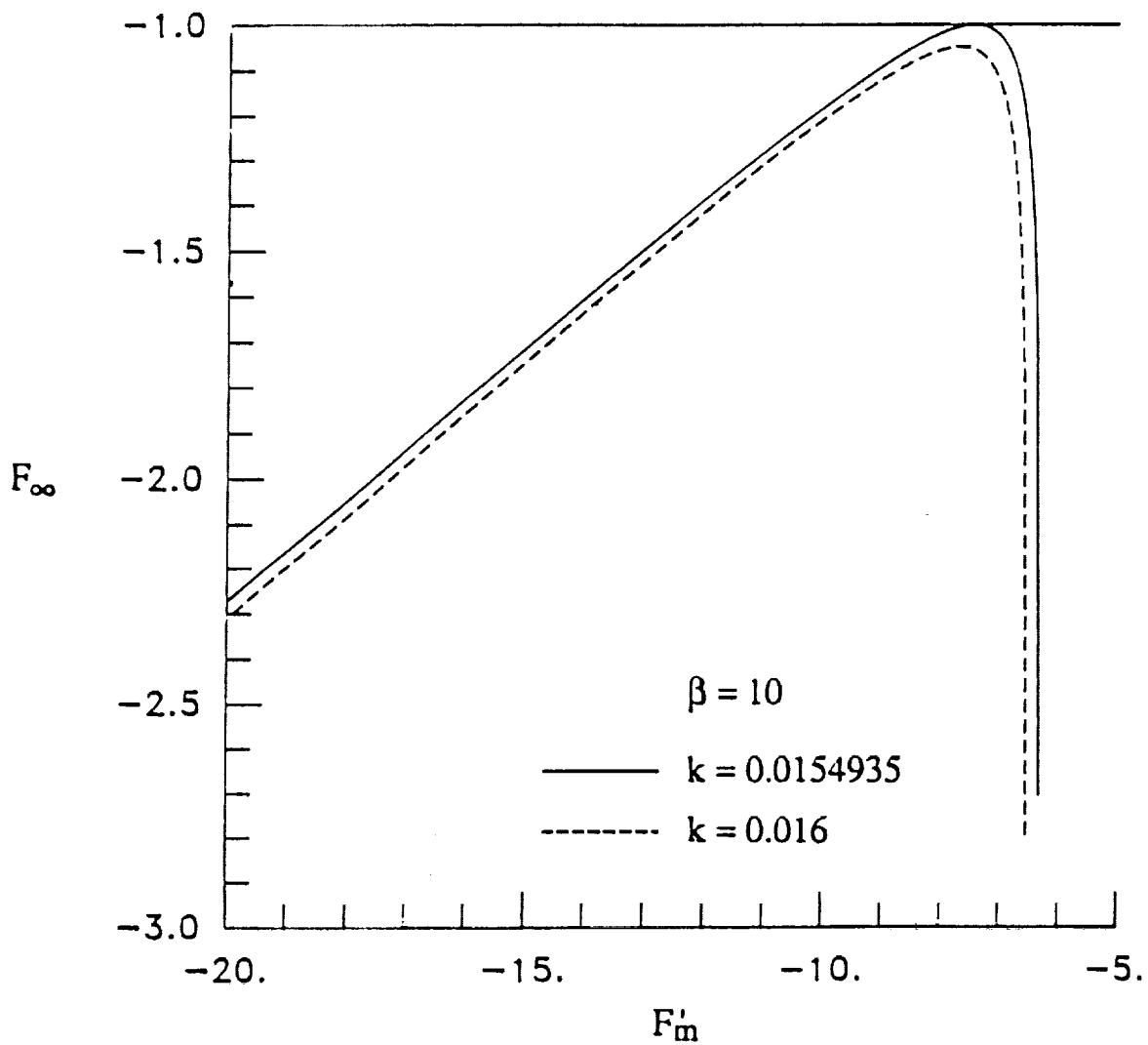
Figure 7.   Effect of the Clauser constant k on convergence with $\beta = 10$
for incompressible flow.
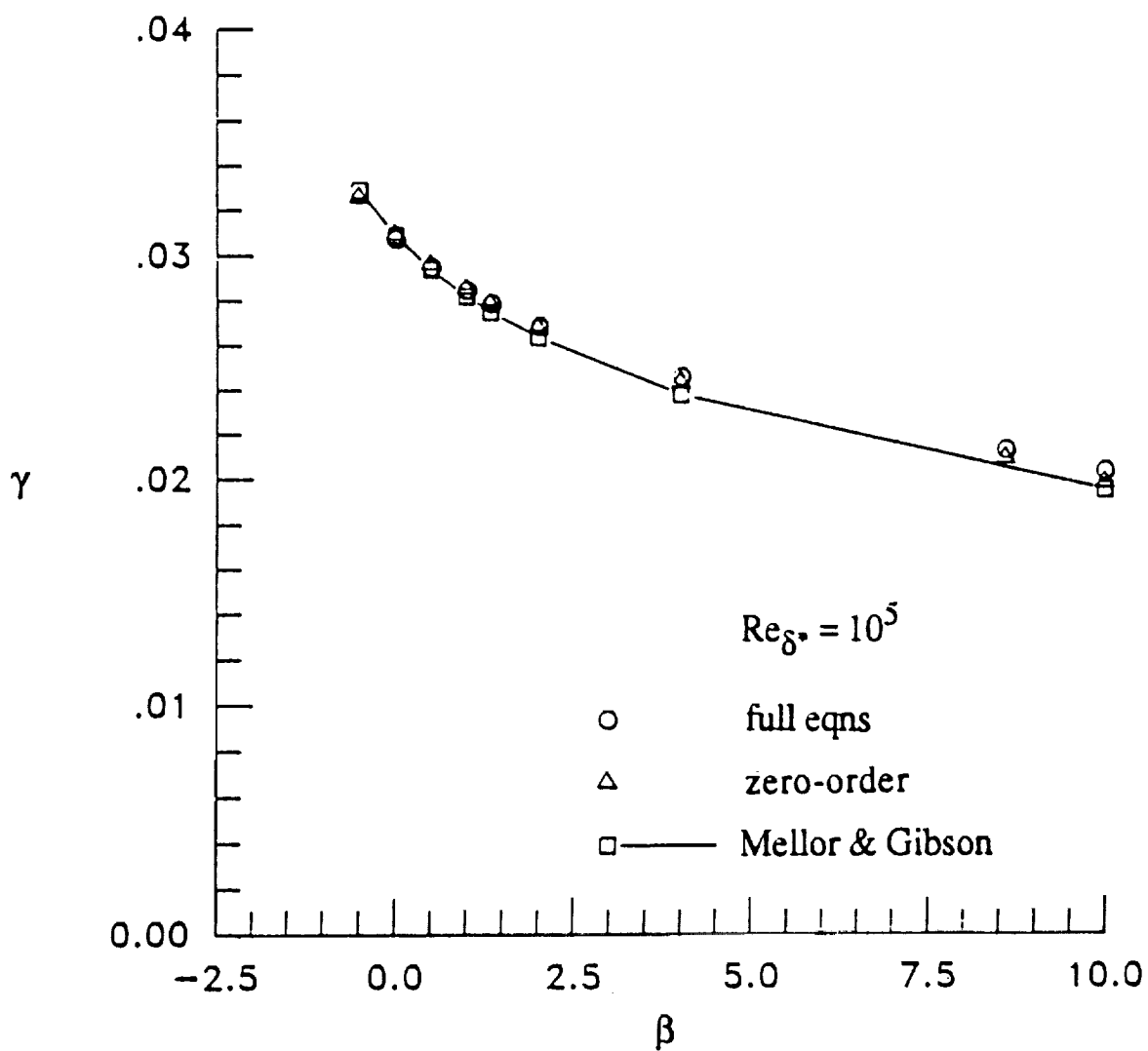
Figure 8.   Shear-stress velocity ratio comparison with $\mathrm{Re}_{\delta^*} = 10^5$
for incompressible flow.
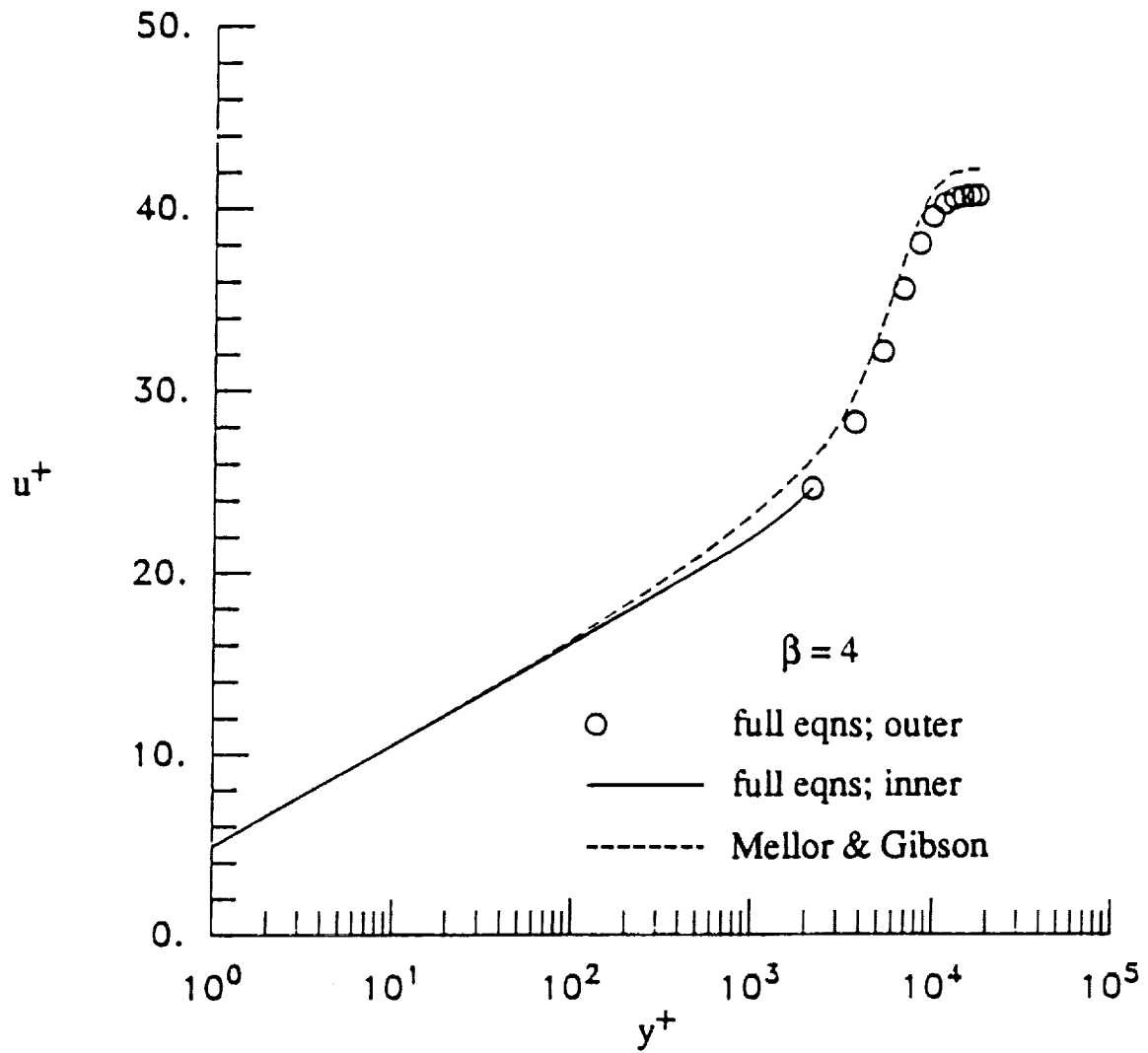
a) Computational comparison with $\beta = 4$ and $Re_{\delta*} = 10^5$.

Figure 9.   Inner variable profiles for several incompressible cases.
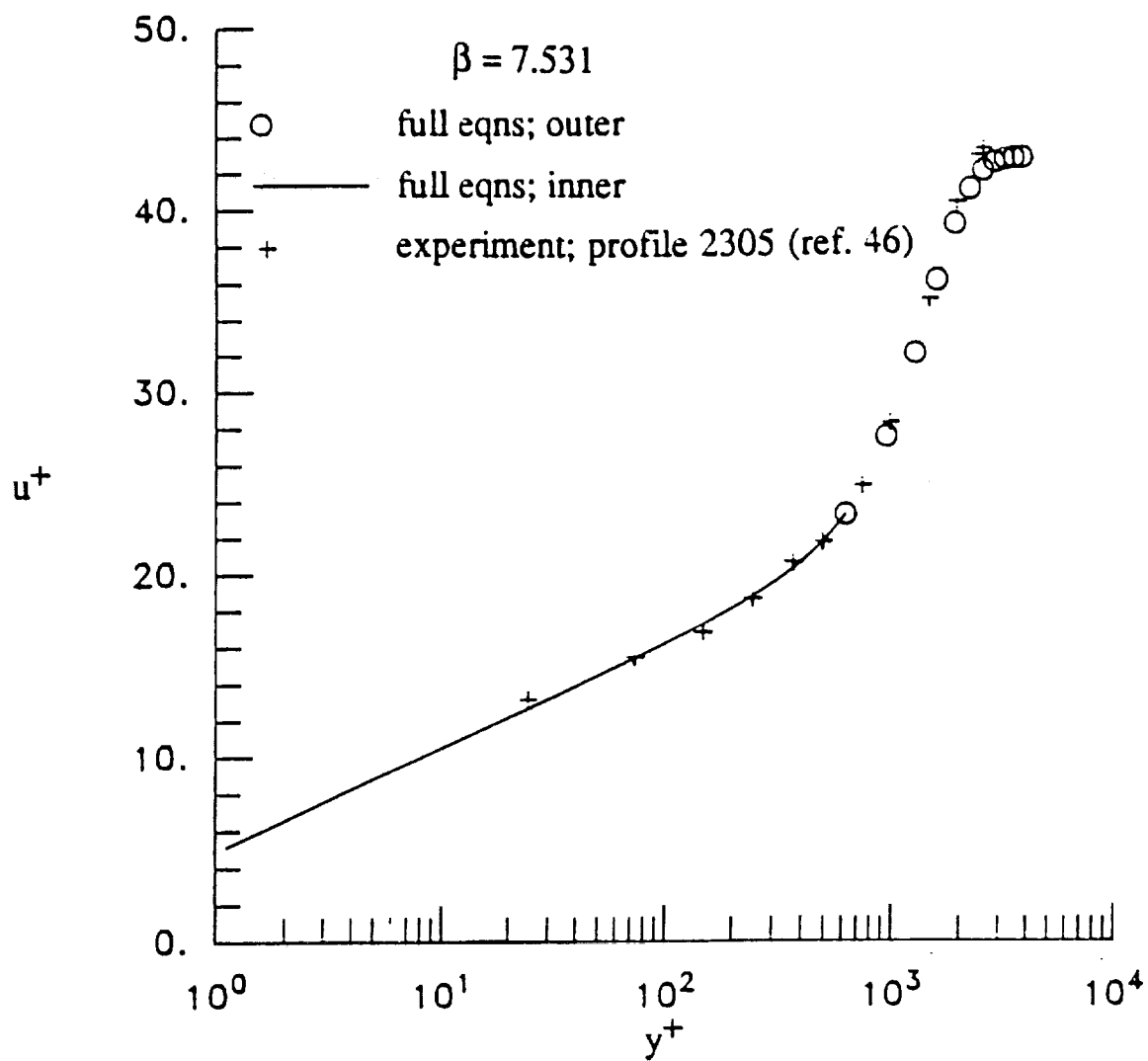
b) Comparison with experimental data with $\beta = 7.531$ and $Re_{\delta^*} = 30,692.5$.

Figure 9.   Concluded.
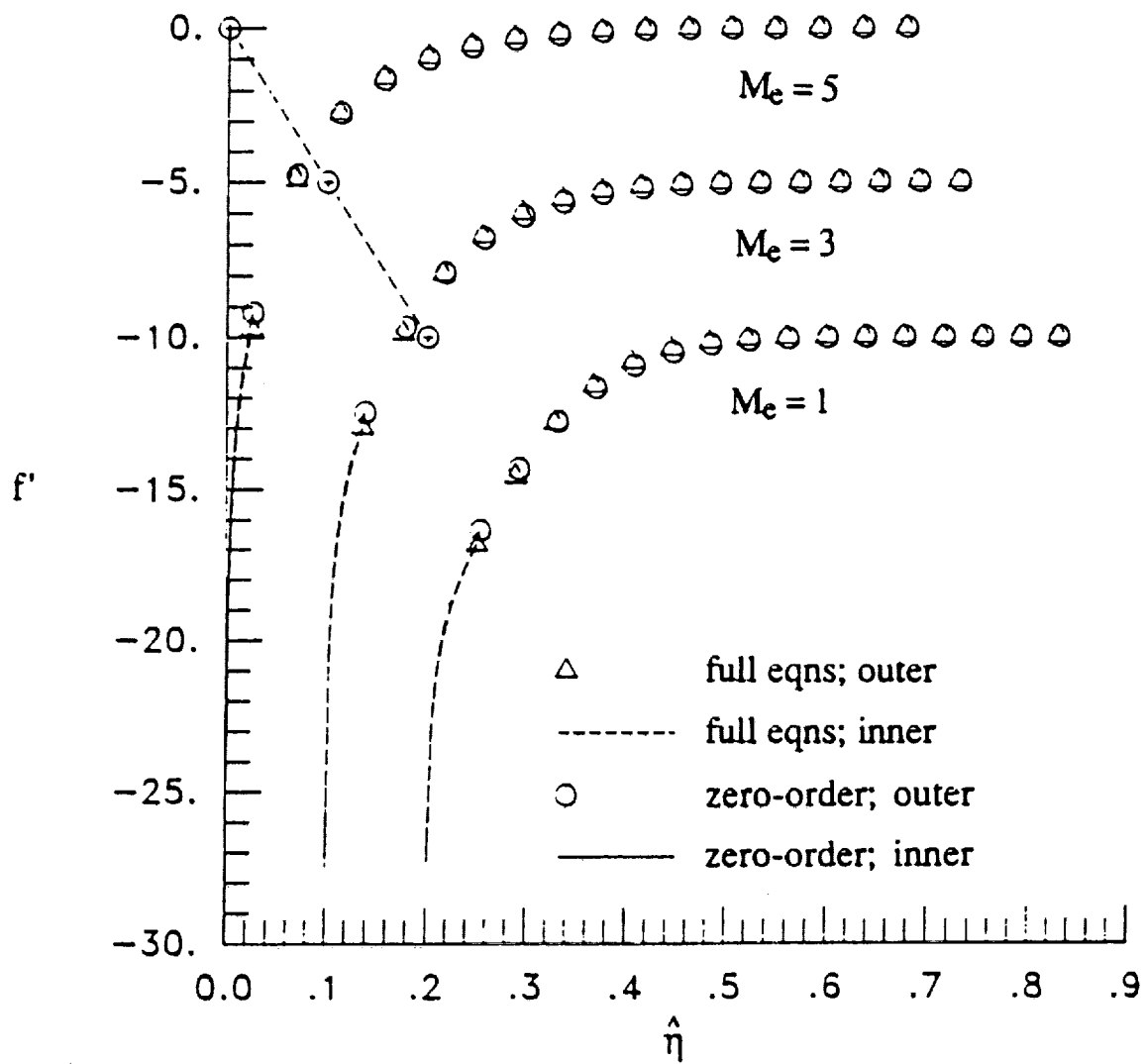
Figure 10. Effect of M_c on the velocity defect profiles with $\hat{\beta} = 0$ and $Re_{\delta^*} = 10^4$.
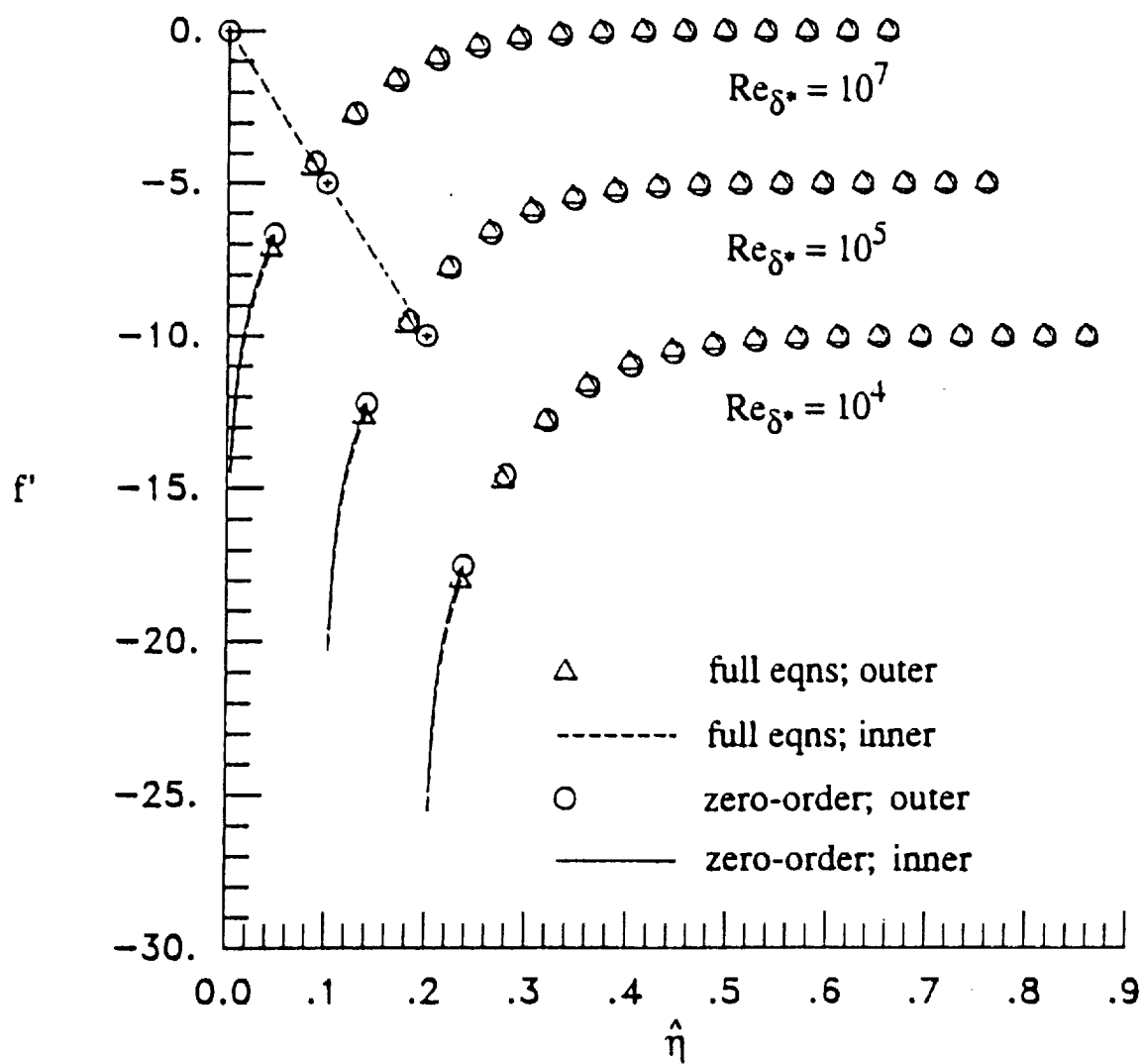
Figure 11. Effect of Re_{δ^*} on the velocity defect profiles with $M_e = 3$ and $\hat{\beta} = 0$.
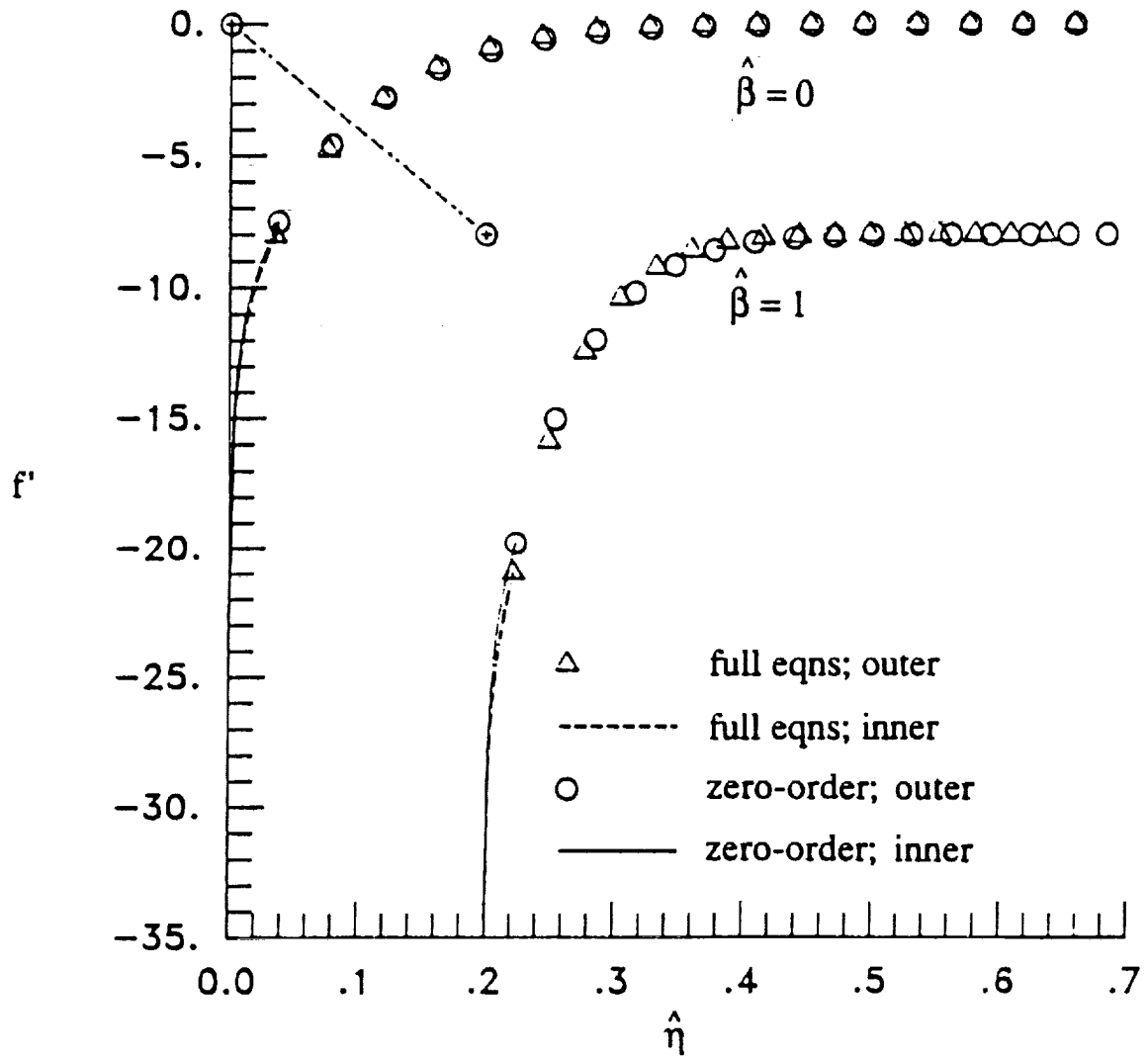
Figure 12. Effect of $\hat{\beta}$ on the velocity defect profiles with $M_e = 3$ and $Re_{\delta^*} = 10^4$.
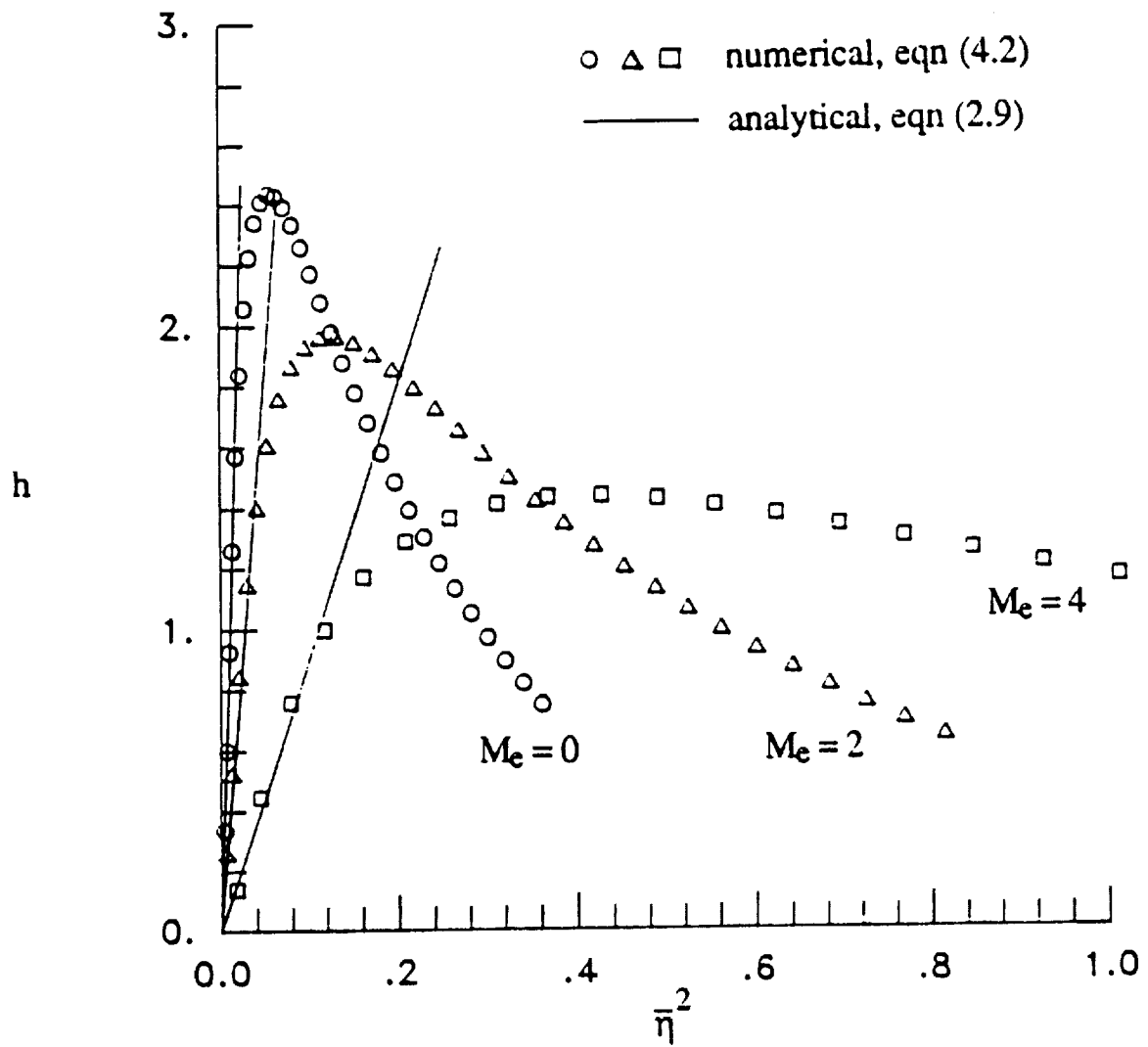
Figure 13. Analytic and numeric values of the law of the wake with $\hat{\beta} = 0$ and $Re_{\delta*} = 10^4$.

O ——	$\hat{\beta} = -0.3$	
□ ——	$\hat{\beta} = 0$	
◇ ——	$\hat{\beta} = 1$	
△ ——	$\hat{\beta} = 2$	
⊕ ——	$\hat{\beta} = 4$	
X	analytical, eqn (4.3)	
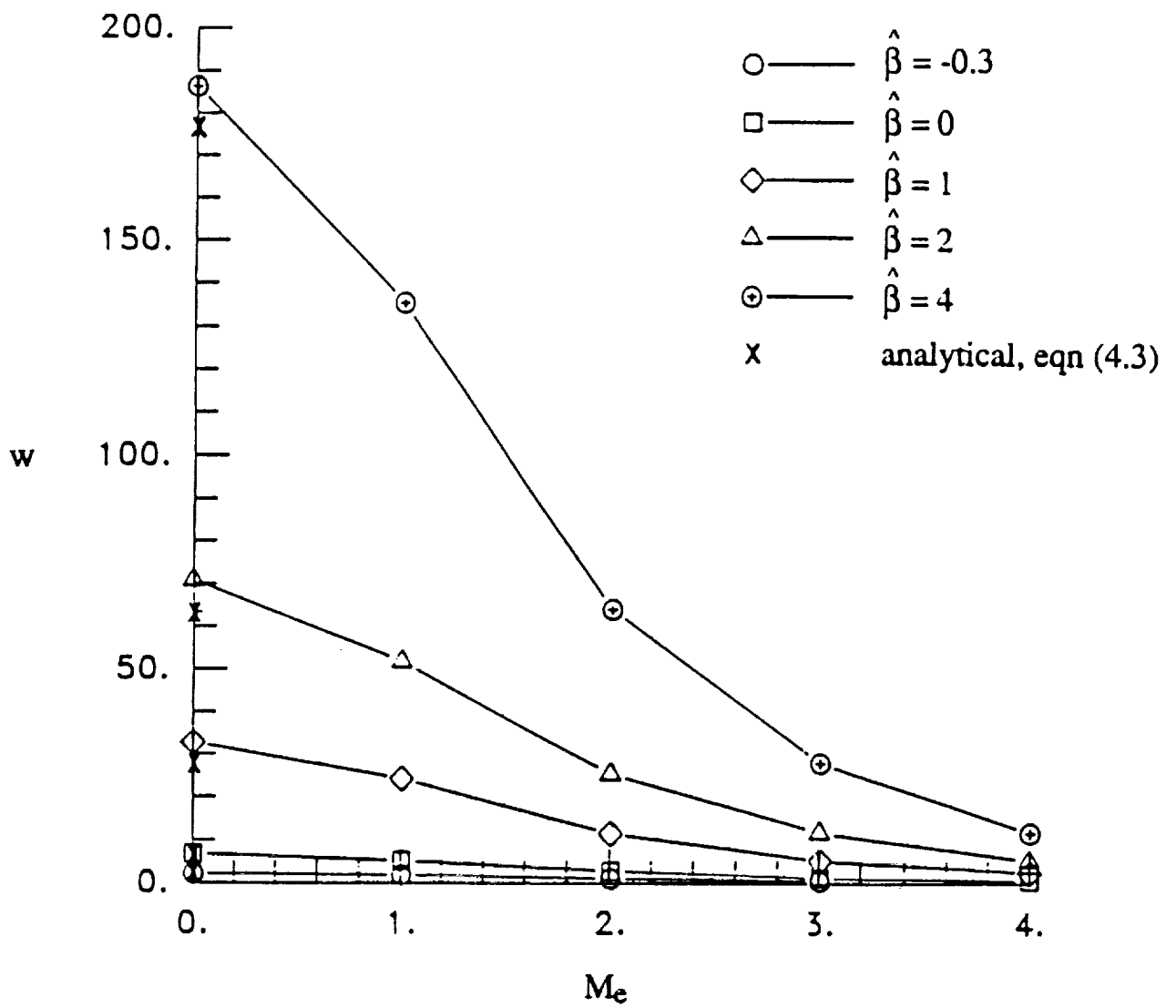
a) Effect of $\hat{\beta}$ and M_e with $Re_{\delta^*} = 10^4$.

Figure 14. Behavior of the the law of the wake coefficient.
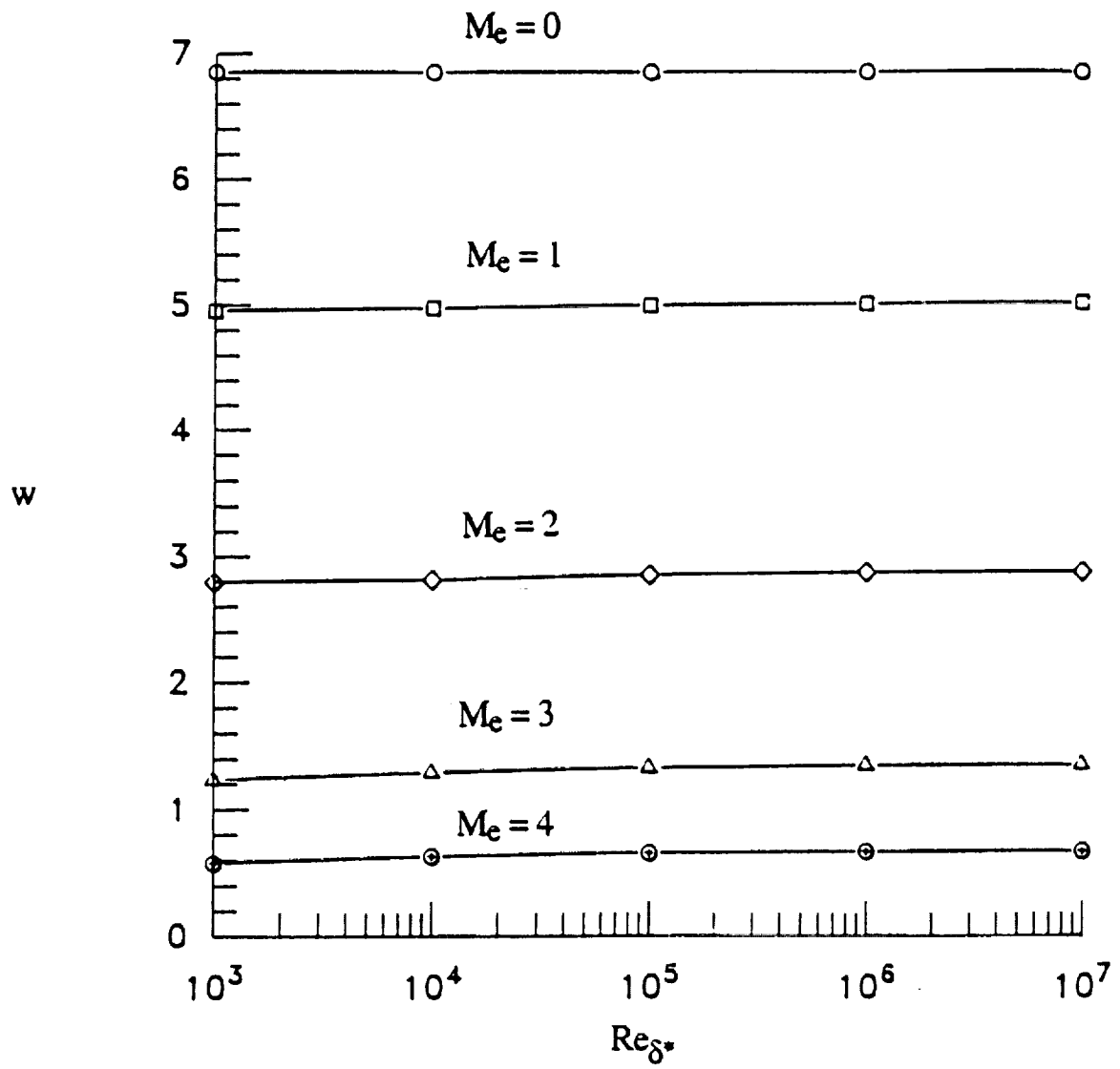
b) Effect of Re_{δ^*} and M_e for flat plate flow.

Figure 14. Concluded.
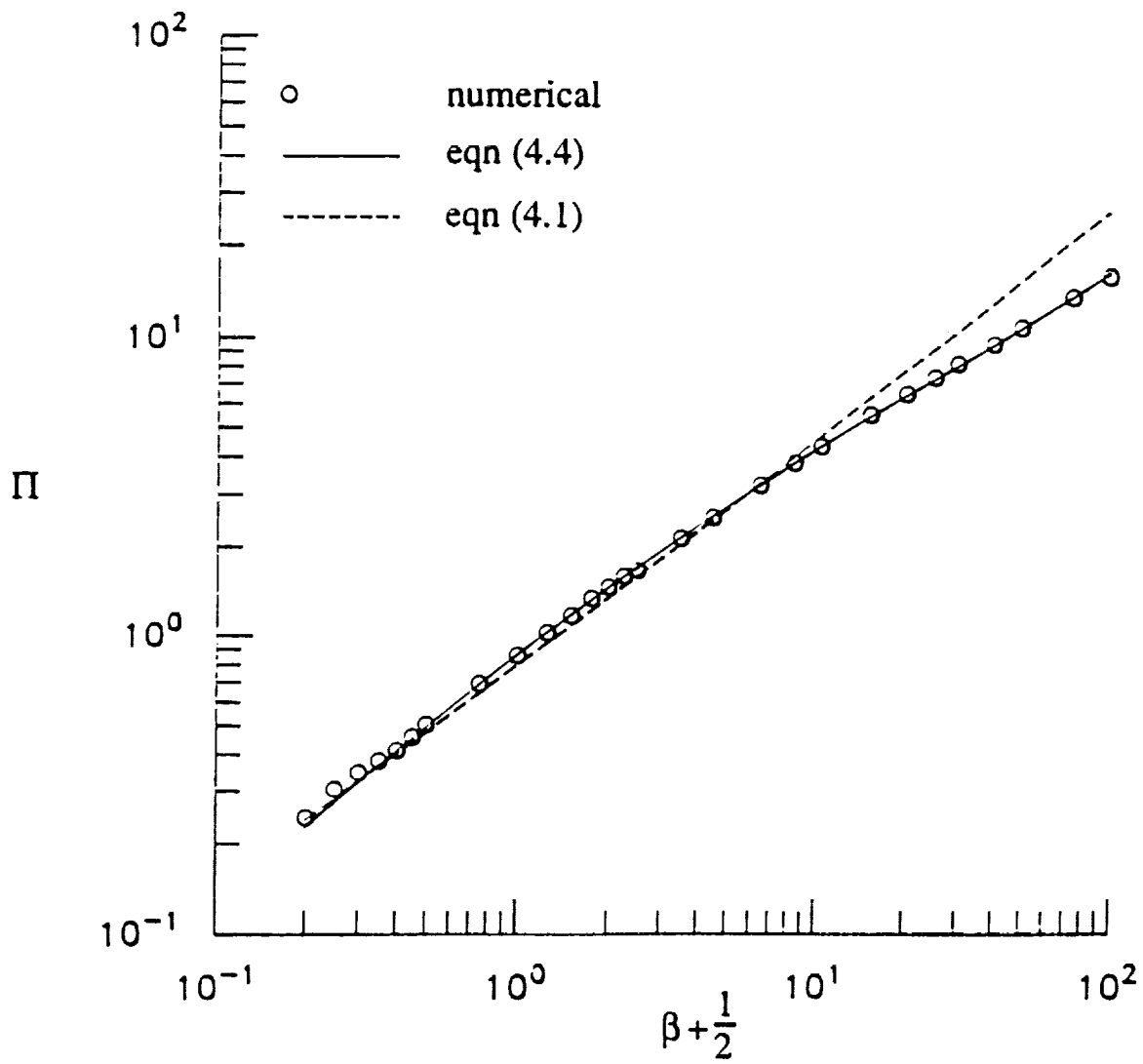
a) Comparison of analytical and numerical values of Π.

Figure 15. The incompressible law of the wake coefficient.
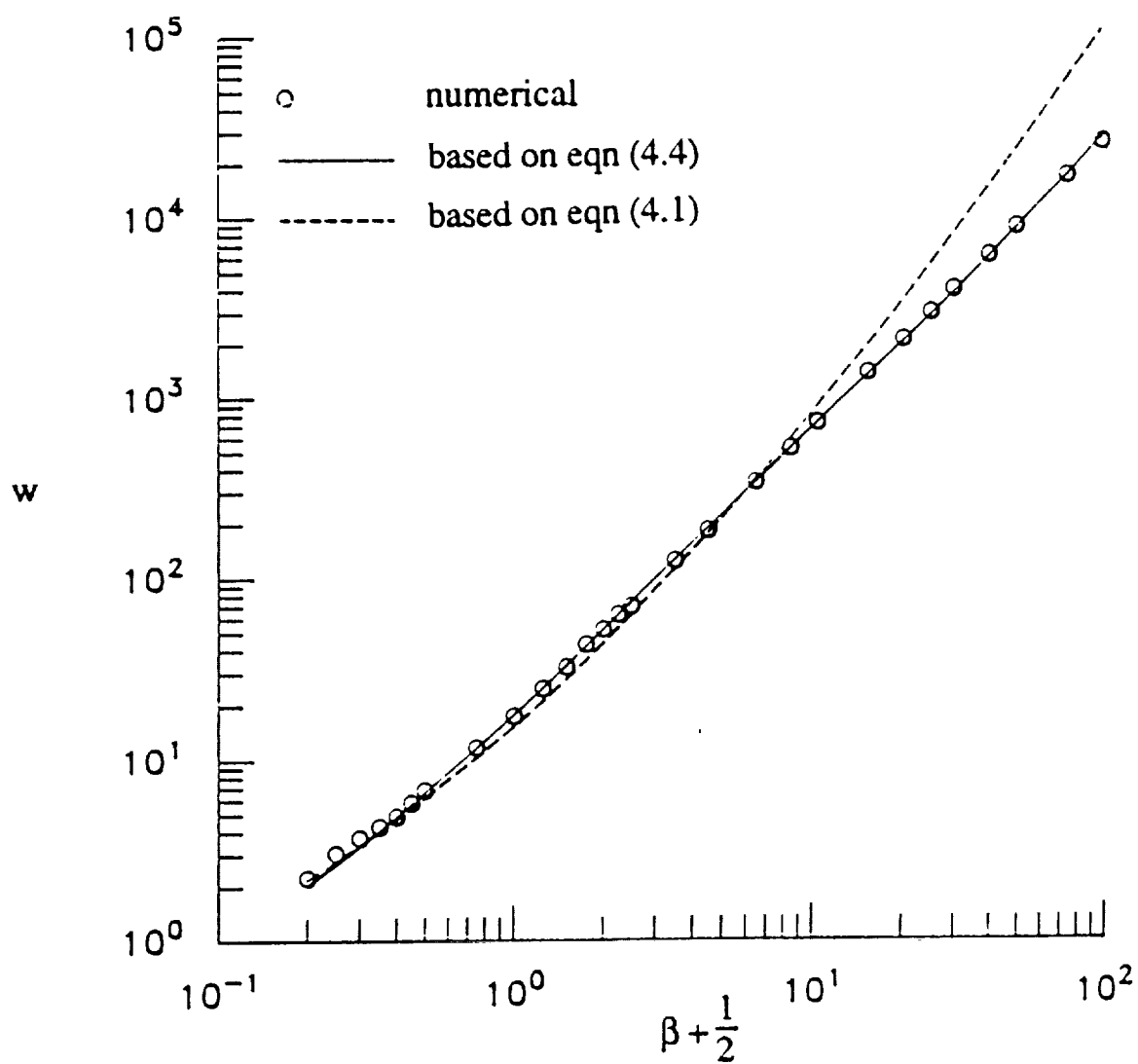
b) Comparison of analytical and numerical values of w.

Figure 15. Concluded.
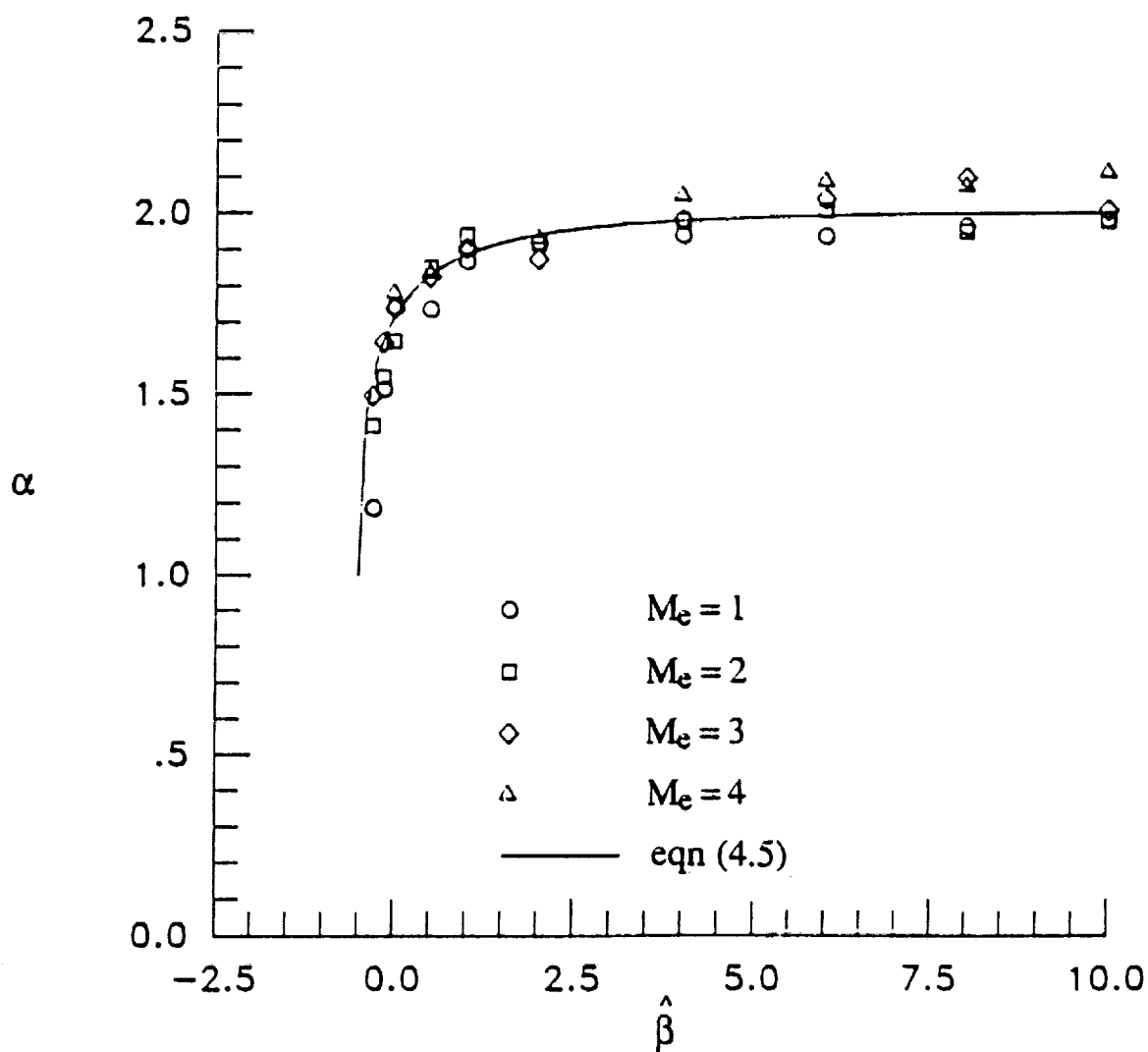
Figure 16. Effect of $\hat{\beta}$ on the law of the wake coefficient exponent α.
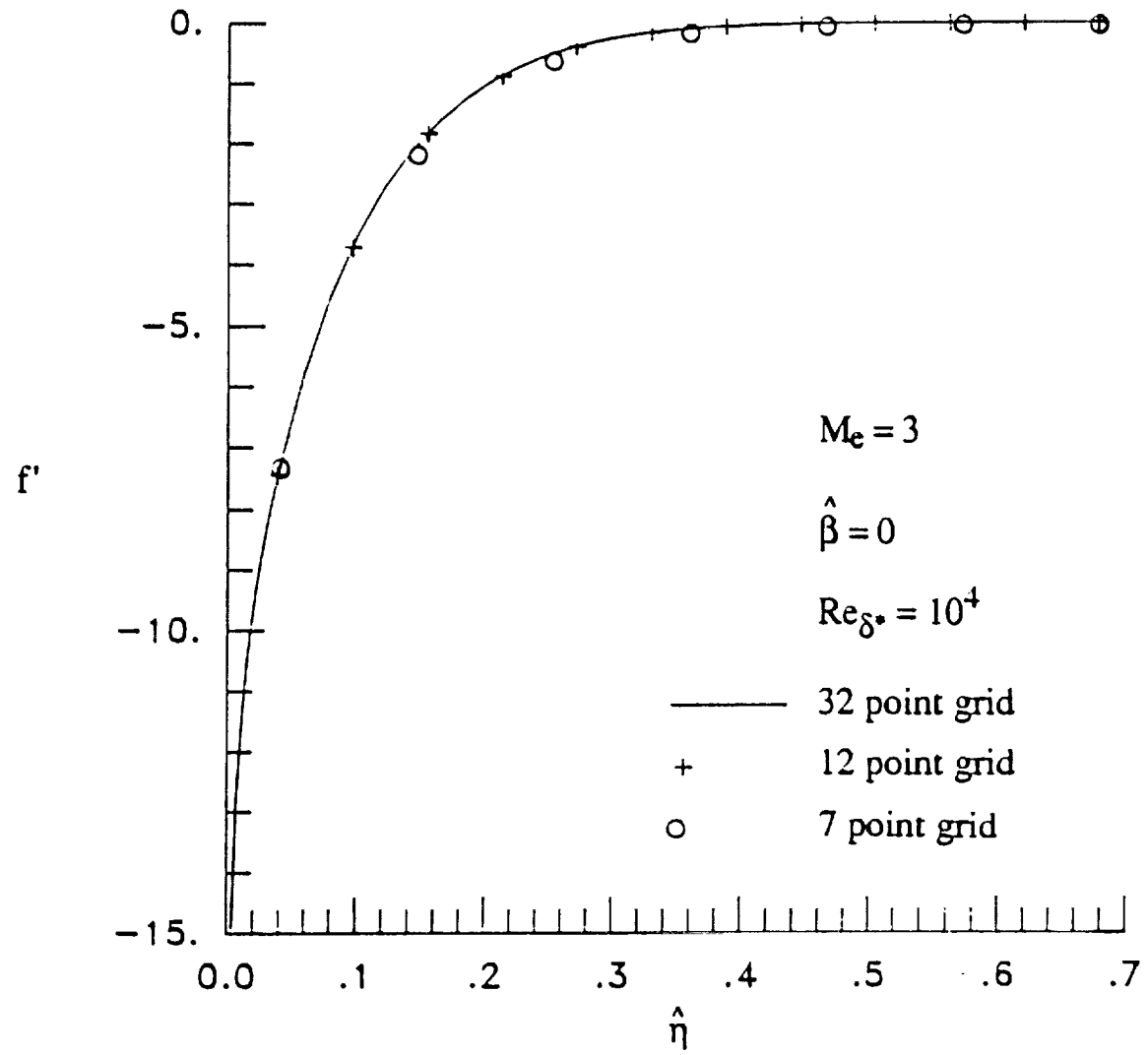
Figure 17. Grid resolution comparison for compressible flow.
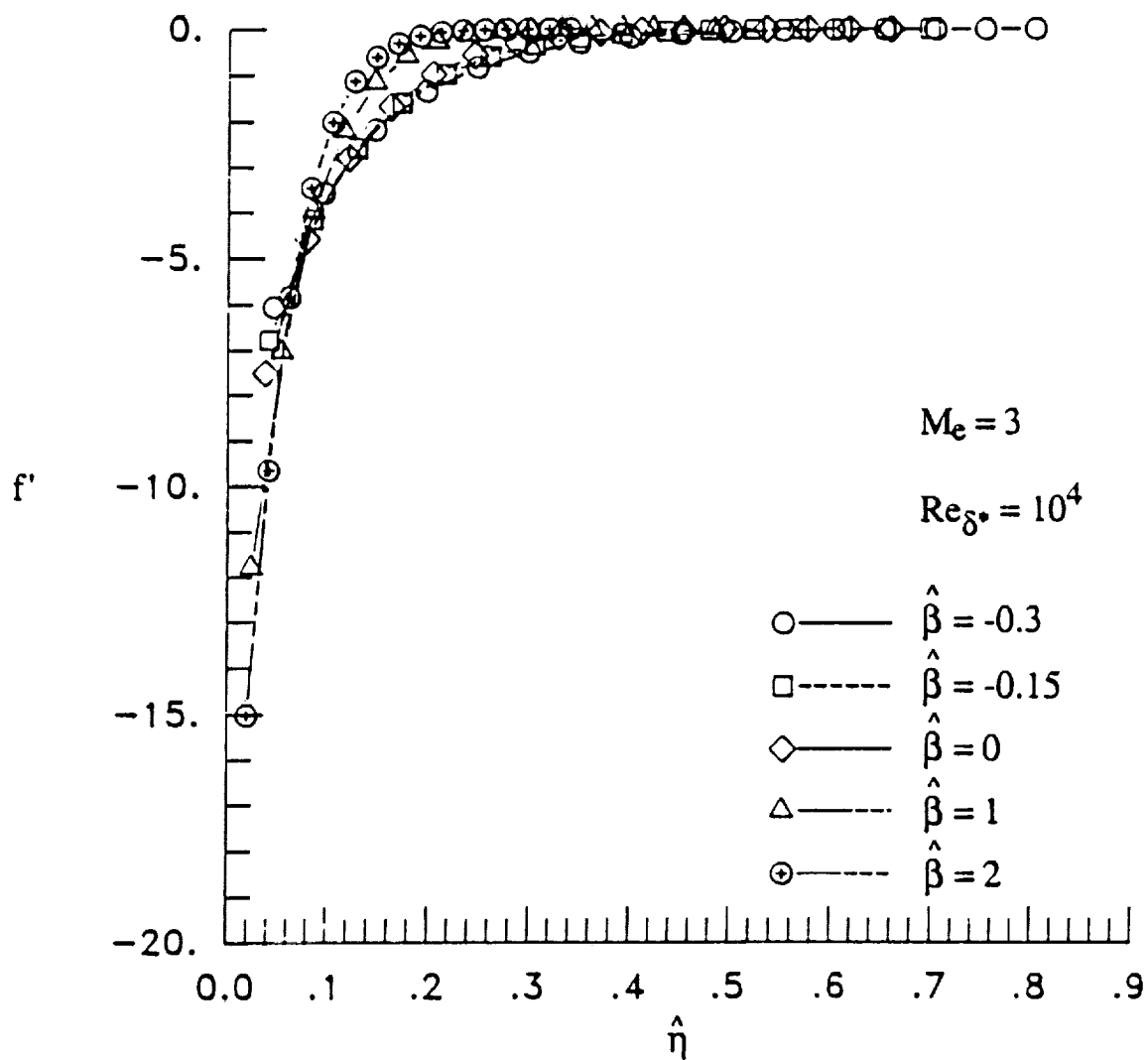
a) Effect on velocity defect profiles.

Figure 18. Effect of $\hat{\beta}$ on various profiles with $M_e = 3$ and $Re_{\delta^*} = 10^4$.
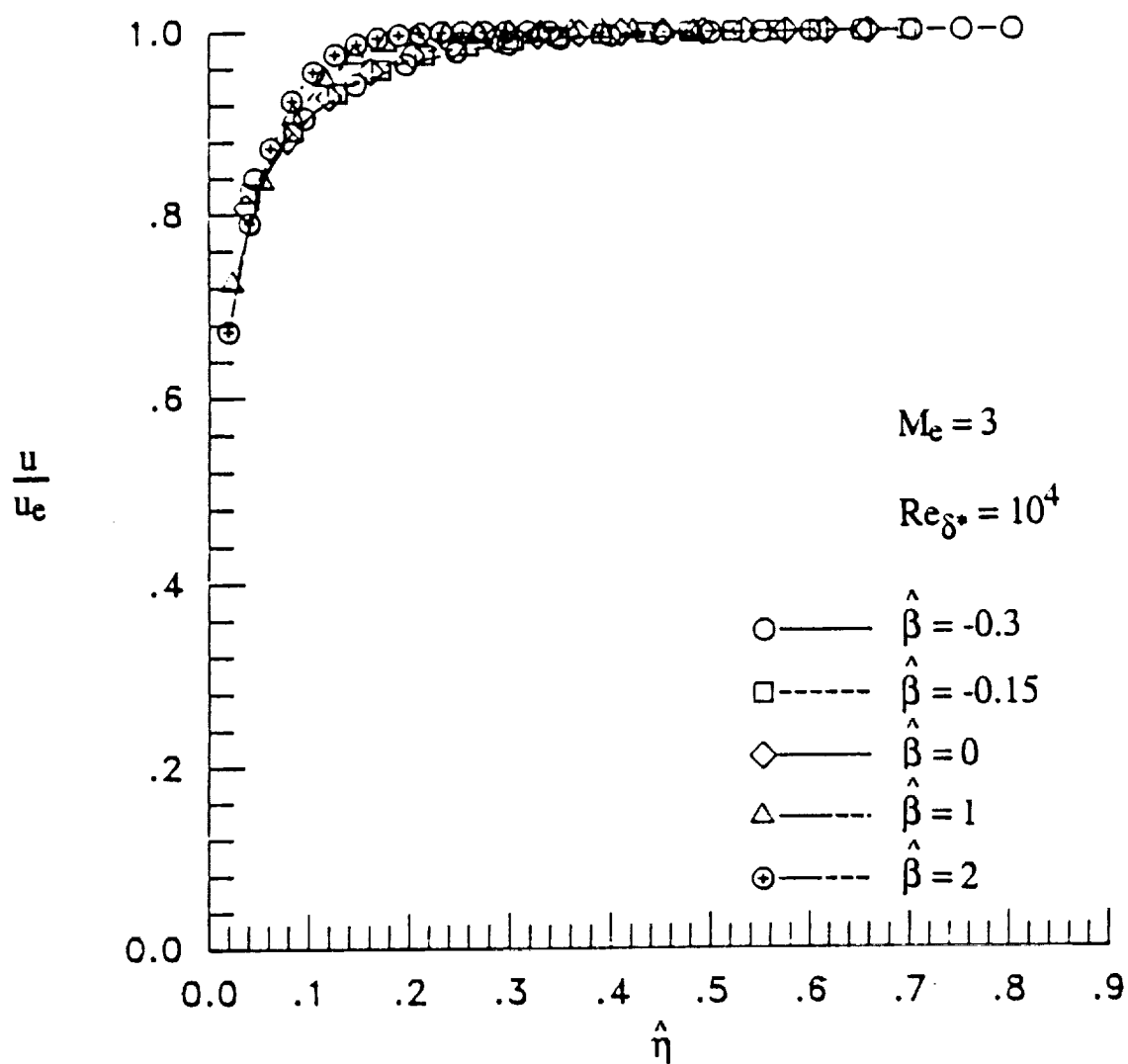
b) Effect on velocity profiles.

Figure 18. Continued.
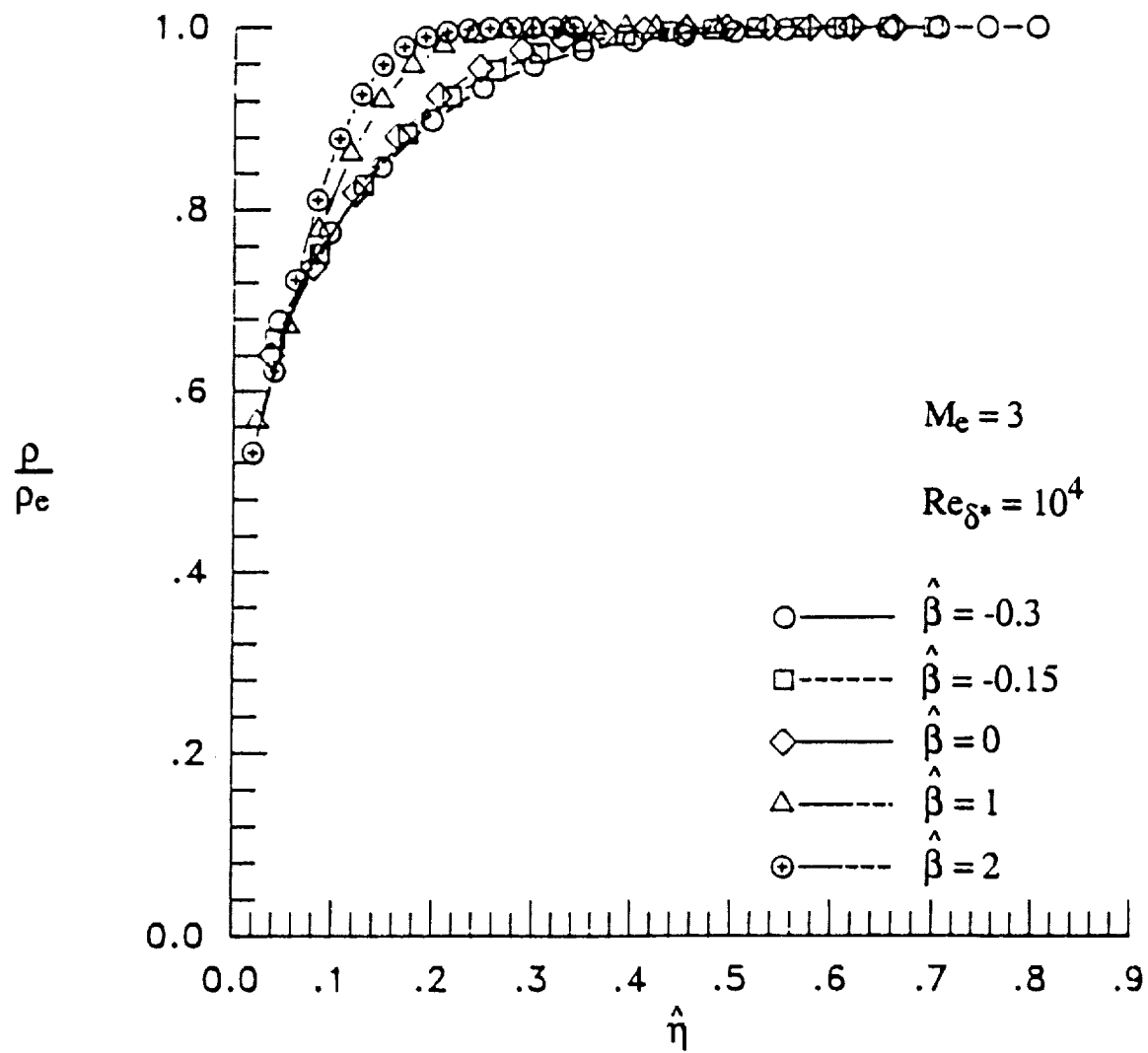
c) Effect on density profiles.

Figure 18. Concluded.
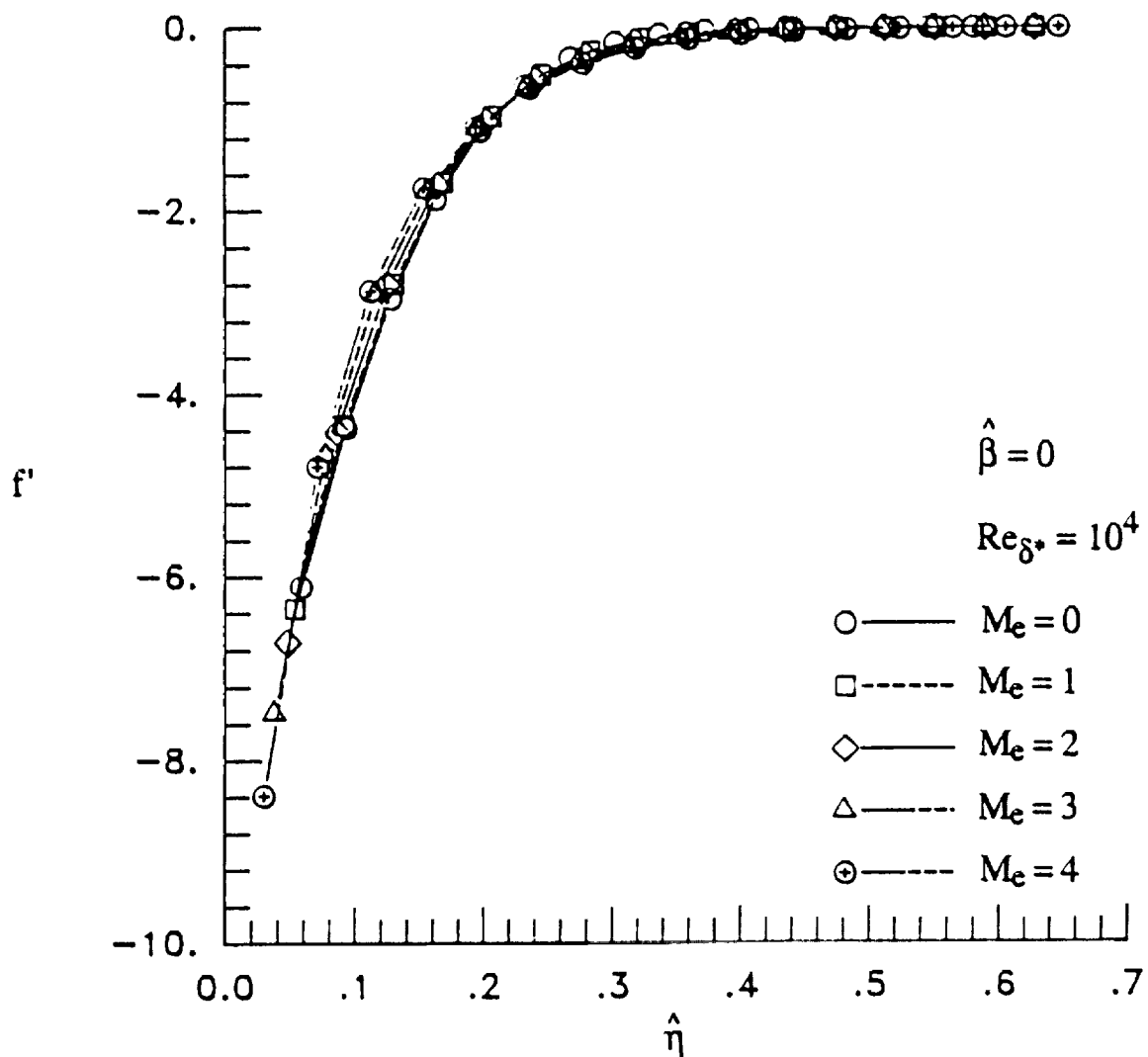
a) Effect on velocity defect profiles.

Figure 19. Effect of M_e on various profiles with $\hat{\beta} = 0$ and $Re_{\delta^*} = 10^4$.
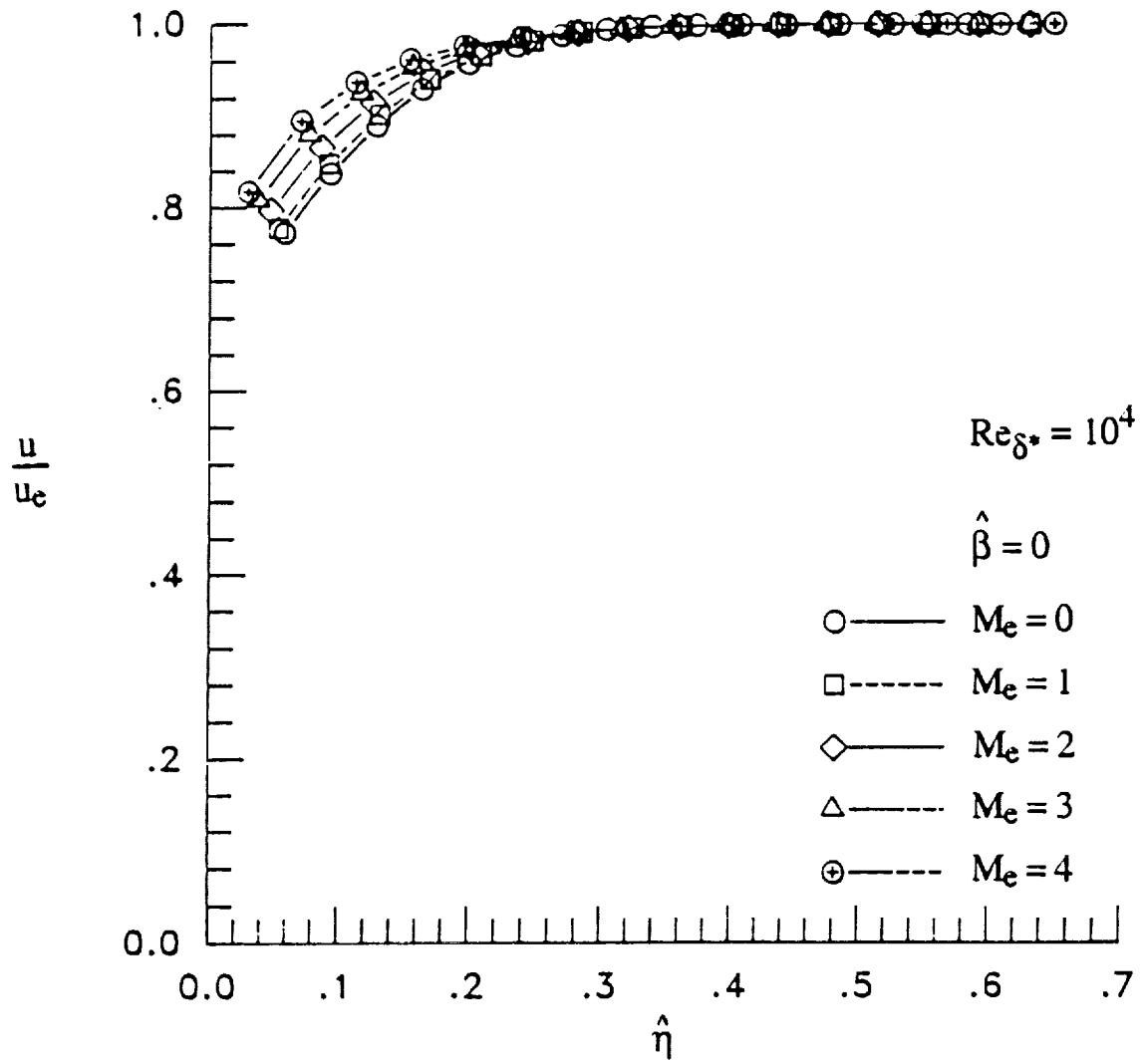
b) Effect on velocity profiles.

Figure 19. Continued.
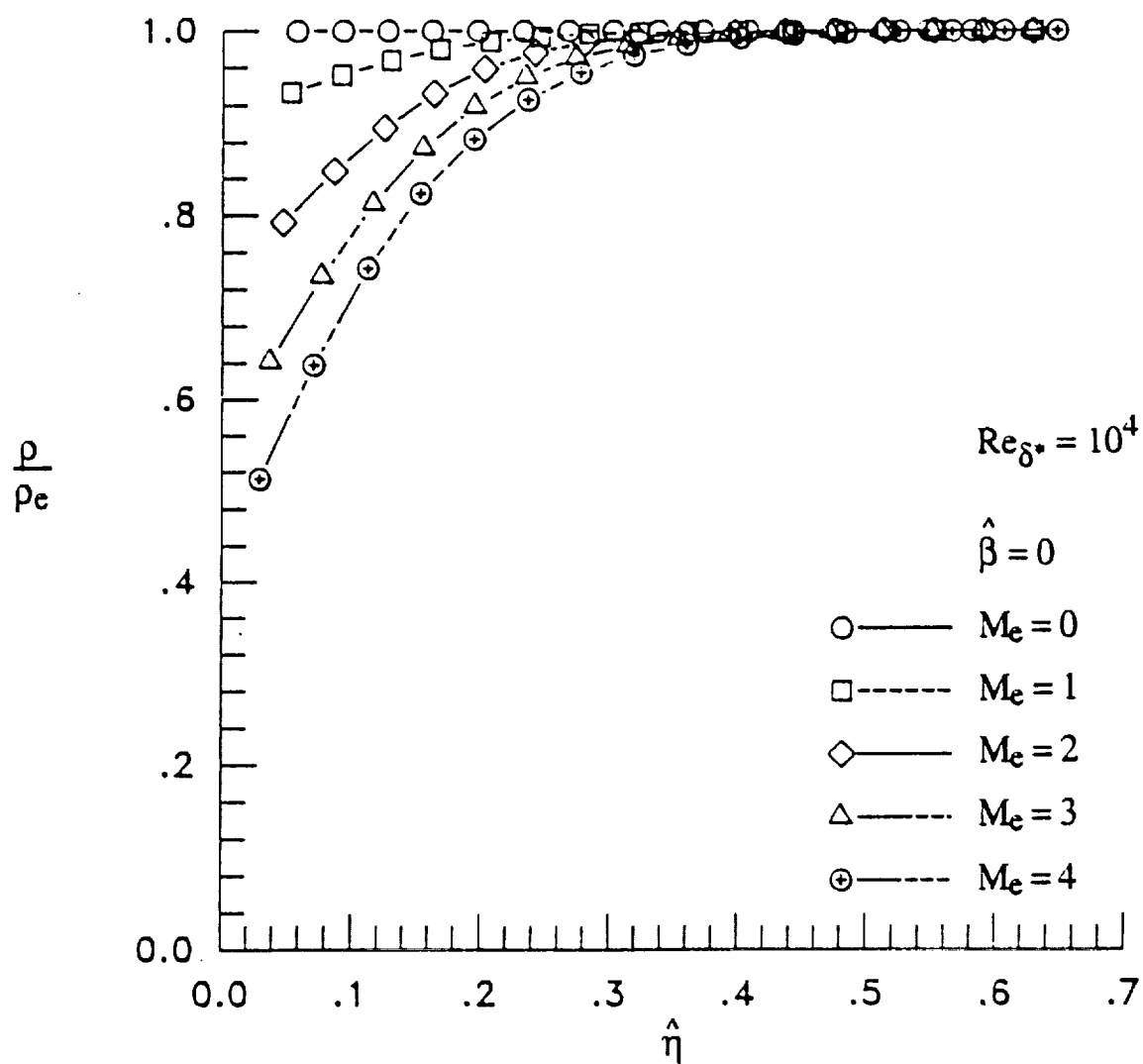
c) Effect on density profiles.

Figure 19. Concluded.
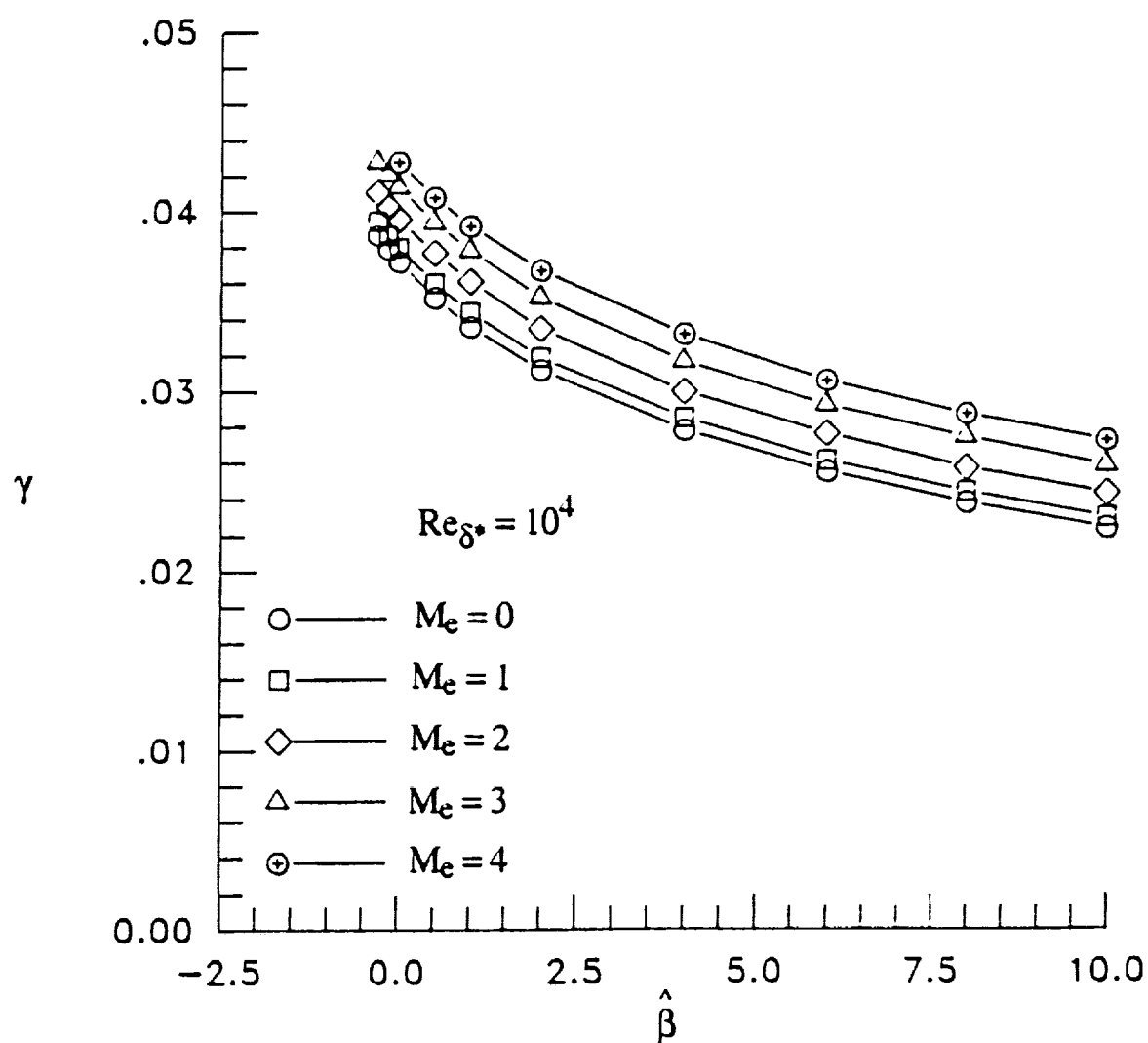
a) Effect of $\hat{\beta}$ and M_e with $Re_{\delta^*} = 10^4$.

Figure 20. Behavior of the shear-stress velocity ratio.
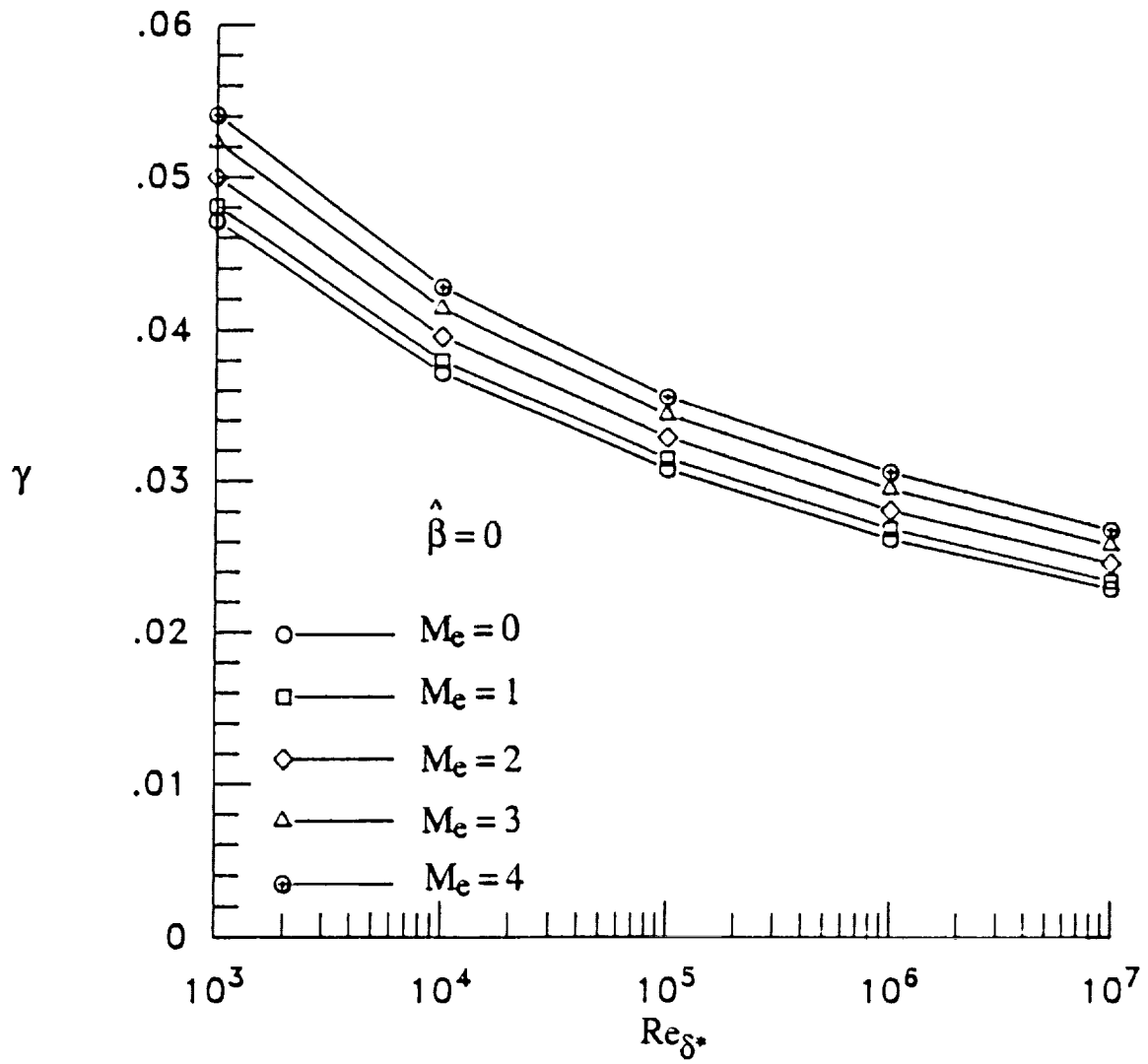
b) Effect of Re_{δ^*} and M_e for flat plate flow.

Figure 20. Concluded.
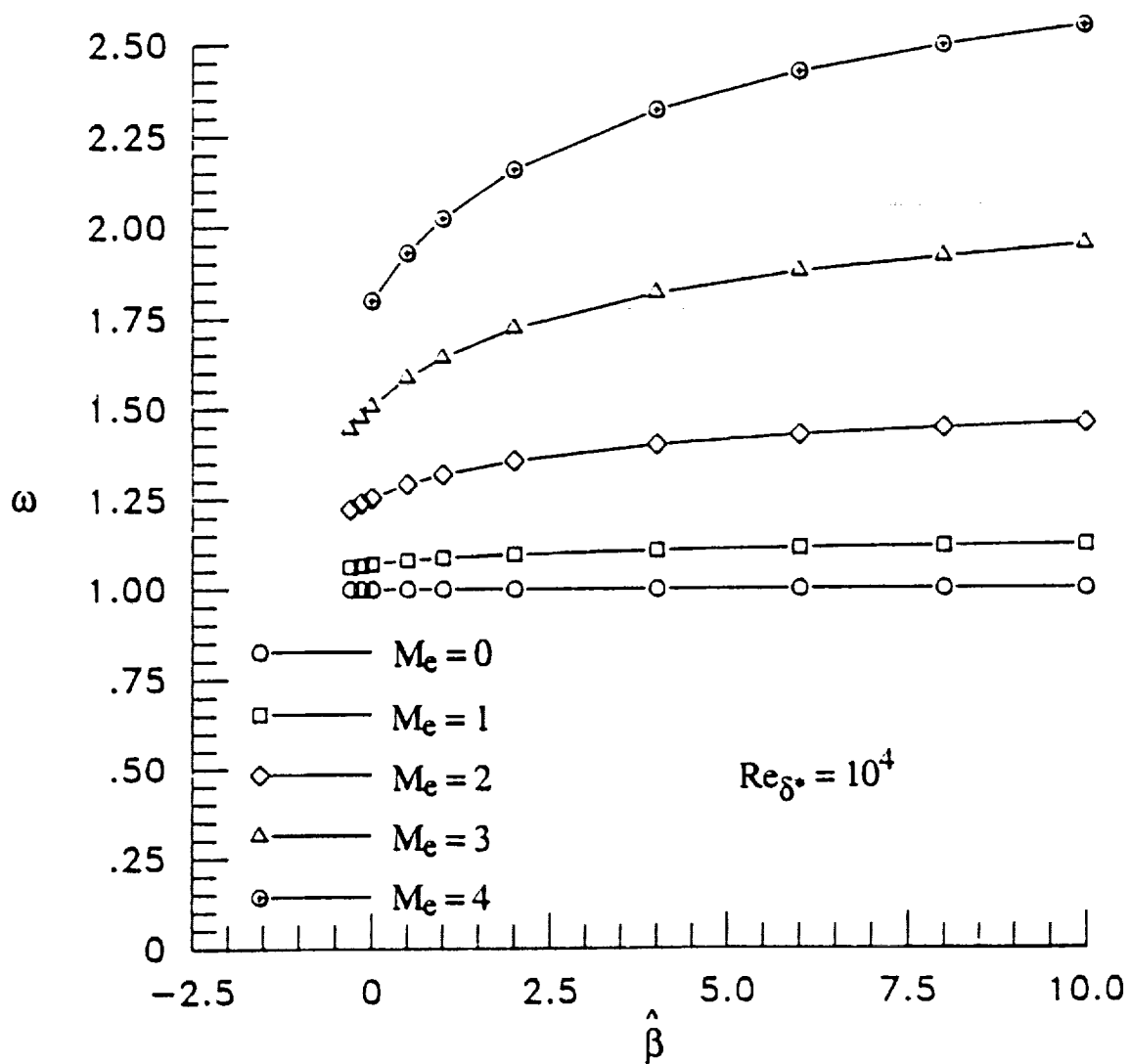
a) Effect of $\hat{\beta}$ and M_e with $Re_{\delta^*} = 10^4$.
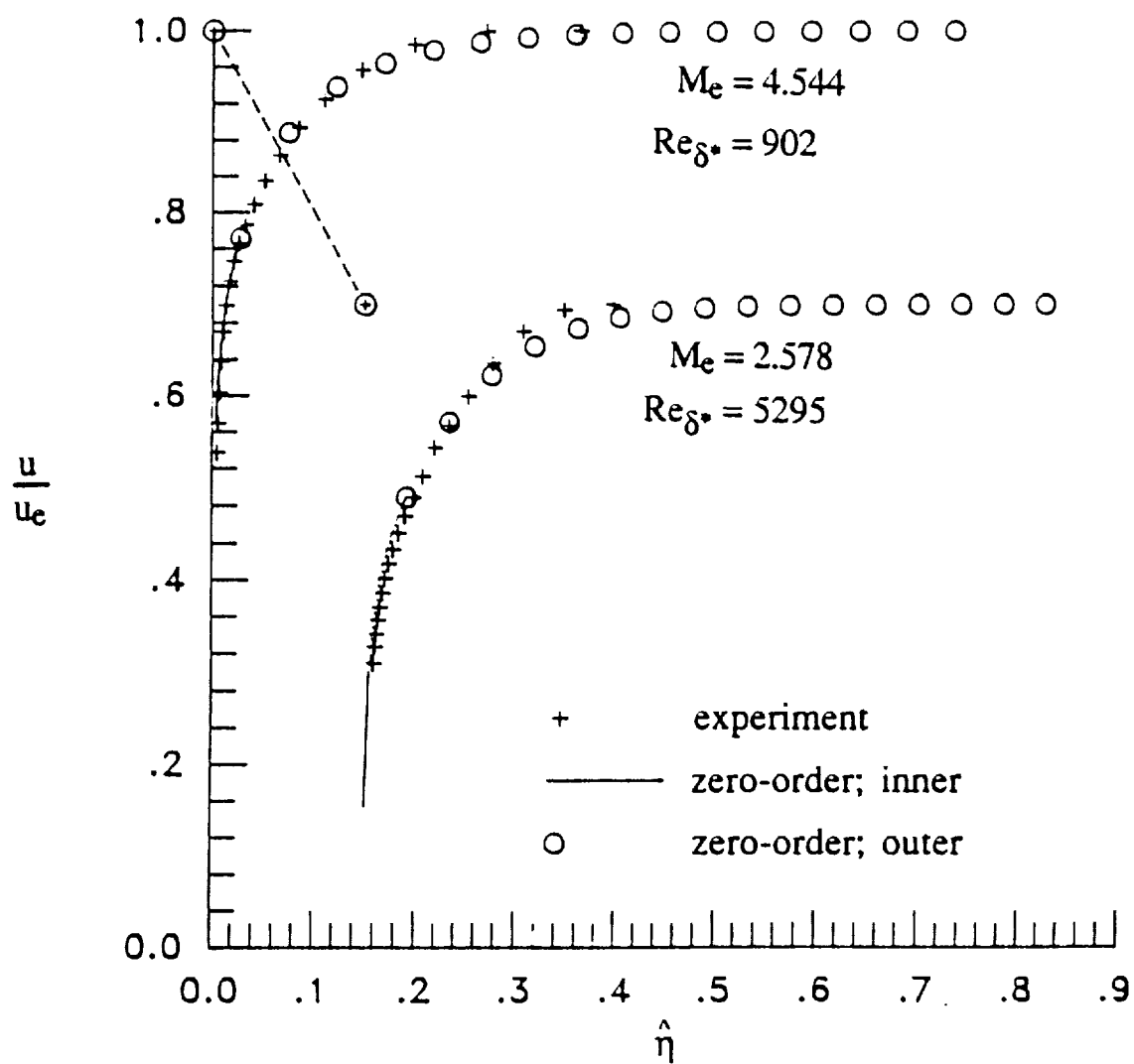
Figure 21. Trends of the compressibility parameter ω.
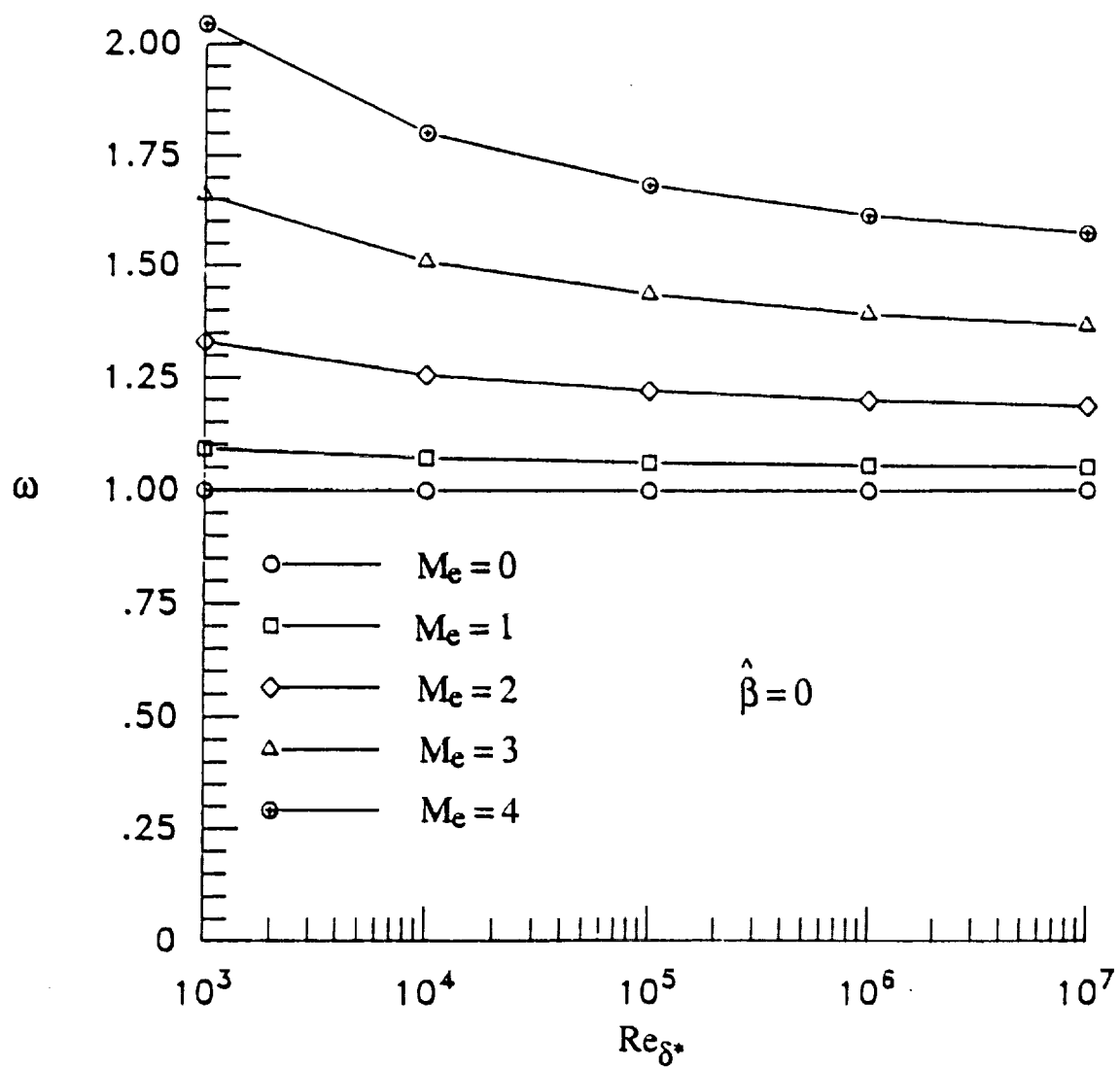
b) Effect of Re_{δ^*} and M_e for flat plate flow.
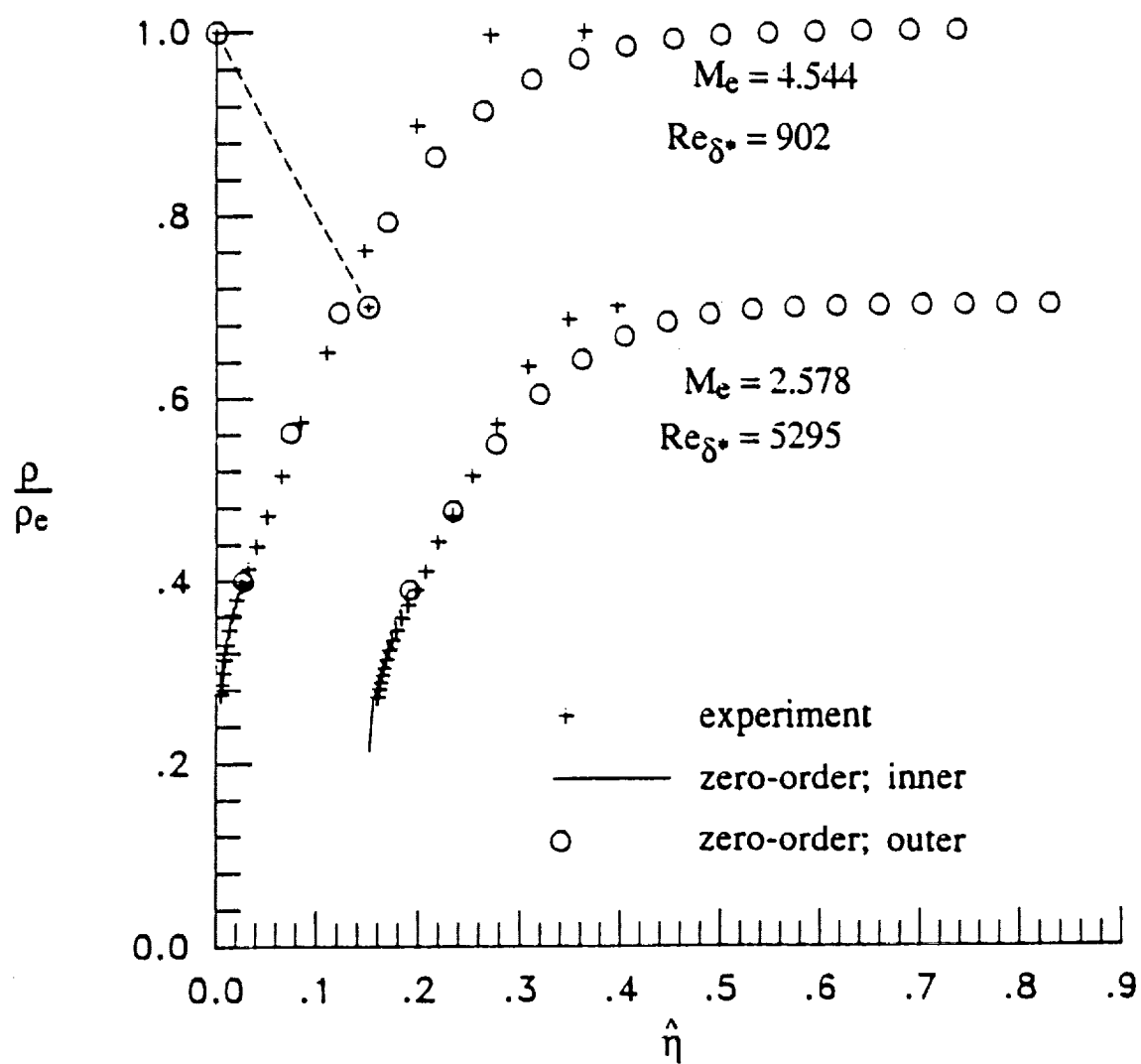
Figure 21. Concluded.
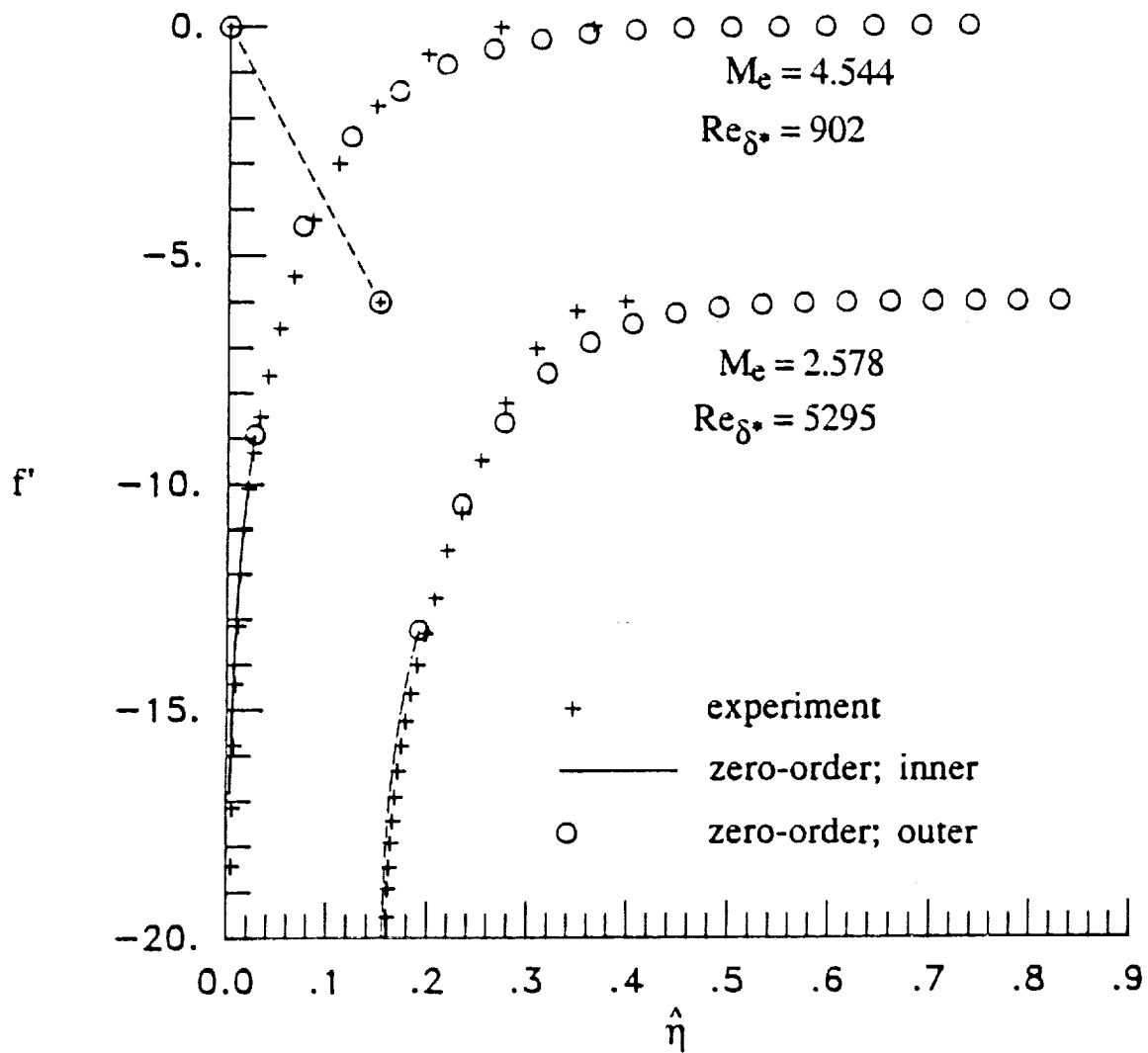
a) Comparison of velocity defect profiles.

Figure 22. Comparison of various profiles with experimental data for compressible flow on a flat plate .
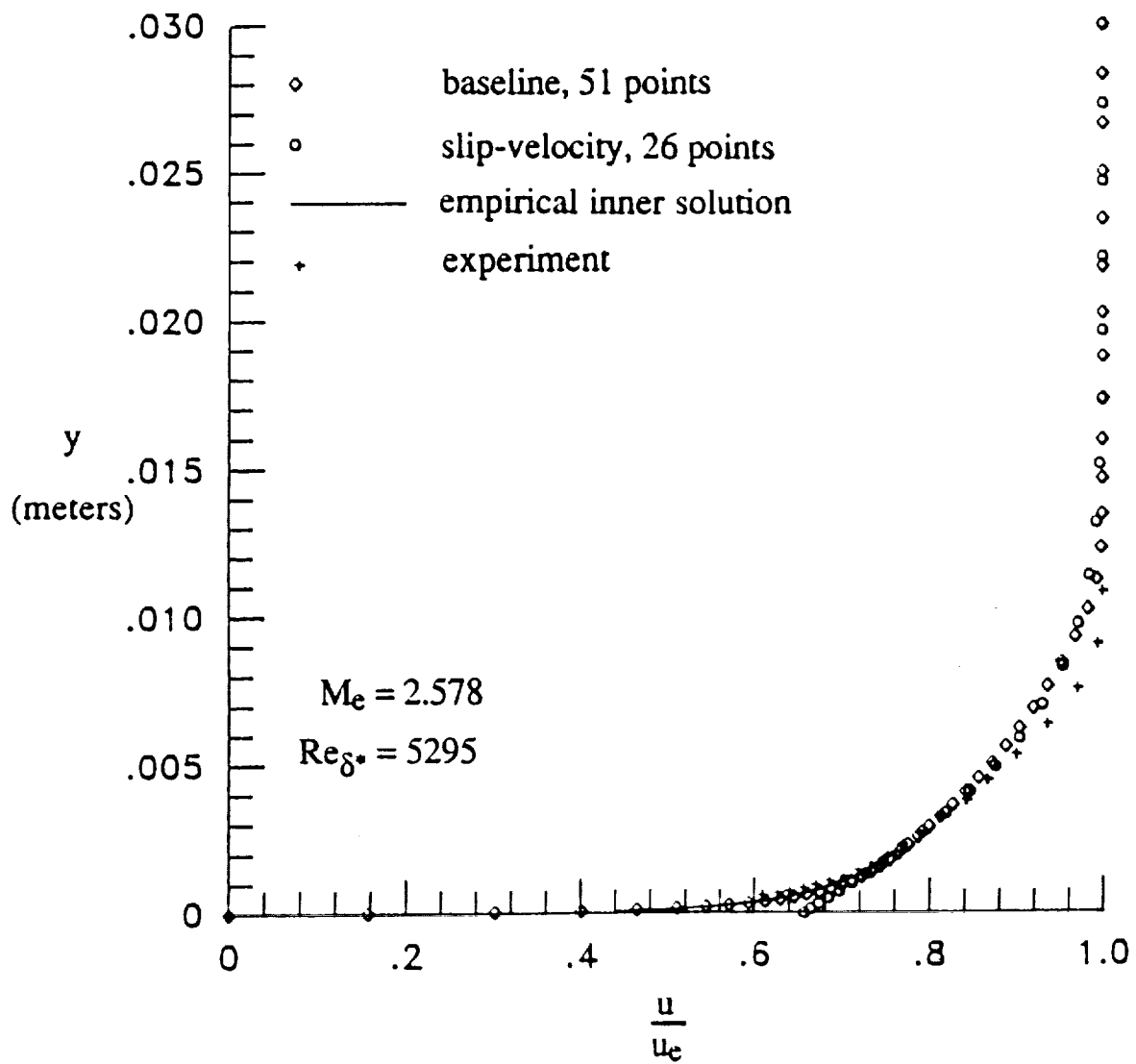
b) Comparison of velocity profiles.
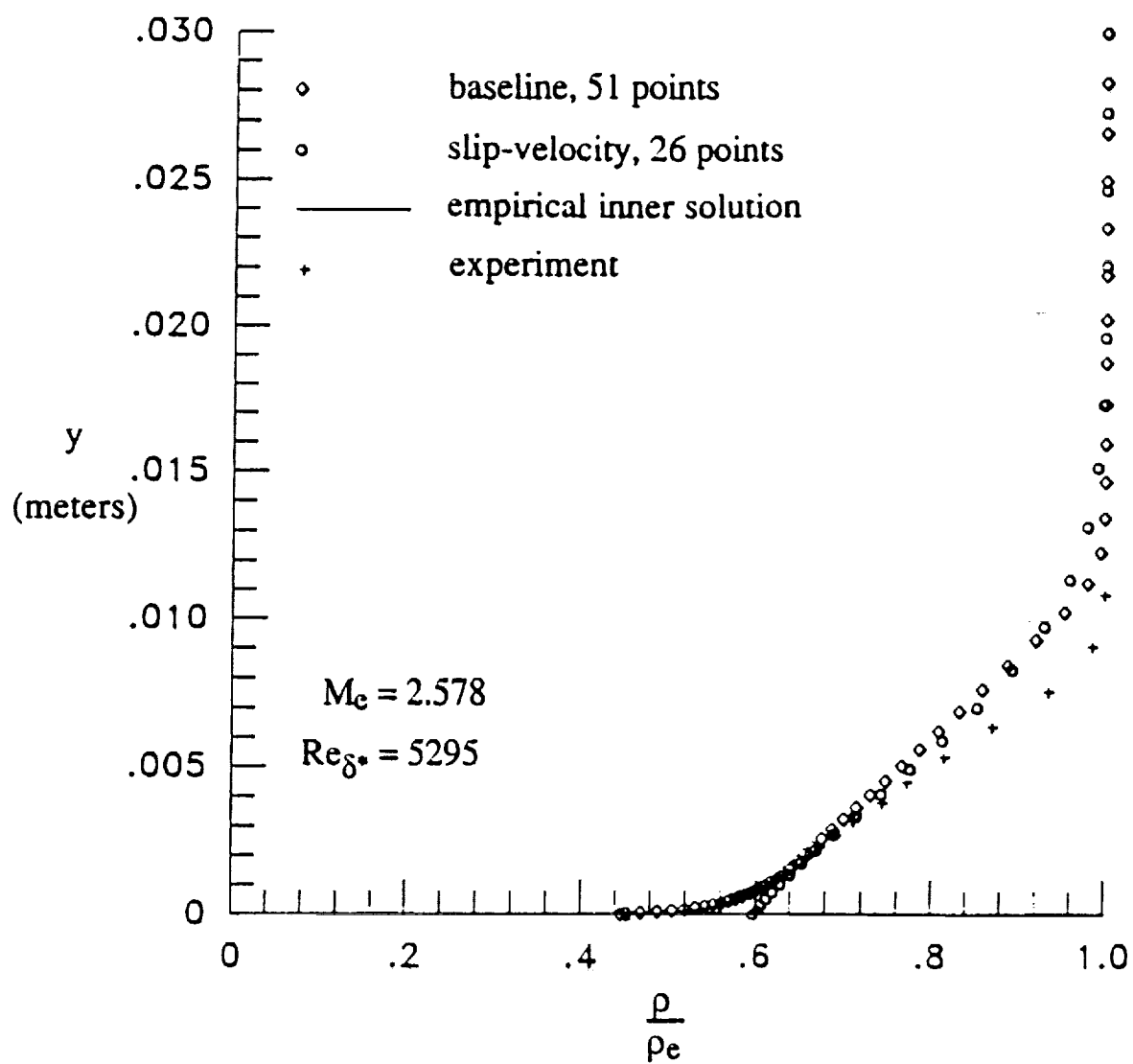
Figure 22. Continued.

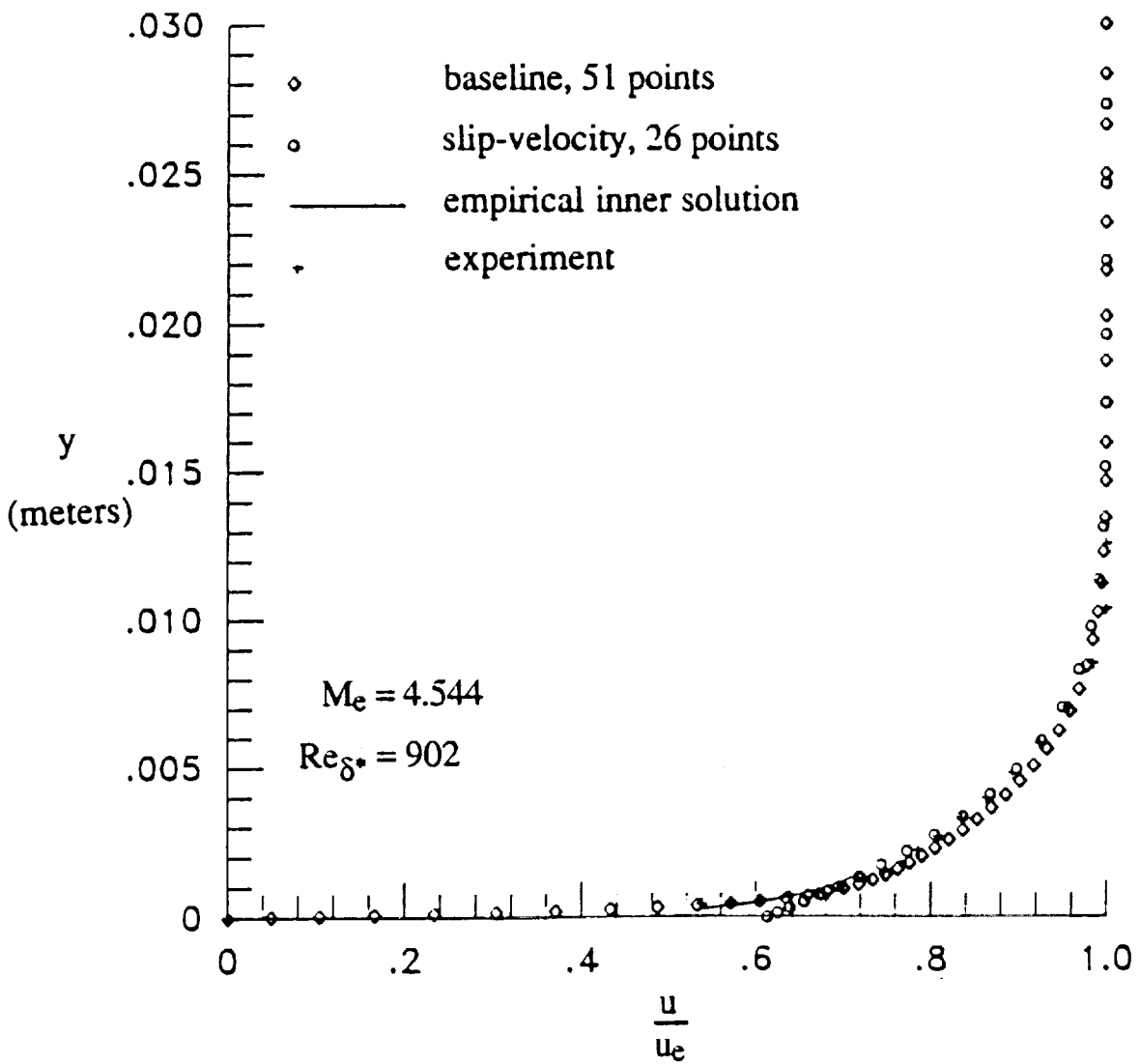c) Comparison of density profiles.

Figure 22. Concluded.

a) Velocity ratio comparison.

Figure 23. Baseline and slip-velocity Navier-Stokes solutions for $M_e = 2.578$.
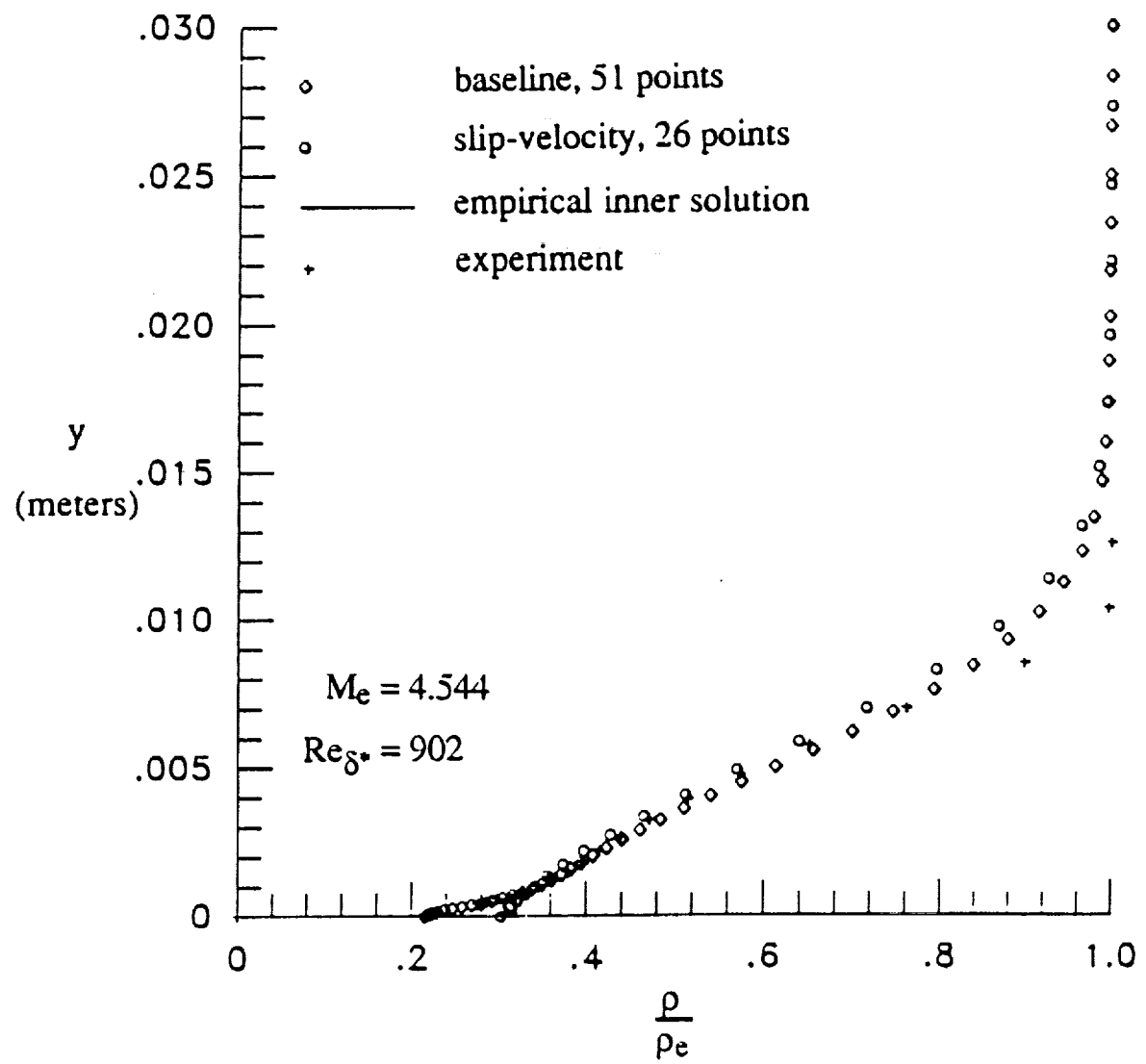
b) Density ratio comparison.

Figure 23. Concluded.

a) Velocity ratio comparison.

Figure 24. Baseline and slip-velocity Navier-Stokes solutions for $M_e = 4.544$.

b) Density ratio comparison.

Figure 24. Concluded.

National Aeronautics and Space Administration

Report Documentation Page

1. Report No. NASA CR-4286	2. Government Accession No.	3. Recipient's Catalog No.

4. Title and Subtitle	5. Report Date
Development of a Defect Stream Function, Law of the Wall/Wake Method for Compressible Turbulent Boundary Layers	March 1990
	6. Performing Organization Code

7. Author(s)	8. Performing Organization Report No.
Richard A. Wahls	
	10. Work Unit No. 505-60-01-02

9. Performing Organization Name and Address	11. Contract or Grant No.
North Carolina State University Department of Mechanical and Aerospace Engineering Raleigh, NC 27695-7910	NCC1-117
	13. Type of Report and Period Covered

12. Sponsoring Agency Name and Address	Contractor Report
National Aeronautics and Space Administration Langley Research Center Hampton, VA 23665-5225	14. Sponsoring Agency Code

15. Supplementary Notes

The information presented in this report was offered as a dissertation in partial fulfillment of the requirements for the Degree of Doctor of Philosphy, North Carolina State University, Raleigh, North Carolina, 1989.

Langley Technical Monitor: David H. Rudy

16. Abstract The method presented is designed to improve the accuracy and computational efficiency of existing numerical methods for the solution of flows with compressible turbulent boundary layers. A compressible defect stream function formulation assuming an arbitrary turbulence model is derived. Previous problems with the defect formulation are eliminated by using empirically based analytic expressions to define the flow near the wall. The need for an inner-region eddy-viscosity model is completely avoided. The near-wall analytic expressions are patched to numerically computed outer-region solutions at a point determined during the computation. A new surface boundary condition is presented; this condition replaces the no-slip condition and enables numerical integration to the surface with a relatively coarse grid. The method has been evaluated for incompressible and compressible equilibrium flows and has been implemented into an existing Navier-Stokes code.

17. Key Words (Suggested by Author(s))	18. Distribution Statement
Law of the Wall Law of the Wake Equilibrium Boundary Layer Turbulent Boundary Layer Compressible Flow	Unclassified-Unlimited Subject Category 34

19. Security Classif. (of this report)	20. Security Classif. (of this page)	21. No. of pages	22. Price
Unclassified	Unclassified	124	A06

NASA FORM 1626 OCT 86